ENTROPY OPTIMIZATION OF AN ADDITIVELY MANUFACTURED HEAT EXCHANGER WITH A DUAL STAGE GIFFORD-MCMAHON CRYOGENIC REFRIGERATOR FOR HYDROGEN LIQUEFACTION

By

JORDAN ALYSE RAYMOND

A thesis submitted in partial fulfillment of
the requirements for the degree of

MASTER OF SCIENCE IN MECHANICAL ENGINEERING

WASHINGTON STATE UNIVERSITY
School of Mechanical and Materials Engineering

JULY 2021

To the Faculty of Washington State University:

The members of the Committee appointed to examine the thesis of JORDAN ALYSE RAYMOND find it satisfactory and recommend that it be accepted.

_____

Jacob Leachman, Ph.D., Chair

_____

Konstantin Matveev, Ph.D.

_____

Steven Saunders, Ph.D.

ACKNOWLEDGMENT

The support that I have received from friends, family, and colleagues throughout my time in graduate school has been invaluable in helping me reach my goals and finish this degree. I want to start by thanking my mentor and advisor, Dr. Jake Leachman. The number of hours that we have spent discussing heat transfer, thermodynamics, and how to succeed in both graduate school as well as the real world are innumerable. He was always willing to answer questions and pushed me to be a better engineer both academically and professionally. I would also like to thank my committee members, Dr. Konstantin Matveev and Dr. Steve Saunders, for providing insight and guidance whenever needed.

The members of HYPER have been invaluable. The discussions, tutorials, and support were never ending, and the enthusiasm never waned. Everyone in the lab is an amazing individual, and when they work together, I don't think there are any limits to what they can accomplish. I would specifically like to thank Ian Richardson, Carl Bunge, all of the undergraduates who have been a part of the liquefaction team, and everyone who has been involved with the Mobile Hydrogen Generation Unit. I can't wait to see what you all do next.

Last but not least, I would like to thank my mom and dad, Heidi and Mike Raymond, my brother, Tanner Raymond, my partner, Michael Brown, and my roommate, Hayley Masterson. My parents fielded many stressed phone calls and always encouraged me to do my best. They raised me to believe that I could accomplish anything and never wavered in that belief. Michael was always interested to hear what I was working on, even when I wasn't, and encouraged me to follow my passion. Last but not least, Hayley has been there for midnight ice cream runs, stressed movie nights, and everything in between. I am so thankful for everyone who has been a part of this journey, and I can't wait to see what comes next.

ENTROPY OPTIMIZATION OF AN ADDITIVELY MANUFACTURED HEAT EXCHANGER WITH A DUAL STAGE GIFFORD-MCMAHON CRYOGENIC REFRIGERATOR FOR HYDROGEN LIQUEFACTION

Abstract

by Jordan Alyse Raymond, M.S.
Washington State University
July 2021

Chair: Jacob Leachman

Small-scale hydrogen liquefaction presents an opportunity to drive down market costs by eliminating the cost associated with transportation. With the decline of fossil fuels and other nonrenewable energy sources, billions of dollars are being invested in large-scale hydrogen liquefaction. Large-scale systems have higher efficiencies, but limit accessibility. Little research has been done to optimize small-scale systems, and the presented options are often not scalable beyond a laboratory setting. The most inefficient system components are the heat exchanger, the nitrogen refrigerator, and the cycle compressor. In this thesis a novel, scalable, heat exchanger design based on principles of entropy minimization is presented. The design utilizes a branching structure with exponentially varying wall thickness and mounts onto a Gifford-McMahon cryogenic refrigerator. Numerical optimization indicates an efficiency increase of 39.21% when compared to a single tube design. The thermal mass is decreased by 43.82% and the length of the optimized design is only 8.61% of that of the single tube design. The heat exchanger is additively

manufactured with an aluminum alloy and the interior is coated with a ruthenium-based catalyst to facilitate the ortho-parahydrogen conversion. Hydrogen enters the heat exchanger at 293 K and 653 kPa. It is cooled to 28.1 K and full ortho-parahydrogen conversion is assumed prior to reaching the storage dewar. The experimental measured rate of liquefaction is determined to be 0.003535 g/s, the upper flange of the heat exchanger resides at 58.0523 K, and the lower flange resides at 26.1631 K. The temperature difference between the lower flange of the heat exchanger and outlet fluid flow is less than 0.5 K. The mass flow rate and operating temperatures are lower than predicted. This is likely due to poor thermal properties of the heat exchanger material and poor thermal contact between the heat exchanger and the cryogenic refrigerator. However, the small temperature difference suggests small temperature gradients within the system, indicating minimum entropy generation. Suggestions are given to improve system performance.

TABLE OF CONTENTS

Page

LIST OF TABLES

Page

LIST OF FIGURES

Page

Dedication

To everyone who has been there along the way –

thank you.

CHAPTER ONE: INTRODUCTION

Fossil fuels are nonrenewable. Assuming current consumption trends continue, BP estimates that current oil reserves will be depleted by 2072 [1]. With the looming demise of nonrenewable fuels, batteries and renewable options such as wind, solar, and geothermal are garnering more interest. Batteries are viewed as a clean alternative to fossil fuels, and this is true while the vehicle is in operation. There are no emissions. However, once the battery is no longer usable, only the mechanical components are recycled, not the lithium cell. The demand for lithium is estimated to surpass the supply by 2025, rendering batteries a nonrenewable and unsustainable option [2]. The only feasible long-term energy sources are those that are renewable. However, energy generation from renewables is inconsistent and requires methods for energy storage. For instance, if the wind stops so does the energy generated from windmills. Even dams, which have a constant flow of water, do not have a constant flow rate and therefore do not have a constant power output. Source inconsistency and energy storage are two of the largest hurdles to clear for large scale utilization of these renewable energies. Without a consistent output or reliable storage of generated power, renewable energy must be supplemented with nonrenewable sources, or else outages could result.

By partnering renewable energy sources with hydrogen liquefiers, the energy can be stored, and inconsistent power generation is no longer a concern. Energy generated by the renewable source can be used to power an electrolyzer connected to the liquefier, generating energy dense hydrogen which can be stored and used on demand. The resulting hydrogen is referred to as green hydrogen due to zero carbon emissions. Plug Power, a company committed to growing the green hydrogen economy as well as a leading provider of hydrogen solutions, has committed to producing 50% of its hydrogen with renewable sources by 2024 [3]. They estimate

a production of 500 tons per day by 2025, and 1,000 tons per day globally by 2028 [4]. In 2020 alone, Plug Power received over $2.5 billion in investments to help achieve the company goals, reflecting an increased interest in liquid hydrogen as a fuel [5, 6].

Industrial and commercial demand for hydrogen is rising. In the industrial sector, where two main uses for hydrogen are in ammonia fertilizer to increase crop output and in oil refining, the global demand for hydrogen has increased more than threefold from 1975-2018 [7]; reflecting this trend is the commercial sector. Hydrogen vehicle sales are increasing around the world; there are over 8,000 hydrogen vehicles in California alone, the 2020 Olympics were set to run exclusively on hydrogen vehicles (and use a hydrogen torch flame), and hydrogen semi-trucks are gaining popularity throughout the US [8, 9]. Demand is also increasing in the aviation industry. Hydrogen is being considered as a fuel source for technology from commercial aircraft to military drones [10]. Airbus has gone on record forecasting the release of their hydrogen aircraft by 2035 [11]. Unfortunately, hydrogen can be costly and difficult to obtain which limits the feasibility of applications.

The current hydrogen infrastructure is not conducive for easy accessibility and could limit the applications of this fuel. There are only 37 commercial hydrogen liquefaction plants in the world, 20 of which are large-scale, meaning the production capacity is more than five tons per day. Of the 17 small-scale systems, eleven are in Asia [12]. For the commercial sector, there are only 44 hydrogen refueling stations in the US, with all but two on the west coast [13]. Therefore, unless a liquefier is nearby, the fuel could be out of reach. Hydrogen liquefiers have notoriously low efficiencies and high costs of manufacture, making it hard to justify installing new plants. Small-scale systems operate around only 20% of second law efficiency, which is a comparison of actual system performance to performance with reversible conditions, and when

building large-scale systems it costs about $5 million for each tonne per day capacity, including the steam methane reformer [14]. Excluding the steam methane reformer, the costs comes down to about $3 million for each tonne per day capacity. Only large-scale systems are economically feasible, because efficiency increases with size. The contrasting efficiencies of large and small-scale systems are reflected in the ratio of cost to hydrogen production. In 2012, the ratio for small-scale systems was about 1,333, whereas that for large-scale systems was about 433 [15]. Cost and capacity projections made by the Department of Energy are shown in Figure 1. There is little financial benefit to increasing system capacity above 30 tonnes per day, and a system of this size is estimated to cost $3 million per tonne per day capacity.

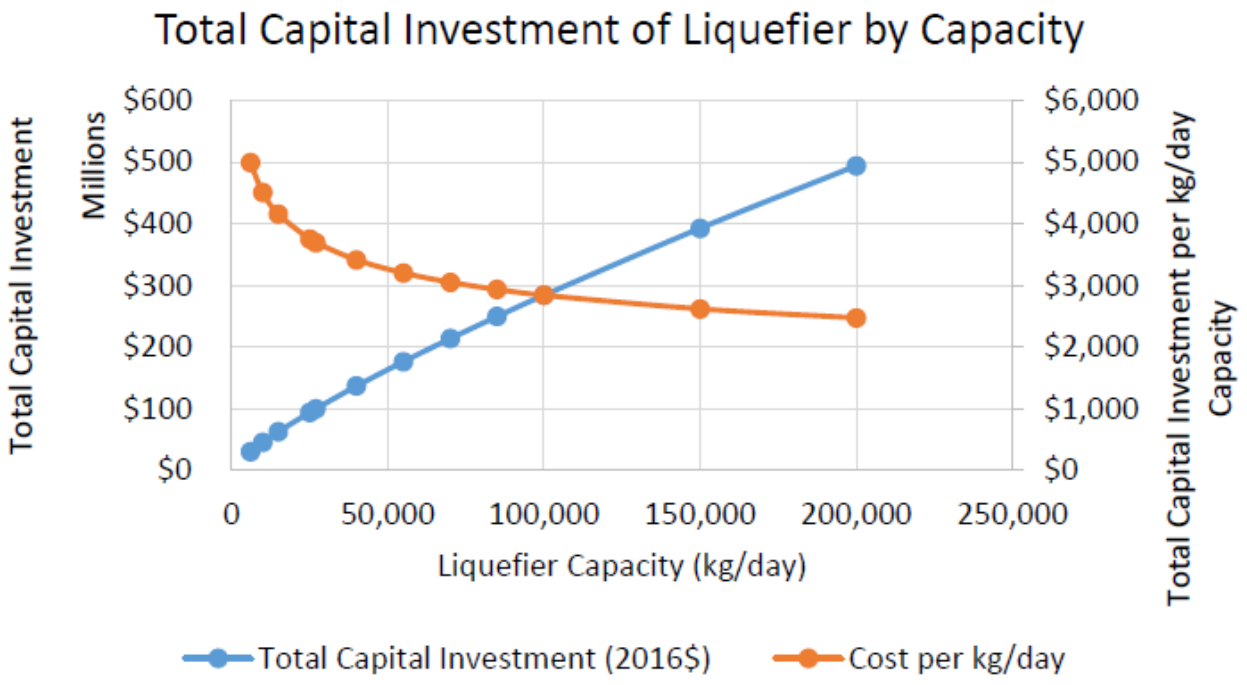

Figure 1: Cost versus hydrogen production capacity [16].

Although large-scale systems are currently more cost-effective, small-scale systems have more opportunity for future applications. They can be dispersed around the globe, eliminating the need to transport fuel from large liquification centers. For a city with an early hydrogen market and a liquefaction plant within 62 miles, the costs associated with hydrogen delivery is estimated at $5-$12 per kilogram. As the market matures, the cost is expected to drop to $2-$4 per kilogram [17]. If the liquefier is more than 62 miles away, as it is in most cases, the cost increases linearly. Liquid hydrogen delivery drivers are paid an estimated $40 per hour and the gas mileage of the trucks is estimated to be 6.5 miles per gallon. Every hour driven, assuming the driver maintains 60 miles per hour and gas costs $3 per gallon, increases the cost by about $70. The closest liquefier to Seattle, WA is in Ontario, CA. The drive between the two cities is almost 18 hours, resulting in an added round-trip cost of $2,520. Assuming a tanker holds 3,000 kg, the transport results in an added cost of $0.84. When combined with a local delivery cost of $0.68 per kilogram, the total cost associated with travel is $1.52 per kilogram [16]. Liquefying on site in a small-scale system would eliminate this cost. In addition to lowering overall costs, on site liquefaction would increase accessibility and usability for the consumer.

To make small-scale systems economically viable and increase accessibility, the system efficiency must be improved. The three lowest efficiency components in a liquefier are the heat exchanger, the cycle compressor, and the nitrogen refrigerator. Heat exchangers experience thermodynamic losses of almost 13%, based on calculated irreversibilities [18]. In this thesis, a novel, optimized design of a heat exchanger for a small-scale hydrogen liquefier is presented. Entropy generation within the system is minimized through utilization of a bifurcating flow structure and varying wall thickness. Results indicate a more efficient heat exchanger with a smaller form factor. Implementation of this design presents an opportunity to make small-scale

systems economically feasible, increase accessibility and viability of hydrogen as a fuel, as well as a method of advancing renewable energy.

CHAPTER TWO: BACKGROUND

A variety of heat exchanger configurations are used in industry, all of which consist of single tubes in different arrangements. The first heat exchanger for cryogenics was developed by Michael Faraday in 1885. Faraday was able to cool gases to 163 K using ether and solid carbon dioxide [19]. James Dewar was the first to liquefy hydrogen and did so on May 10, 1898 [20]. Since then, heat exchangers have been researched extensively and optimized for a multitude of scenarios. One of the most common designs are shell-and-tube heat exchangers. This style of heat exchanger, shown in Figure 2, can be counter flow, parallel, or cross flow, contain tube bundles or single tubes, and utilize fins.

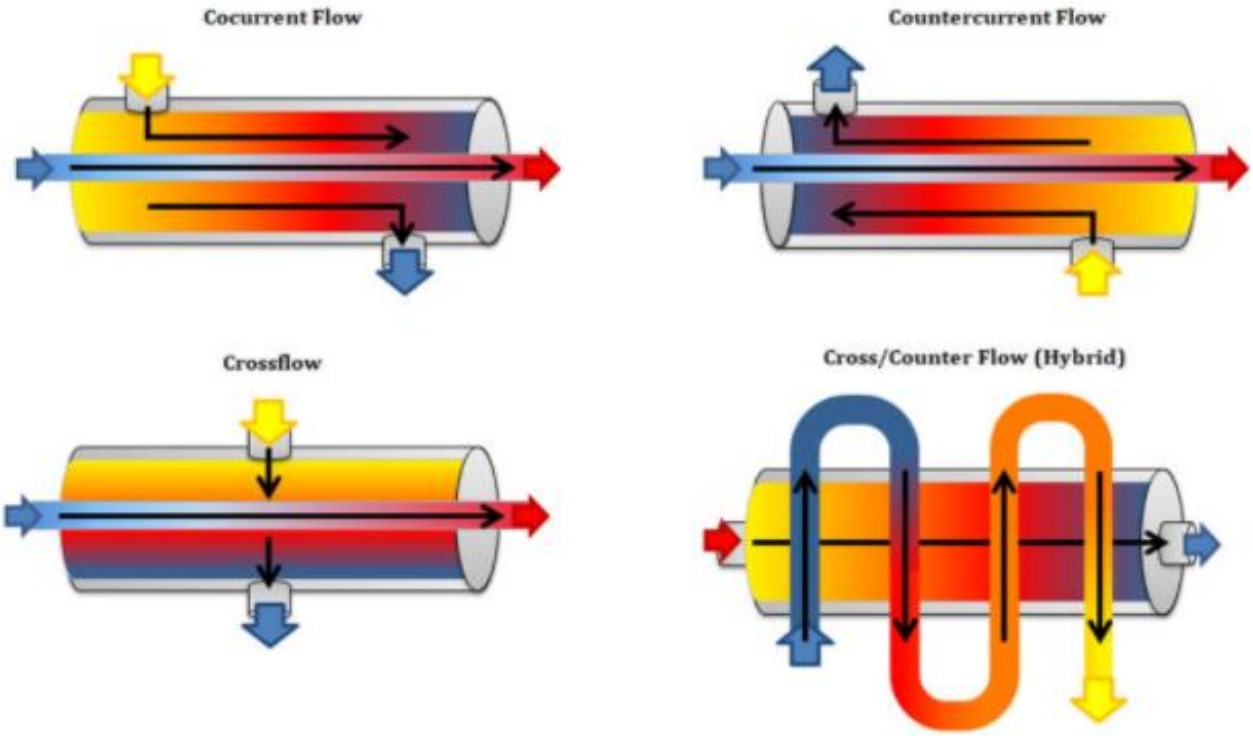

Figure 2: Common heat exchanger configurations [21].

In addition to manipulating the flow configuration, the cooling fluid can be modified to achieve a desired heat capacity, the flow rate of either fluid can be changed, and the overall geometry can vary. With so many design options, there is an optimum for each application which will maximize efficiency while achieving the desired temperatures. Heat exchangers are typically one of the greatest limiters for system efficiency. As such, heat exchanger optimization is critical for increasing overall efficiency. Historically, heat exchanger optimizations have focused on geometry, fins, and precooling. Hydrogen specific heat exchangers be further optimized by accounting for the ortho-para conversion of hydrogen.

In a heat exchanger, significant entropy is generated as a result of the pressure drop within the system and the temperature difference between the fluids, resulting in a low efficiency. Some of the ways to minimize the pressure drop include increasing tube diameter, selecting fluids with lower viscosities, or ensuring smooth surfaces. To minimize the temperature difference, heat transfer must be maximized. This can be done by increasing the surface-area-to-volume ratio, increasing the number of channels in the system, or modifying the inlet temperatures of the fluids. These general suggestions are outlined by Timmerhaus and Schoenhals [22]. These suggestions have been followed and applied to variety of heat exchanger types. Ordonez and Bejan and Lerou et al optimized counterflow heat exchangers. Their variables of interest include mass flow rates, inlet and outlet pressures, inlet and outlet temperatures, and channel geometry such as length and diameter [23, 24]. Ogulata and Doba optimized cross-flow heat exchangers, and focused more broadly on optimizing the heat transfer area, rather than specific geometries [25]. Guo et al optimized a shell-and-tube heat exchanger, focusing on baffle spacing, allowable pressure drops, and length-to-diameter ratios. Guo et al found that increasing heat exchanger effectiveness drastically decreases required pumping power

[26, 27]. Farzaneh-Gord et al optimized a helical heat exchanger and found an optimum diameter ratio between the inner tube and annulus [28]. Giaque optimized the coiled-tube heat exchanger, originally designed by Hampson for hydrogen liquefaction by increasing number of tubes in a shell-and tube heat exchanger and wrapping them around the central core. This yielded increased heat transfer and system efficiency, but the design was very expensive to manufacture and could not be cleaned mechanically [29]. All of the listed optimizations succeed in increasing system performance as suggested by Timmerhaus and Schoenhals but are not close to reaching the optimum Carnot efficiency and are generally only applicable to niche scenarios.

Fins have been introduced to heat exchangers to increase heat transfer by increasing surface area while maintaining the size of the system. This increases system efficiency by decreasing the temperature difference in the fluid streams. Fins can be a variety of shapes and sizes. Although they decrease the entropy generation related to temperature, they increase that from pressure. They also increase system complexity and difficulty of manufacturing. Optimizations have been performed to determine ideal fin spacings, diameters, and heights[30-34]. Pin-fins have been determined to be the optimal geometry for most scenarios, with heights, diameters, and spacing varying based on the fluid selection. Chart Industries has commercialized a plate fin heat exchanger for natural gas, air separation, and petrochemical processes which is considered industry leading [35]. The addition of fins increases the system efficiency, but it is still far from optimum.

Pre-cooling has been introduced as another way of increasing system efficiency. This allows for staged cooling. The primary advantage of this system is the decreased difference in temperature between the fluids and the resulting decrease in entropy generation. One fluid can be used to cool the system from point A to B, and a separate fluid can be used to cool the system

from point B to C. Not only does this decrease the temperature difference, it also allows for multiple fluids with different thermal properties to be used. This increases system efficiency but also drastically increases system complexity and size. Most models utilizing precooling are either highly theoretical or small-scale. Researchers such as Kanoglu et al, Krasae-in et al, Berstad et al are investigating novel methods of cooling to achieve unique thermal properties, rather than using the standard methods with nitrogen or helium [36-38]. Their systems are all small, laboratory scale. Quack and Cardella et al proposed configurations with precooling for large-scale hydrogen systems, estimating a system efficiency upwards of 60%, but as of yet have not been implemented in practice [39, 40]. The use of precooling represents a promising method of increasing heat exchanger efficiency, with an estimated increase from 20-30% of second law efficiency to 30-40% [40]. Unfortunately, the technology is not currently scalable for industry applications.

A simple, scalable way of increasing system efficiency that has been adopted by the hydrogen industry is applying catalyst to heat exchangers to aid in the ortho-para conversion. Hydrogen can exist as either orthohydrogen or parahydrogen, and at any temperature there exists an ideal ratio. Orthohydrogen resides at odd rotational energy levels and both nuclei spin in the same direction. Parahydrogen resides at even rotational energy levels and the nuclei spin in opposite directions. At room temperature, 293 K, hydrogen is about 75% orthohydrogen while at liquefaction temperatures, 20 K, hydrogen is over 99% parahydrogen. The room temperature concentration, 75% orthohydrogen, is referred to as normal hydrogen. The ideal ortho-para ratio at a given temperature is referred to as equilibrium hydrogen. The equilibrium orthohydrogen concentration as a function of temperature is shown in Figure 3. The concentration of orthohydrogen does not significantly decrease until the temperature decreases below 100 K.

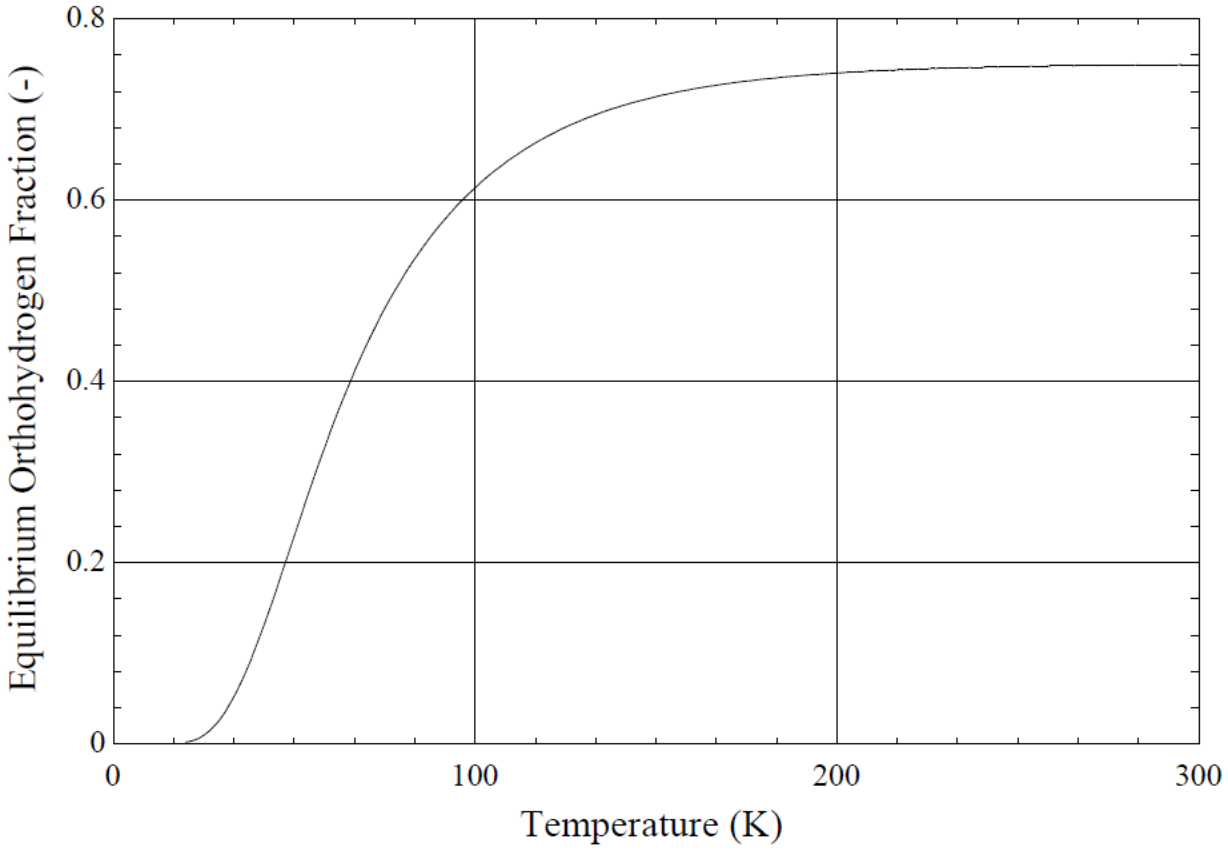

Figure 3: Equilibrium orthohydrogen concentration as a function of temperature [41].

The conversion of hydrogen from orthohydrogen to parahydrogen is an exothermic reaction, with an energy release of 702 kJ/kg, and the natural reaction rate is on the order of weeks. If hydrogen is cooled from room temperature to liquefaction without catalyst, the liquefied hydrogen will be normal hydrogen, and the natural conversion to parahydrogen will result in boil off of the liquefied product of up to 2% per day [42]. Using catalyst allows the heat of conversion to be removed from the system during active liquefaction, which does not negatively affect the final product. A more complete discussion on ortho-para hydrogen and the accompanying conversion can be found elsewhere [43-46]. In this thesis hydrogen is always

assumed to be equilibrium, and in the experiment, catalyst is added to the system to validate this assumption. This represents another method of increasing system efficiency. The efficiency losses in the system are due to entropy generation, with less optimized systems generating more entropy.

One of the most effective forms of system optimization for fluids is branching. This is exemplified by the Hess-Murray rule. The Hess-Murray rule was derived as a result of cardiovascular research in the 1920s when Hess and Murray noticed a trend in the diameters and lengths of parent and daughter vessels. The rule can be derived by doing an energy balance on the cardiovascular system, with the goal of minimizing energy input required to synthesize, maintain, and pump blood, as well as a multitude of other parameters [47]. With this concept, there is an optimal length and diameter for a system that minimizes entropy generation with the given system parameters. Once the minimum is reached, the system is allowed to bifurcate and search for a new minimum with a new geometry. The Hess-Murray rule indicates that this minimum is reached by using length and diameter ratios of $2^{1/3}$. This rule is not valid for systems larger than human veins and capillaries which are similar in fluid properties to water. Nor is it valid for turbulent or external flows. However, the pattern can be observed in nature in larger structures such as tributaries and tree branches that also flow viscous fluids similar to water. The design represents a system with the minimum entropy generation, and therefore the maximum achievable efficiency.

Adrian Bejan has published many papers on the concept of branching and wrote an entire chapter on it in his book on thermodynamics [48]. Example problems within his text refer to physical systems, and his papers detail theoretical structures such as fluid flow within a finite volume [49]. However, all of Bejan's proposals are theoretical, and outside of a few example

problems in his textbook, not strongly linked to real world applications. Despite focusing on fluid flow problems, Bejan has not proposed an optimized heat exchanger utilizing branching principles. This is likely because until recent advances in additive manufacturing, it was not possible to create a branching structure in line with this theory. In this thesis a heat exchanger is optimized for small-scale hydrogen liquefaction and constructed using additive manufacturing. The use of new manufacturing techniques allows for the design of a branching heat exchanger, suggested by the Hess-Murray rule to be an optimum, as well as the implementation of more well-known design principles. The method of manufacture also lowers the production cost and makes the design easily optimizable for a multitude of systems. Theoretical calculations suggest an increase in system performance of about 23% over a single tube heat exchanger for the same application.

CHAPTER THREE: THEORY

This chapter begins with an entropy analysis of a tube without a wall. This is used to determine what factors significantly impact entropy generation in a flow scenario. An optimal geometry of a branching flow structure is then determined for a tube without a wall for two scenarios – an isothermal condition and a linear temperature gradient. Next, a wall is added, and a heat transfer problem for a real scenario is established. Resistances, pressure drops, and boundary conditions are assessed. Energy and entropy balances are conducted and implemented using numerical integration to predict temperature and pressure profiles. Finally, the effect of varying wall thickness is evaluated.

3.1 Entropy Optimization of a Tube

Entropy minimization increases system efficiency. Entropy is generated whenever energy flows through a gradient. Within a tube, entropy is generated as a result of pressure and temperature gradients. The gradients are affected by a variety of parameters including the surface temperature and the cross-sectional area.

3.1.1 Entropy Balance on a Tube

The general equation for an entropy balance is shown in Equation 1.

$$\dot{S}_i + \dot{S}_{gen} = \dot{S}_o + \frac{dS}{dt} \tag{1}$$

Where an i subscript denotes a quantity entering the system, an o subscript denotes a quantity leaving the system, $\dot{S}$ is an entropy rate, $\dot{S}_{gen}$ is the rate of entropy generation within the system, and $\frac{dS}{dt}$ is the change in entropy as a function of time. Figure 4 shows the system being analyzed – a tube without a wall.

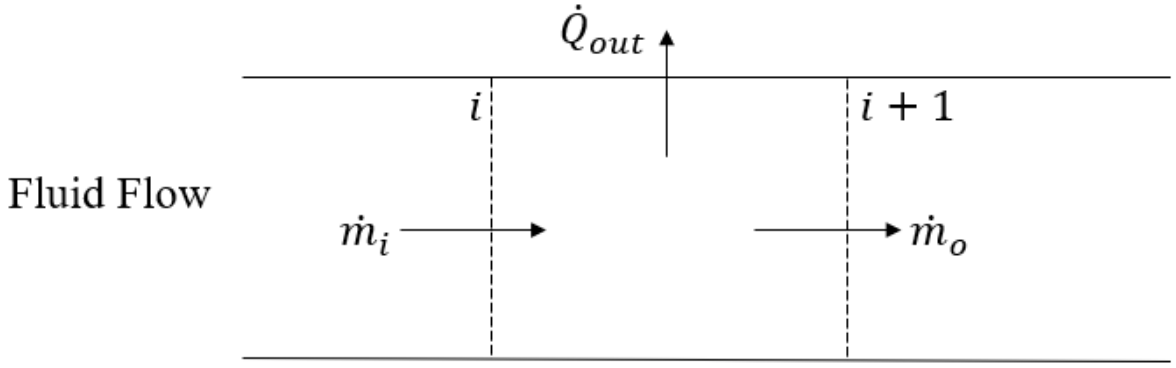

Figure 4: System diagram of a tube, without a wall, containing a flowing fluid.

In this scenario, entropy is generated through mass flow and heat transfer. Mass flow generates a pressure drop due to the fluid viscosity which leads to a lower pressure state with higher entropy. Heat transfer occurs because the fluid and the surface are not at the same temperature. The heat transfer is not reversible; therefore, some heat is lost, and entropy is generated as a result. For pure fluids entropy can cross a system boundary only with mass or heat. Assuming a steady state, open system and expanding the terms in Equation 1 leads to Equation 2.

$$\dot{m}_i s_i + \frac{\dot{Q}_{in}}{T_o} + \dot{S}_{gen} = \dot{m}_o s_o + \frac{\dot{Q}_{out}}{T_o} \tag{2}$$

Where $\dot{m}$ is the mass flow rate, s is entropy at the point, $\dot{Q}$ is rate of heat transfer, and T_o is the reference temperature. Assuming the only mode of heat transfer is internal convection and solving for $\dot{S}_{gen}$ results in Equation 3.

$$\dot{S}_{gen} = \dot{m}(s_o - s_i) + \frac{\dot{Q}_{out}}{T_s} \quad \text{where } \dot{m}_i = \dot{m}_o = \dot{m} \tag{3}$$

Where T_s is the surface temperature. The rate of entropy generation in the system is used to evaluate the efficiency of the system.

3.1.2 Relationships Between System Properties and Entropy Generation

To determine how changes in system properties affect entropy generation one property must be varied while holding the others constant. The property values in Table 1 are assigned unless the variable is being manipulated.

Table 1: Fixed property values within the simulation.

Property	Value
Length	4.5 m
Mass Flow Rate	0.093 g/s
Inner Diameter	0.01 m
Surface Temperature	20 K
Inlet Pressure	758.42 kPa
Surface Roughness	0.01

The pipe flow correlation detailed by Nellis and Klein is used to determine the pressure drop and coefficient of heat transfer for internal convection [50]. All physical property data is determined using the equation of state developed by Leachman et al and correlations for viscosity and thermal conductivity developed by Muzny et al and Assael et al [51-53]. All functions are used as implemented in the 64-bit professional version of EES [54].

Assuming the tube has an isothermal surface temperature, varying that temperature changes the rate of entropy generation within the system. Above 50 K the surface temperature has minimal effect on entropy generation. This is shown in Figure 5 for 0.003175 m to 0.0127 m tube diameters. Decreasing the tube diameter increases the entropy generation.

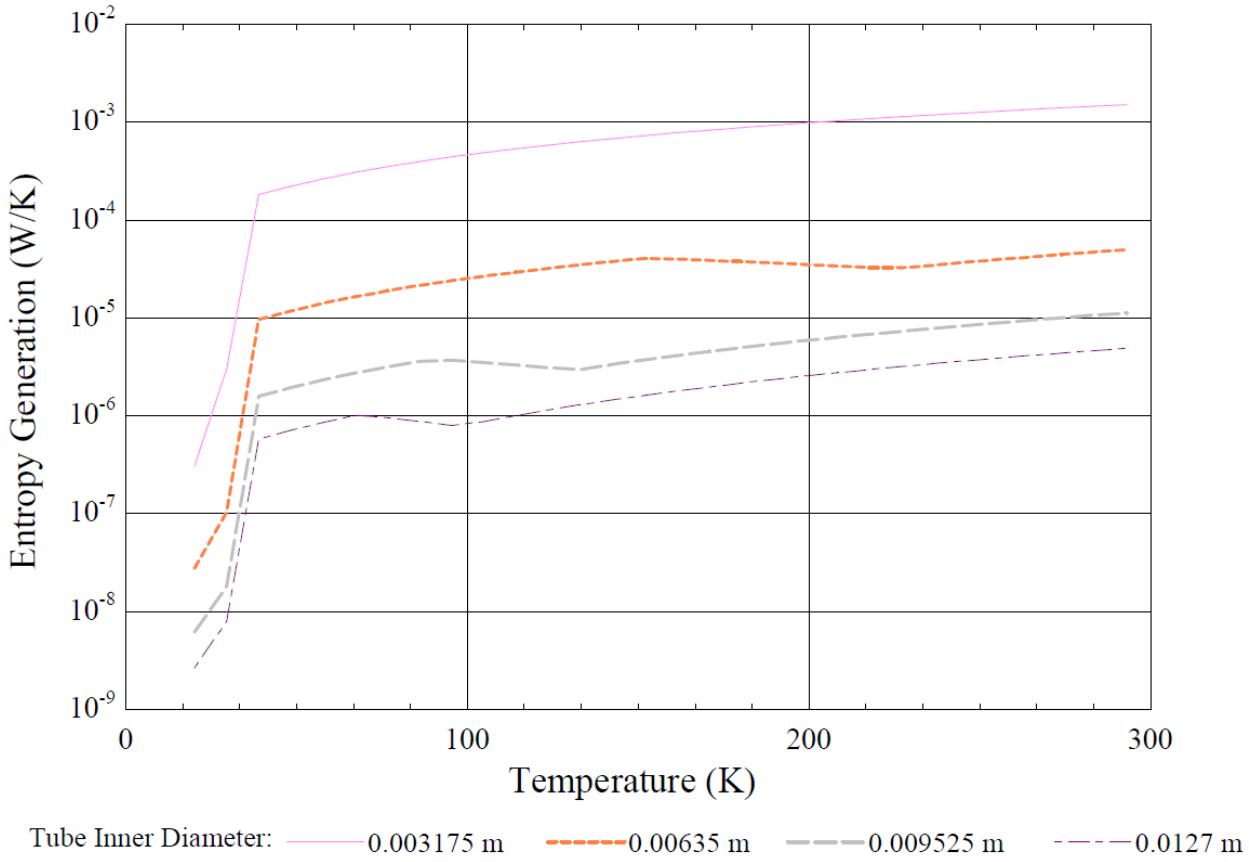

Figure 5: Entropy generation versus isothermal surface temperature for various tube diameters assuming a length of 4.5 m, a mass flow rate of 0.093 g/s, and a relative roughness of 0.01.

The effect of varying the surface roughness on entropy generation is shown in Figure 6. Varying the roughness does not impact the rate of entropy generation. The rate of entropy generation increases with decreasing tube diameter.

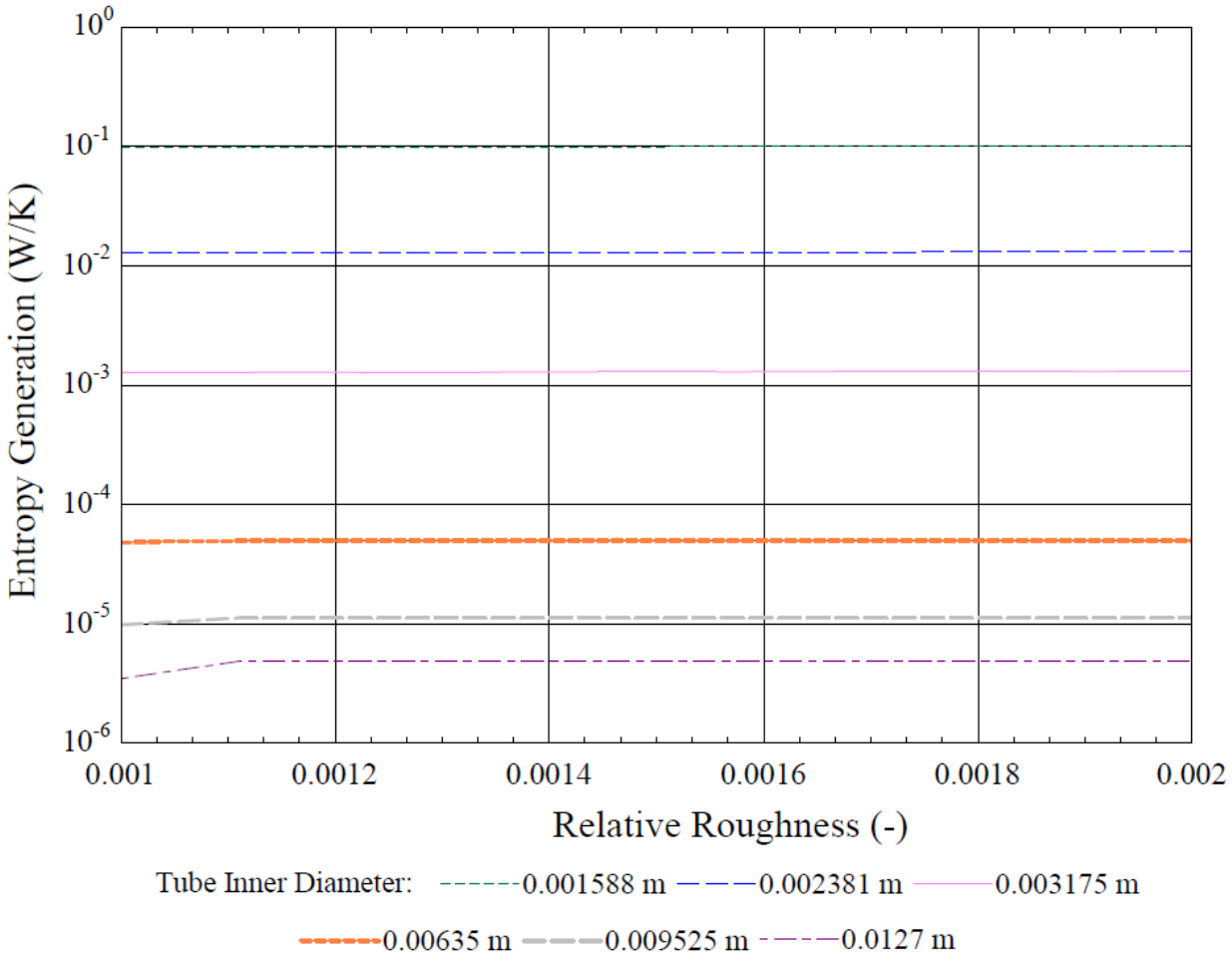

Figure 6: Entropy generation versus relative roughness for a variety of tube diameters assuming a length of 4.5 m, an isothermal surface temperature of 293 K, and a mass flow rate of 0.093 g/s.

The effect of varying the tube length on entropy generation and pressure drop are shown in

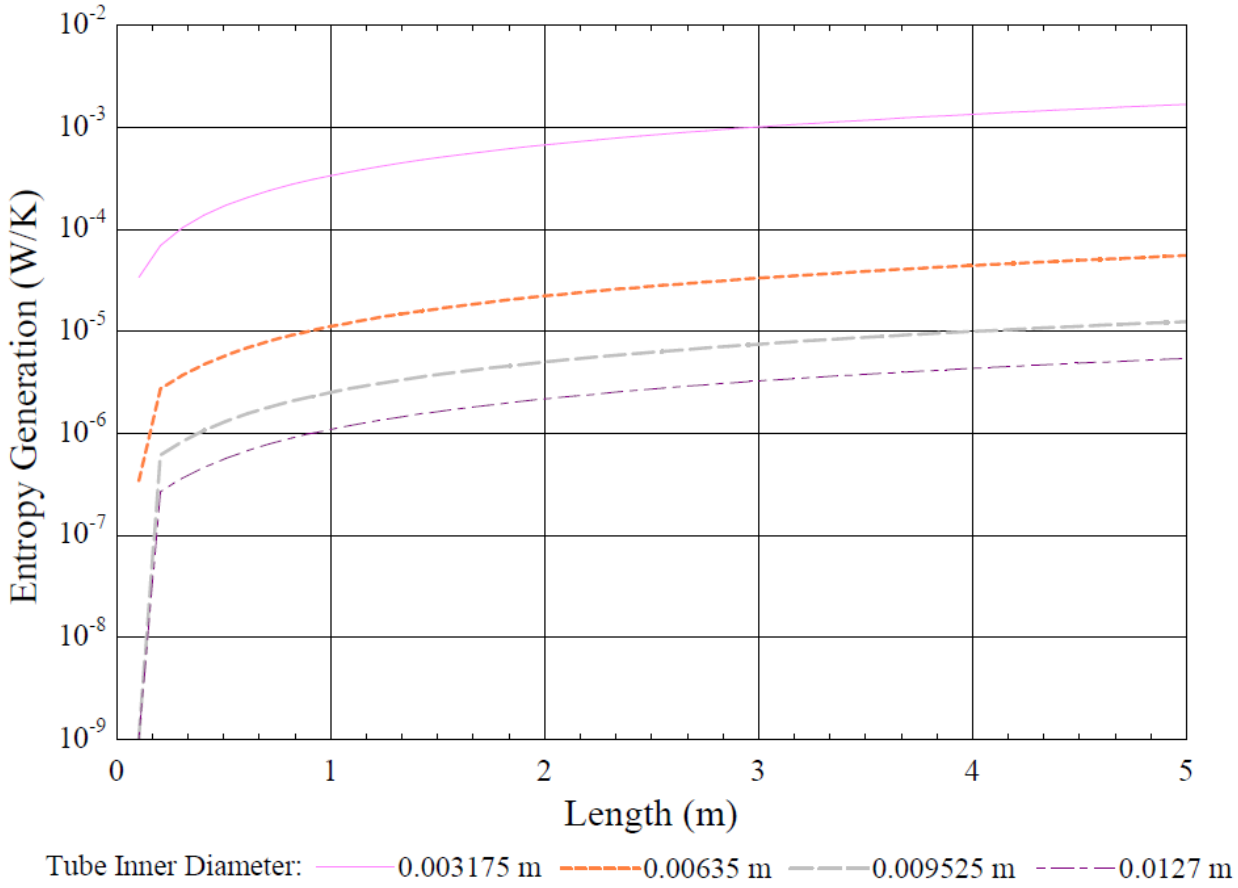

Figure 7 and Figure 8. Increasing the tube length causes minimal increases in entropy generation in tubes with inner diameters greater than 0.003175 m. In a 0.003175 m inner diameter tube increasing length causes a linear increase in entropy generation. Increasing tube length does not affect the pressure drop. However, the pressure drop increases significantly in tubes with inner diameters 0.003175 m or smaller.

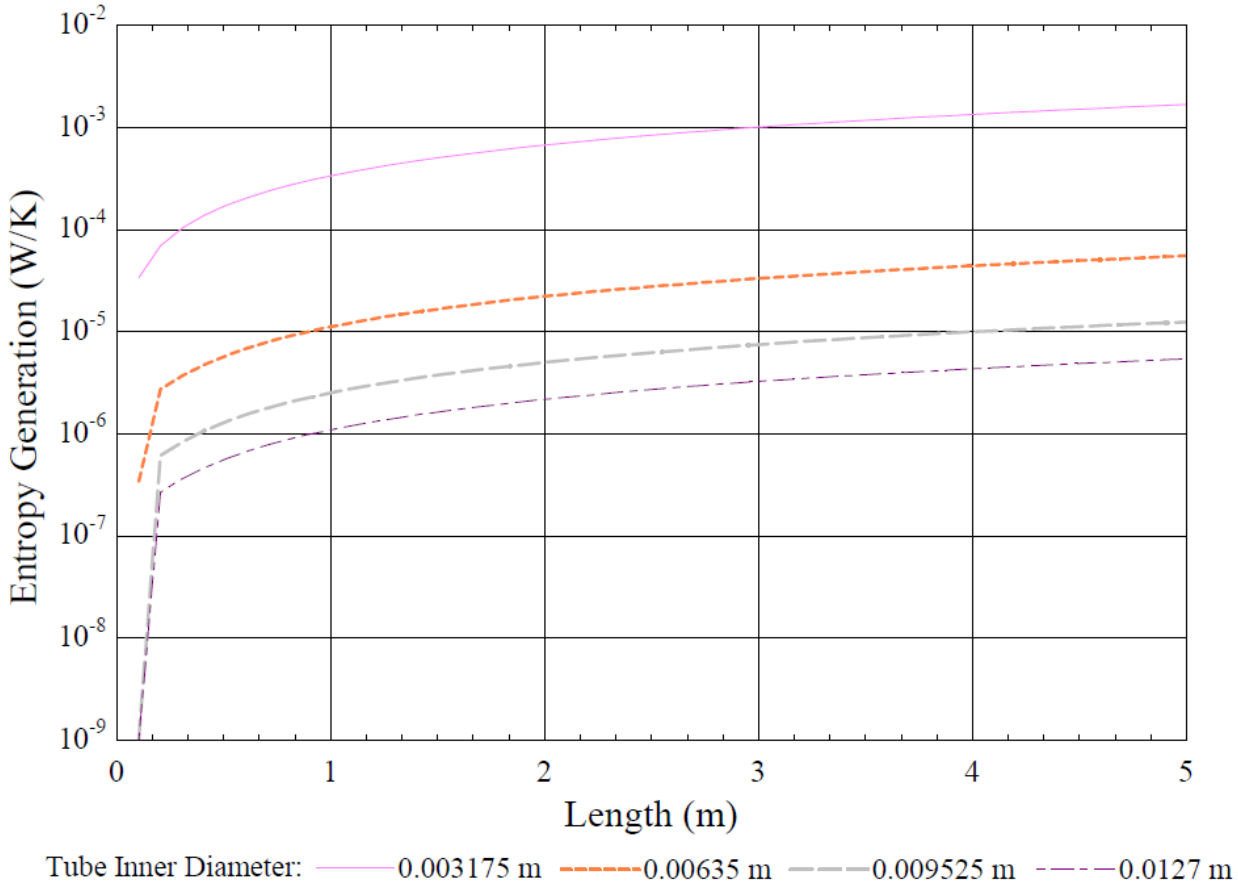

Figure 7: Entropy generation versus length for a variety of tube diameters assuming an isothermal surface temperature of 293 K, a relative roughness of 0.01, and a mass flow rate of 0.093 g/s.

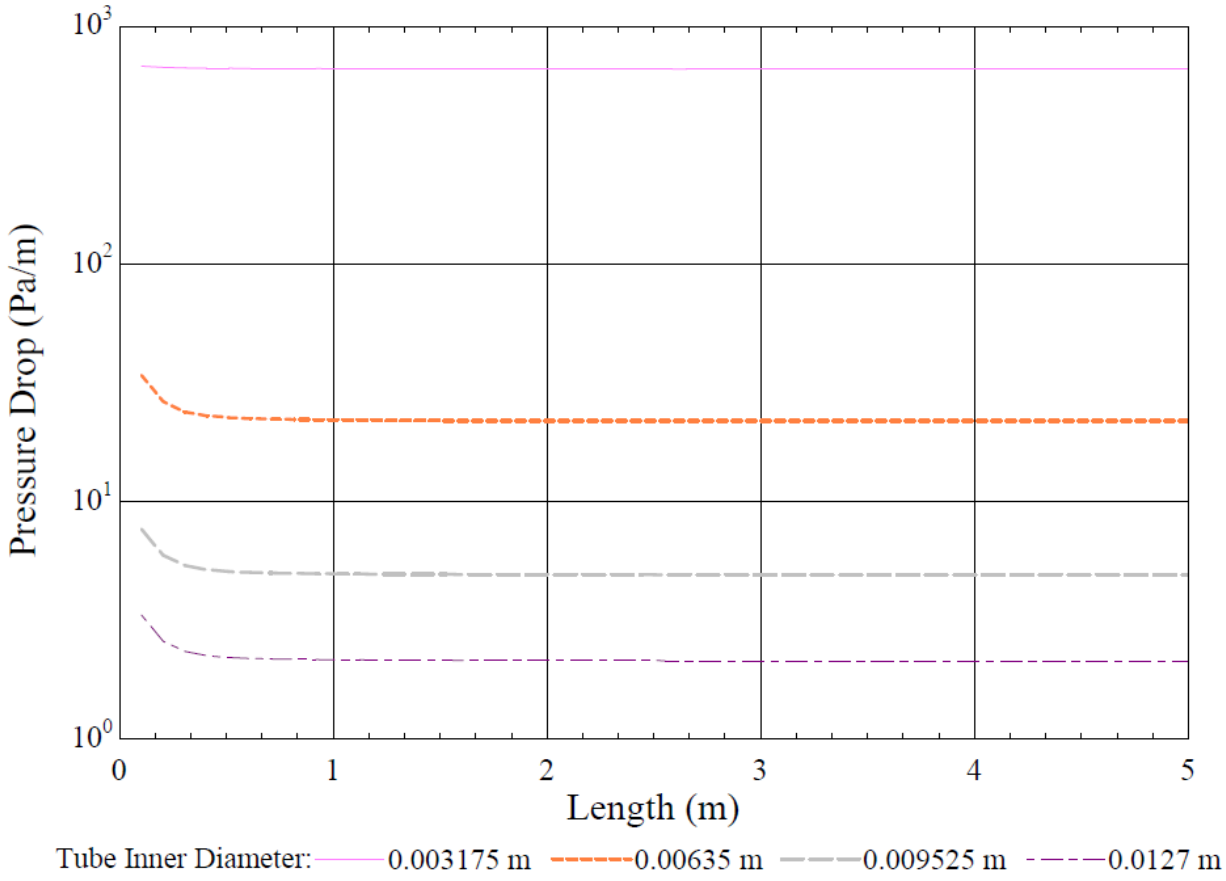

Figure 8: Pressure drop versus length for a variety of tube diameters assuming an isothermal surface temperature of 293 K, a relative roughness of 0.01, and a mass flow rate of 0.093 g/s.

The effect of varying mass flow rate on entropy generation and pressure drop is shown in Figure 9 and Figure 10. Increasing mass flow rate does not cause significant changes in entropy generation in tubes with inner diameters greater than or equal to 0.003175 m. In tubes with inner diameters smaller than 0.003175 m increasing mass flow rate causes an exponential increase in entropy generation. The same relationships between mass flow rate and entropy generation exist between mass flow rate and pressure drop. In tubes with inner diameters greater than or equal to 0.003175 m the pressure drop is minimally affected by increasing the mass flow rate. In tubes

with an inner diameter smaller than 0.003175 m the pressure drop increases exponentially as mass flow rate increases.

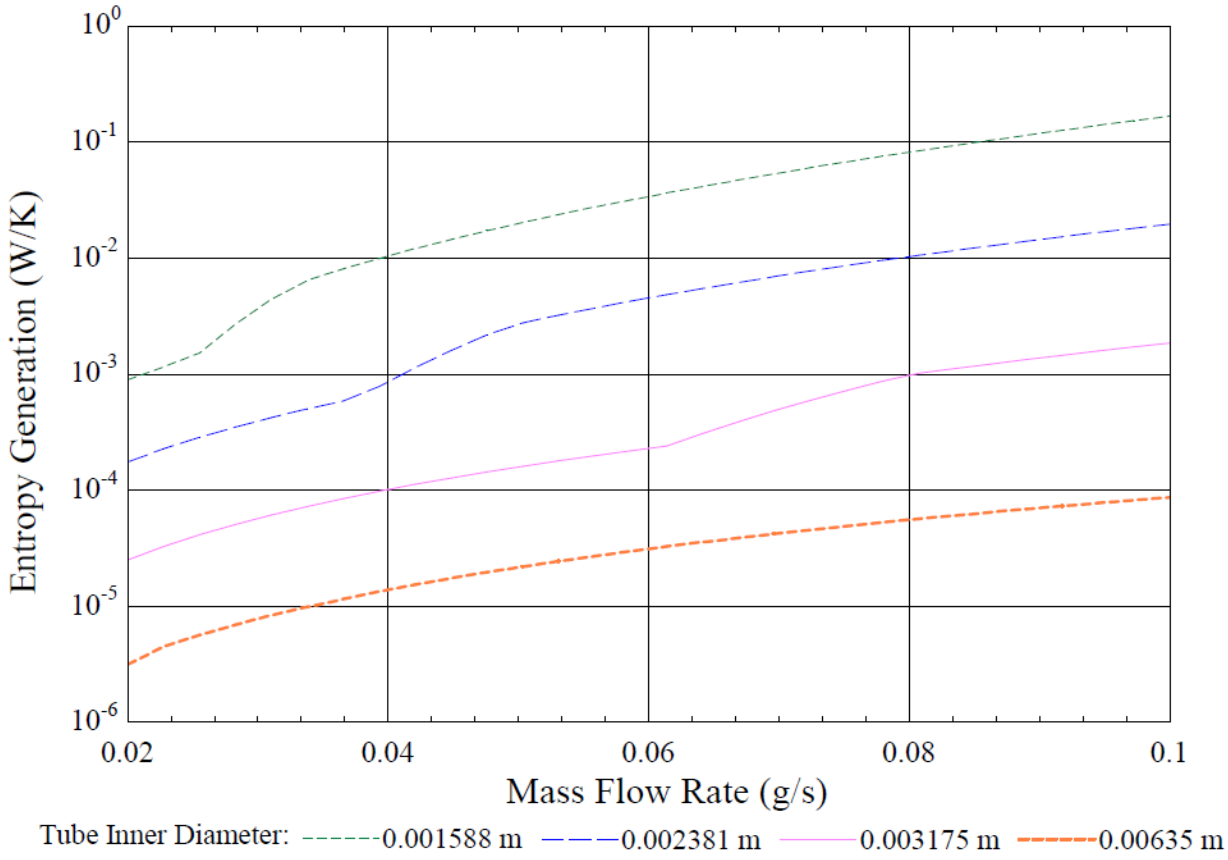

Figure 9: Entropy generation versus mass flow rate for a variety of tube diameters assuming an isothermal surface temperature of 293 K, a relative roughness of 0.01, and a length of 4.5 m.

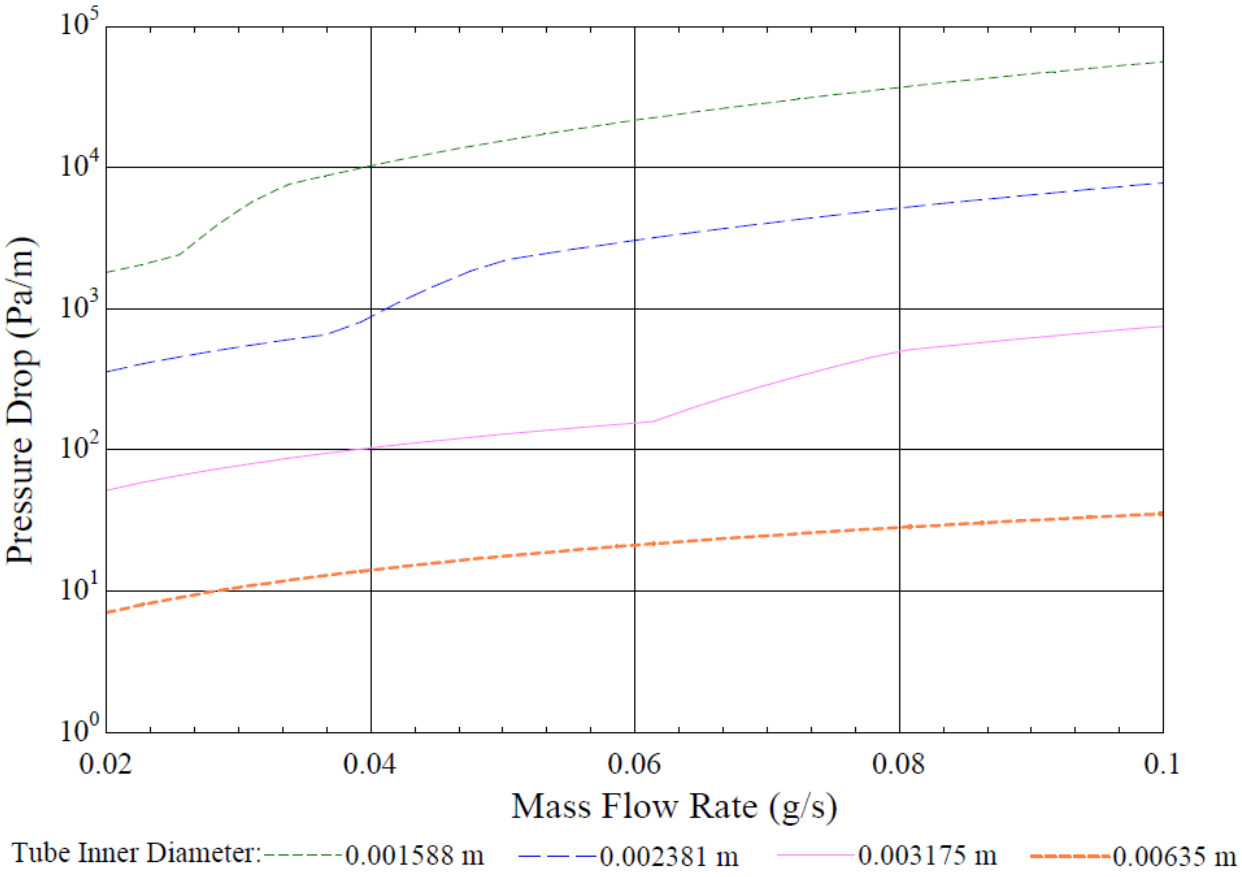

Figure 10: Pressure drop versus mass flow rate for varying tube diameters assuming an isothermal surface temperature of 293 K, a relative roughness of 0.01, and a length of 4.5 m.

In Figure 5–Figure 10 the only mode of heat transfer is internal convection. In Figure 11, 10 W is removed from the system in addition to the heat loss from natural convection. The entropy generated in Figure 11 is less than that in Figure 9, likely due to smaller temperature gradients. The trends do not change.

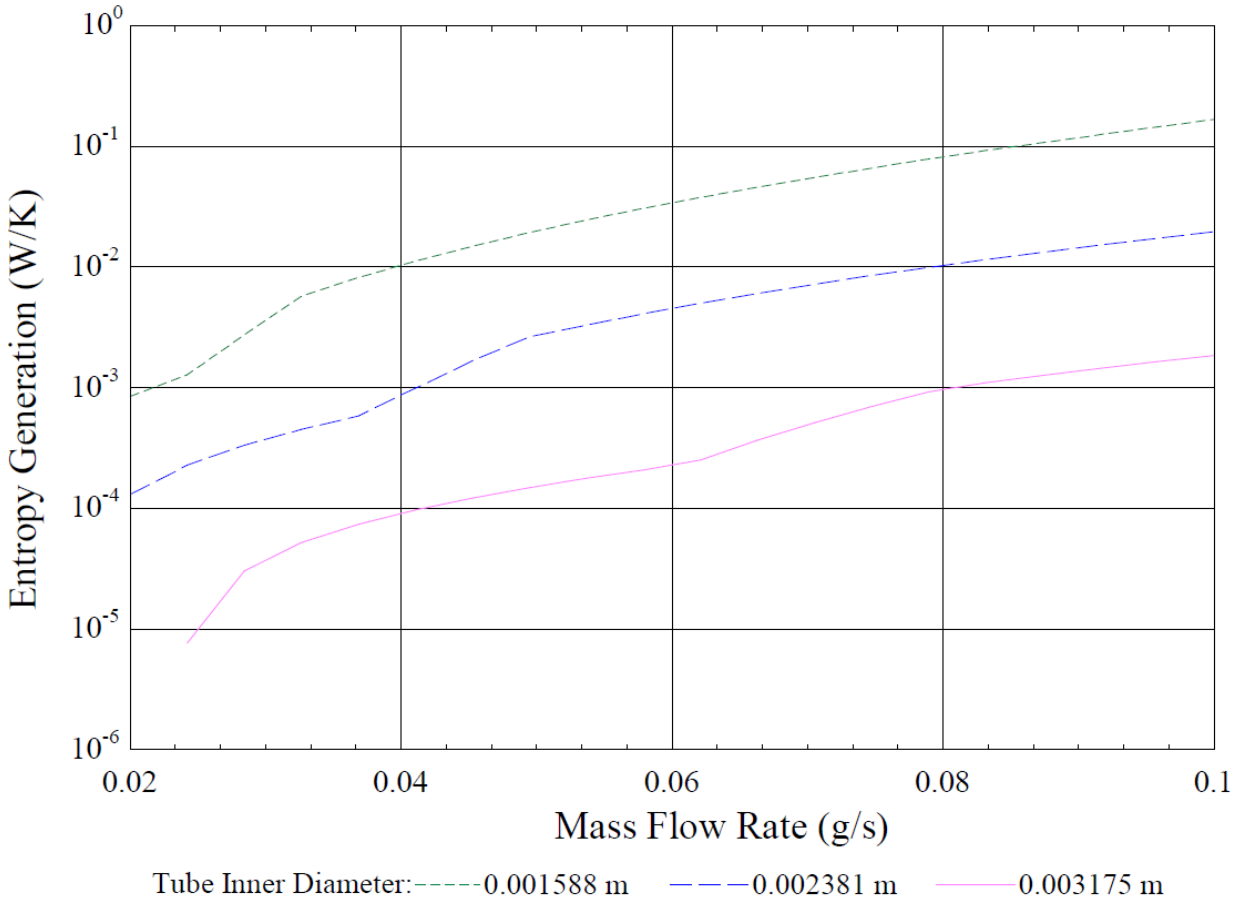

Figure 11: Entropy generation versus mass flow rate for a variety of tube diameters assuming an isothermal surface temperature of 293 K, a relative roughness of 0.01, a length of 4.5 m, and an additional heat removal of 10 W.

In summary, tube roughness does not affect entropy generation, isothermal surface temperatures have no effect above 50 K, changing tube length does not affect entropy generation as long as the inner diameter is greater than 0.003175 m, changing the mass flow rate has minimal effect as long as the inner diameter is greater than 0.001588 m, and forcibly removing heat has no effect. Also, with the given system parameters, changing tube length does not affect the pressure drop and changing the mass flow rate has minimal effect as long as the inner diameter is greater than

0.001588 m. Notable changes in entropy generation and pressure drop occur only when the inner diameter is 0.003175 m or smaller.

3.1.3 Entropy Generation from Temperature and Pressure Differentials

In a tube, the two modes of entropy generation are a function of heat transfer and the pressure drop. Figure 12 depicts an entropy versus temperature graph for flow in a tube. The initial state is point 1, the ideal final state is point 2', and the actual final state is point 2. Along a single isothermal tube at temperature T_s, entropy generated from heat transfer is due to the difference between the outlet temperature and the surface temperature. In Figure 12, this is the difference between points 2' and 2. The entropy generation from the pressure drop is due to the difference between P_{in} and P_{out}. In an ideal scenario, the inlet pressure would be constant throughout the tube and the outlet temperature would equal the surface temperature. The entropy generation represents inefficiencies that require larger work inputs to achieve the ideal output.

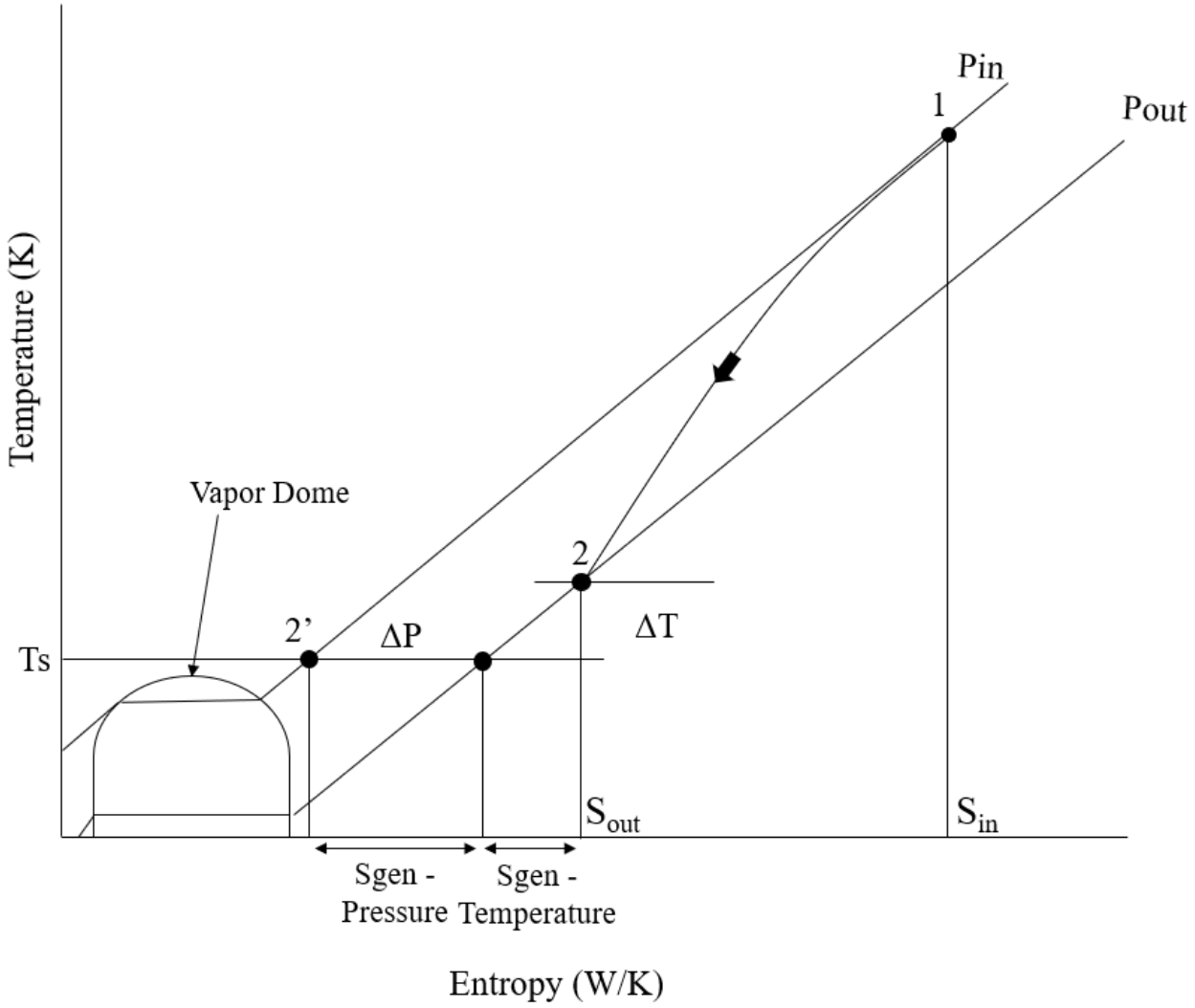

Figure 12: Entropy versus temperature diagram for cooling flow in a pipe.

The goal is to minimize temperature and pressure gradients to reach an ideal state with minimal entropy generation. To solve for the entropy generation from pressure and heat transfer the following relation shown in Equation 4 is used. The relation is a combination of the first and second laws of thermodynamics.

$$dh = Tds + vdP \tag{4}$$

Where dh is a change in enthalpy, T is a set temperature, ds is a change in entropy, v is a specific volume and dP is a change in pressure. Solving Equation 4 for ds yields Equation 5.

$$ds = \frac{dh}{T} - vdP \tag{5}$$

dh can be expressed using Equation 6 assuming small changes in temperature where the heat capacity is essentially constant. Subbing Equation 6 into Equation 5 yields Equation 7.

$$dh = C_p dT \tag{6}$$

$$ds = \frac{dT}{T} C_p - \frac{v}{T} dP \tag{7}$$

Where C_p is the heat capacity at constant pressure. Next the ideal gas equation, shown in Equation 8, is solved for v/T.

$$Pv = RT \tag{8}$$

Where R is the ideal gas constant. Although Equation 8 is not valid during liquefaction, the compressibility factor for hydrogen is greater than 0.9 above 40 K, therefore the equation is valid for most of the applicable temperature range. Subbing Equation 8 into Equation 7 yields Equation 9.

$$ds = \frac{dT}{T} C_p - \frac{dP}{P} R \tag{9}$$

Equation 9 can be broken into two parts to individually express entropy generation from pressure drop and heat transfer. In Equation 9 dT is the difference in temperature between the outlet and the surface, T is the surface temperature, dP is the difference in the inlet and outlet pressure, and P is the inlet pressure. Equation 9 must be multiplied by the mass flow rate to determine the rate of entropy generation, as opposed to the change in entropy. Subbing in the expressions for pressure and temperature, multiplying by mass flow rate, and breaking apart Equation 9 yields Equation 10 for entropy from heat transfer, and Equation 11 for entropy from pressure drop.

$$\dot{S}_{gen_{HT}} = \dot{m}\, C_p \frac{T_{out} - T_s}{T_s} \tag{10}$$

$$\dot{S}_{gen_P} = \dot{m}\, R \frac{P_{in} - P_{out}}{P_{in}} \tag{11}$$

where P_{in} is the inlet pressure, and P_{out} is the outlet pressure, T_{out} is the outlet temperature, and T_s is the surface temperature. The entropy generation from heat transfer decreases with increasing tube length, whereas that from pressure increases. Summing the two modes of entropy generation yields a minimum point. An example of this is shown in Figure 13 for a tube with a 0.0127 m inner diameter, a surface temperature of 200 K, and a mass flow rate of 0.093 g/s, and a packed bed. The minimum entropy generation occurs at a length of about 13 cm. Flow through a packed catalyst bed is assumed to make the entropy generation from pressure drop similar in magnitude to that from heat transfer.

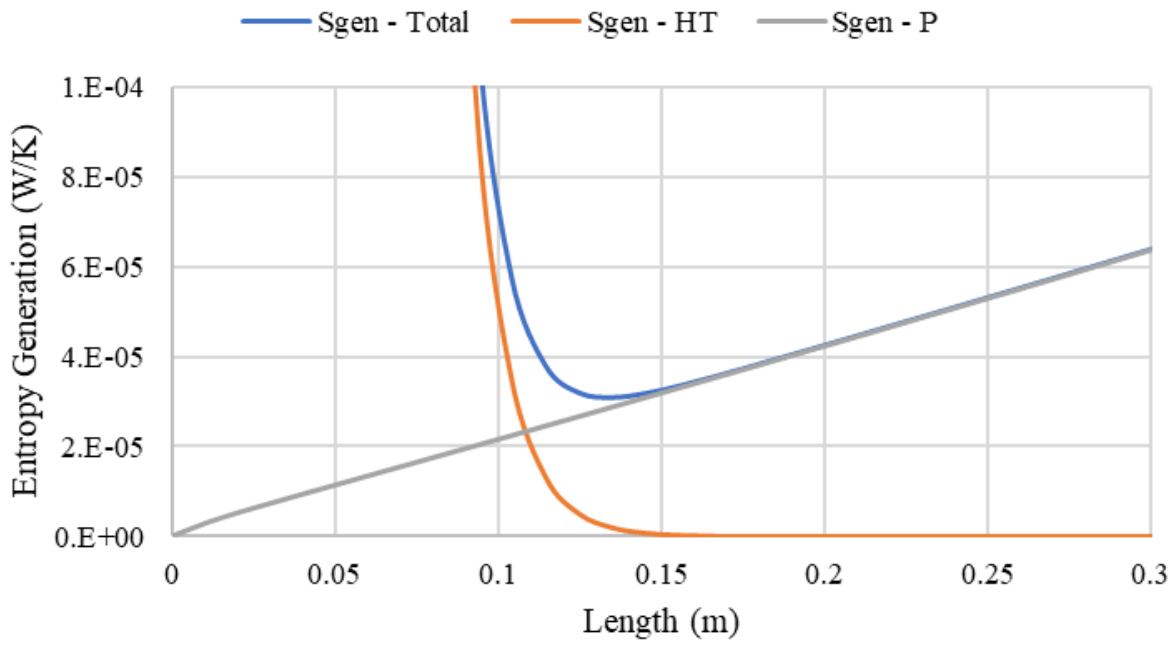

Figure 13: Entropy generation versus length with multiple modes of entropy generation.

If the length is increased beyond the optimum the total entropy generation increases. In this scenario the outlet temperature decreases, as well as the outlet pressure. Once the outlet temperature reaches the surface temperature, which occurs in Figure 13 around 15 cm, the entropy generation from heat transfer approaches zero. The entropy generation from pressure continues to increase linearly. If the length is decreased below the optimum the total entropy generation again increases. The outlet temperature moves further away from the surface temperature, causing entropy generation from heat transfer to increase. Entropy generation from pressure decreases, with the outlet pressure moving closer to the inlet.

3.2 Theoretical Model of a Heat Exchanger without Wall

A theoretical model is created in Engineering Equation Solver (EES) to simulate a heat exchanger without a wall. The heat exchanger is assumed to have a single inlet and bifurcate into branches each layer. The bifurcation aids in entropy minimization. The mass flow rate is assumed to divide evenly between the new branches. The branching segments are referred to as layers, with the single inlet tube being layer one, the two tubes resulting from the first bifurcation as layer two, and so on. The hydrogen is assumed to be equilibrium at all temperatures.

Gifford-McMahon cryocoolers are traditionally used in liquefiers to assist in the cooling of gases. In this model, a Sumitomo RDK-415D Gifford-McMahon cryocooler, shown in Figure 14, is referenced to bound the total length of the heat exchanger.

Figure 14: Sumitomo RDK-415D Gifford-McMahon cryocooler [55].

The heat exchanger fits over the Gifford-McMahon cryocooler like a sleeve, mounting to the upper and lower stages. The upper portion of the heat exchanger resides between the top plate and the upper stage. The lower portion of the heat exchanger resides between the upper and lower stages. Each portion of the heat exchanger has a different branching structure, with the lower portion dependent on the upper. The total lengths of the upper and lower sections, determined by measuring the Gifford-McMahon cryocooler, are 14.2 cm and 23.9 cm. For modeling purposes, only the upper portion of the heat exchanger is considered. The fixed system parameters are shown in Table 2.

Table 2: Fixed simulation parameters for a tube without a wall.

	Value
Surface Roughness	0.01
Total Mass Flow Rate	0.012 g/s
Inlet Pressure	652.93 kPa
Total Length	14.2 cm
Inlet Temperature	293 K
Inlet Pressure	648.11 kPa

The number of layers are varied from one to five, allowing diameters and lengths between layers to vary, while keeping all tubes within a layer consistent. The implementation can be seen in Appendices 7.2-7.7. The variable metric method minimization function in EES is used to determine the heat exchanger geometry that results in the minimum entropy generation. This minimization function operates by creating a matrix that characterizes the function within given bounds of select variables. The minimum value of the variable of interest is then determined. The possible diameters are bounded from 0.0001 – 0.009525 m, and the possible lengths are bounded from 0.001 m to the total. The variable of interest is the total entropy generation.

There are two scenarios to consider depending on the axial conduction parameter, which is calculated using Equation 12.

$$\lambda = \frac{1}{\frac{L}{k_{avg}\frac{\pi}{4}\left(OD^2 - ID^2\right)}\dot{m}\, c_{min}} \tag{12}$$

Where λ is the axial conduction parameter, L is the total length, and c_{min} is the minimum heat capacity of the tube. The axial conduction parameter is an expression of the ratio of heat transfer due to axial conduction versus the heat transfer that would occur without axial conduction. If this parameter is low, it indicates that the temperature profile is linear, and if it is high, it indicates that the temperature profile is a constant, or the wall is isothermal. A system with a low axial

conduction parameter has a higher efficiency than a system with a higher value because the temperature gradients are much smaller. Section 3.2.2. considers the isothermal scenario, and Section 3.2.3. considers the linear gradient scenario.

3.2.1 Temperature Profile of a Tube Without a Wall

The temperature profile along the fluid stream shown in Figure 4 is determined using thermophysical property data. First, the resistance to internal convection is determined using Equation 13.

$$R_{conv_{inner}} = \frac{1}{h_{conv}A_s} \tag{13}$$

Where $R_{conv_{inner}}$ is the resistance from internal convection, h_{conv} is the coefficient of heat transfer, and A_s is the internal surface area. Next, the heat transfer out of the stream is calculated using Equation 14.

$$\dot{Q} = \frac{T_{avg} - T_s}{R_{conv_{inner}}} \tag{14}$$

Where $\dot{Q}$ is the heat transferred out of the fluid stream, T_{avg} is the average temperature in the stream node, and T_s is the surface temperature. T_{avg} is calculated using Equation 15.

$$T_{avg} = \frac{T_i + T_{i+1}}{2} \tag{15}$$

Where T_i is the temperature at the beginning of the section and T_{i+1} is the temperature at the end. Equations 14 and 15 are solved simultaneously with Equations 16 and 17.

$$\dot{Q} = \dot{m}\Delta h \tag{16}$$

$$h_{i+1} = h_i - \Delta h \tag{17}$$

Where $\dot{m}$ is the mass flow rate, Δh is the change in enthalpy over the section, h_i is the enthalpy at the beginning of the section, and h_{i+1} is the enthalpy at the end of the section. There is only one value for T_{i+1} that satisfies all four equations when solved simultaneously. This is the solution

that Engineering Equation Solver is able to implicitly determine. Solving all four equations repeatedly results in the complete temperature profile.

3.2.2 Isothermal Scenario

It is assumed that all tubes have a high axial conduction parameter, such that each tube is isothermal. To determine the temperature of the tubes in each layer, a linear function from 293 – 25 K is imposed along the entire length. This function is used to determine the temperature at the end of each layer. That temperature is then superimposed along the length of the entire layer. For example, if the entire system is 10 cm long, and the first layer is 1 cm, the end of the first layer corresponds to a temperature of 266.2 K. The entire first layer is assumed to be isothermal at 266.2 K.

The total entropy generation of the system decreases with increasing layers as shown in Figure 15. The pressure contribution to the total entropy is on the order of 10^{-10}. Therefore, only the temperature contribution is significant. The maximum value of entropy generation with one layer is 79.49 W/K, and the minimum value with four layers is 23.81 W/K. The percent difference between the two extremes is 107.80%. The model could not be run with five layers because the outlet temperature was below saturation. The raw data is shown in Table 3.

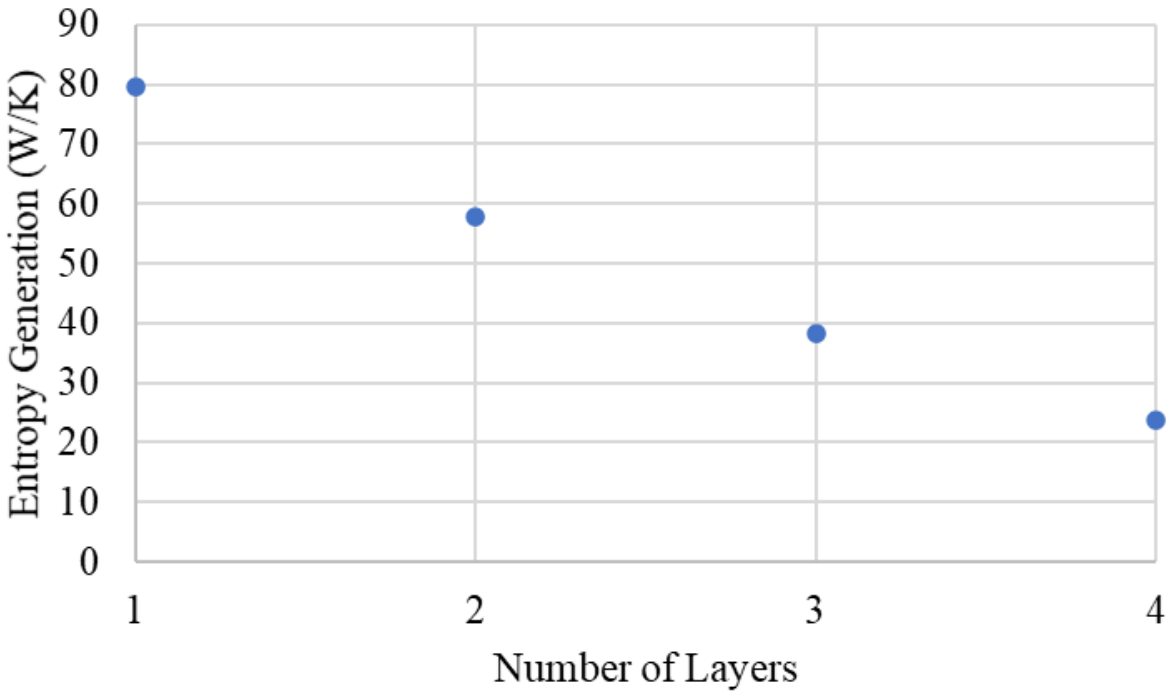

Figure 15: Entropy generation as a function of the number of layers for a tube with an isothermal surface temperature.

Table 3: Outlet temperature, outlet pressure, and entropy generation for a tube with an isothermal surface temperature and increasing layers.

Number of Layers	Total Entropy Generation (W/K)	Final Pressure (Pa)	Final Temperature (K)
1	79.4900	648100	88.91
2	57.8900	647661	56.54
3	38.2400	647049	37.10
4	23.8100	646806	28.86

The outlet temperature decreases with increasing layers and the pressure does not experience any significant change. The length and diameter values are shown in Table 4. As the number of layers increases the length of the initial branches decrease and the final increase. This trend

towards increasing aspect ratio with layer is contrary to what is typically observed in nature and to the Hess-Murray rule for water-based systems. This is likely due to the large variability in thermophysical properties between the inlet and outlet of the heat exchangers. As hydrogen is cooled the viscosity and thermal conductivity each decrease nearly an order of magnitude. Typical systems obeying the Hess-Murray rule exist in near isothermal conditions and experience little change in thermophysical properties. The diameters remain fairly consistent along the total length due to the low pressure-based contribution to entropy generation.

Table 4: Lengths and diameters of an isothermal tube with increasing layers.

Total Number of Layers		Layer 1	Layer 2	Layer 3	Layer 4
1	Length (m)	0.142			
	Diameter (m)	0.009525			
2	Length (m)	0.001	0.141		
	Diameter (m)	0.002242	0.003174		
3	Length (m)	0.001	0.00139	0.1396	
	Diameter (m)	0.000407	0.002566	0.00292	
4	Length (m)	0.001	0.001	0.0136	0.1264
	Diameter (m)	0.001745	0.001926	0.001973	0.001982

3.2.3 Linear Temperature Gradient

In the ideal scenario the temperature gradient across the surface is linear from 293-25 K to minimize gradients that result in entropy generation. Assuming a small value for axial conduction, and therefore a nonisothermal surface yields differing length and diameter ratios from the isothermal scenario. Imposing a linear temperature gradient on the surface and using the same test conditions as the isothermal case shows decreasing entropy generation with increasing

layers, shown in Figure 16. The maximum and minimum entropy generation, 13.50 W/K and 6.064 W/K, occur with one and five layers respectively. The percent difference is 76.01%.

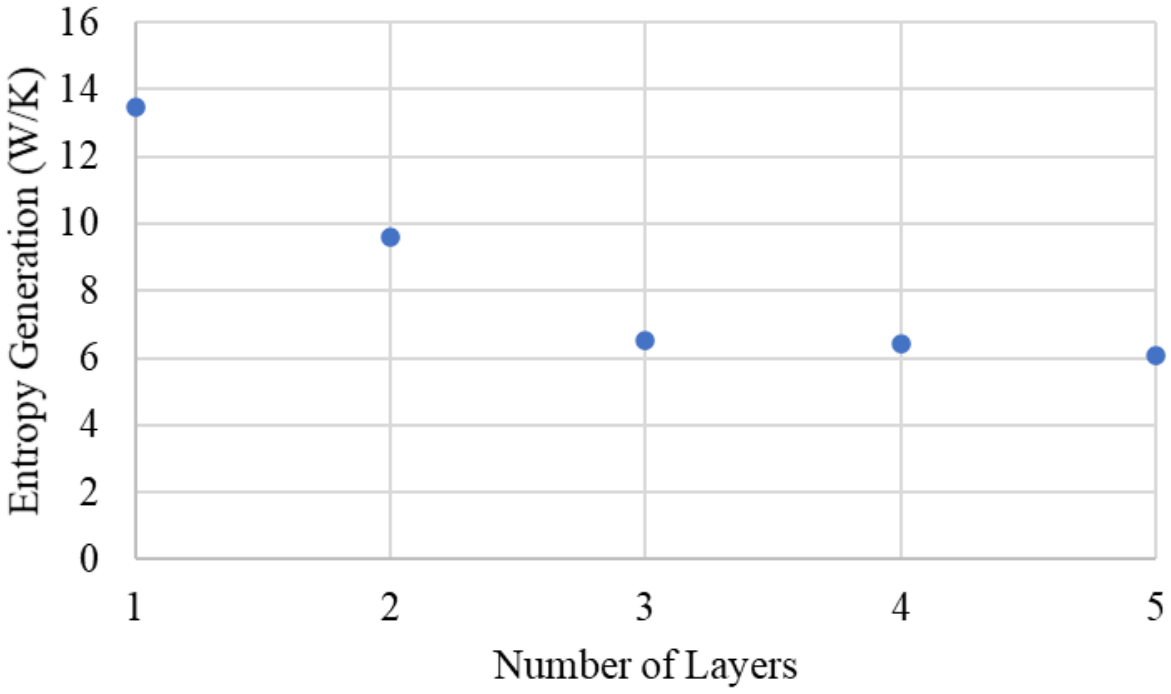

Figure 16: Entropy generation as a function of the number of layers for a tube with a linear temperature gradient along the wall.

The total entropy generation, output temperature, and output pressure are shown in Table 5. Increasing the number of layers decreases both the outlet temperature and the total entropy generation while having a negligible effect on the outlet pressure.

Table 5: Outlet temperature, outlet pressure, and entropy generation for a tube with a linear temperature gradient along the wall and increasing layers.

Number of Layers	Total Entropy Generation (W/K)	Final Pressure (Pa)	Final Temperature (K)
1	13.500	648095	156
2	9.614	647640	118.7
3	6.533	648091	87.82
4	6.403	646962	65.57
5	6.064	646970	51.04

The resulting lengths and diameters are shown in Table 6. The diameters remain fairly consistent along the total length. Layer one has the shortest length. The lengths and diameters are consistent with those from the isothermal scenario and neither trend with the Hess-Murray rule which was developed for water-based systems.

Table 6: Lengths and diameters of a tube with a linear temperature gradient along the wall and increasing layers.

Total Number of Layers		Layer 1	Layer 2	Layer 3	Layer 4	Layer 5
1	Length (m)	0.142				
	Diameter (m)	0.009525				
2	Length (m)	0.001	0.0141			
	Diameter (m)	0.003195	0.003175			
3	Length (m)	0.001	0.001	0.14		
	Diameter (m)	0.006747	0.009525	0.006038		
4	Length (m)	0.001	0.01013	0.01035	0.1205	
	Diameter (m)	0.0018	0.0022	0.003	0.0035	
5	Length (m)	0.001	0.01011	0.01046	0.01019	0.1102
	Diameter (m)	0.0018	0.0022	0.003	0.0035	0.003175

Modeling a tube without a wall is useful in determining geometry based on fluid flow parameters but the wall temperature profile is superimposed. In a real system the temperature profile of the wall is more variable, and dependent on external factors such as wall thickness and material.

Modeling the fluid flow shows how, in both isothermal and linear temperature gradient scenarios, increasing the number of layers leads to decreased entropy generation and how lengths and diameters vary between layers, inconsistent with the Hess-Murray rule. This is expected because the system being modeled is not water-based. The two modes of entropy generation being considered, heat transfer out of the fluid and pressure drop, determine system geometry independent of axial heat transfer along the wall. To model a real system the wall must be included in the analysis. The wall geometry determines the temperature profile and dictates the amount of heat transfer out of the fluid stream, thereby significantly impacting entropy generation within the system. In the following section, a wall is added to the model. Resistance comparisons are conducted, the axial conduction parameter is estimated, entropy and energy balances are conducted, and a method for numerical integration is detailed.

3.3 Theoretical Model of Heat Exchanger with Wall

The following sections detail the theoretical analysis of a tube with a wall. The wall is assumed to be aluminum 6061, and all properties are determined using data correlated by the National Institute of Standards and Technology [56-58]. All correlations are used as implemented in the 64-bit professional version of EES [54].

3.3.1 Resistance Comparison and Axial Conduction Parameter

There are four potential types of resistance in the system. These include axial conduction, radial conduction, external convection, and internal convection. To determine which are relevant in this system a resistance comparison is conducted. The parameters shown in Table 7 are assumed. The longest continuous length in the system, that from the upper stage to the lower stage, is used because it will yield the largest resistances and is most likely to develop a temperature gradient.

Table 7: System properties held constant to determine the resistance and axial conduction values for the system.

Property	Value
Material	6061 Aluminum
Thermal Conductivity (Integrated Average, 25-293 K)	115 W/m-K
Relative Roughness	0.01
Mass Flow Rate	0.012 g/s
Length	0.239 m
Minimum Heat Capacity	18.28 J/kg-K

The calculated resistance values and accompanying equations are shown in Table 8.

Table 8: Resistance values for the system with varying wall thicknesses and inner diameters.

		Resistance (K/W)			
		0.5 mm Wall Thickness		5 mm Wall Thickness	
Resistance Type	Equation	0.0127 m ID	0.003175 m ID	0.0127 m ID	0.003175 m ID
Axial Conduction	$\frac{L}{k_{int\ avg}\frac{\pi}{4}(OD^2 - ID^2)}$	133.6	479.7	9.96	21.57
Radial Conduction	$\frac{\ln\left(\frac{OD}{ID}\right)}{2\pi k_{int\ avg} L}$	0.0003293	0.00119	0.002523	0.006183
		0.0127 m ID or OD		0.003175 m ID or OD	
Internal Convection	$\frac{1}{h_{internal}\pi IDL}$	1.263		1.263	
External Convection	$\frac{1}{h_{external}\pi ODL}$	2.098		2.098	

A Biot number comparison between the resistance from radial conduction and any of the other resistances is more than three orders of magnitude less than one. Therefore, resistance from radial conduction can be ignored. It is assumed that the gas flow outside of the heat exchanger is

stagnant, therefore external convection can also be ignored. Next, the axial conduction parameter is calculated. The resulting values are shown in Table 9.

Table 9: Calculated axial conduction parameters with varying wall thicknesses and inner diameters.

	Wall Thickness (mm)	
Inner Diameter (m)	0.5	5
0.003175	4.362	97.04
0.0127	15.67	210.1

A large value of the axial conduction parameter, close to 25, indicates that the system is isothermal. A small value of the axial conduction parameter, close to 0.0025 indicates that the system is nonisothermal. The calculated value with an inner diameter of 0.003175 m and a wall thickness of 0.5 mm is small enough that the system can likely be assumed nonisothermal. However, for any other scenario with larger tube thicknesses, the system should be assumed isothermal.

3.3.2 Pressure Drop from Branching

Branching results in a pressure drop related to head loss. Each branch can be approximated as a y-fitting with an associated minor head loss that corresponds to a pressure drop in the system. The pressure drop is calculated using Equation 18.

$$\Delta P = \frac{K \rho V^2}{2} \tag{18}$$

Where ΔP is the pressure drop, K is the loss coefficient, V is the fluid velocity, and ρ is the fluid density. For a y-fitting, the loss coefficient is equal to 3 [59]. Assuming a temperature of 100 K and a pressure of 652.93 kPa, the density of normal hydrogen is 1.585 kg/m^3. To achieve a

pressure drop of 1 Pa at the setpoint, the fluid stream velocity must be 0.6486 m/s. The theoretical velocity in the heat exchanger with the same temperature and pressure, a total mass flow rate of 0.008 g/s split between eight tubes, and an inner diameter of 3.175 mm, is 0.07969 m/s. Therefore, the pressure drop due to the heat exchanger bifurcating is not expected to exceed 1 Pa, and the associated pressure drop can be ignored.

3.3.3 Entropy Balance

In a heat exchanger entropy is generated through heat transfer from the fluid stream into the wall, heat transfer along the wall, and pressure drop along the fluid stream. Entropy generated as a result of the pressure drop is assumed negligible in comparison to the other modes of generation as illustrated in Section 1.2.1. A system diagram is shown in Figure 17.

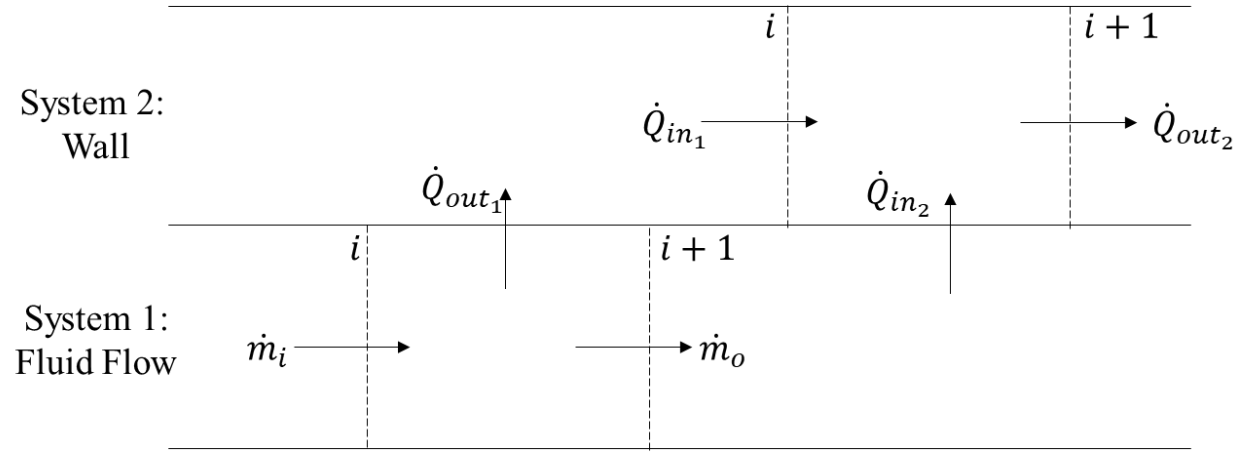

Figure 17: System diagram of a tube with a wall and a flowing fluid. $\dot{Q}_{out_1}$ is equal to $\dot{Q}_{in_2}$, and $\dot{m}_i$ is equal to $\dot{m}_o$.

Looking at System 1, the fluid flow, in Figure 17 and simplifying Equation 2 yields Equation 19.

$$\dot{m}_i s_i + \dot{S}_{gen} = \dot{m}_o s_{i+1} + \frac{\dot{Q}_{out_1}}{T_{o_1}} \tag{19}$$

Where T_{o_1} is the wall temperature at i+1, and $\dot{Q}_{out_1}$ is equal to Equation 20.

$$\dot{Q}_{out_1} = \dot{m}(h_{i+1} - h_i) \tag{20}$$

Where h is the enthalpy of the fluid. Substituting Equation 20 into Equation 19 and solving for $\dot{S}_{gen}$ yields the function for the total entropy generation in the fluid flow, shown in Equation 21.

$$\dot{S}_{gen} = \frac{\dot{m}(h_{i+1} - h_i)}{T_{o_1}} + \dot{m}(s_{i+1} - s_i) \tag{21}$$

Looking at System 2, the wall, in Figure 17 and simplifying Equation 2 yields Equation 22.

$$\dot{m}_i s_i + \frac{\dot{Q}_{in_1}}{T_{o_2}} + \frac{\dot{Q}_{in_2}}{T_{o_1}} + \dot{S}_{gen} = \dot{m}_o s_{i+1} + \frac{\dot{Q}_{out_2}}{T_{o_3}} \tag{22}$$

Where T_{o_2} is the wall temperature at i, $T_{o_3}$is the wall temperature at i+1, $\dot{Q}_{in_2}$ is equal to $\dot{Q}_{out_1}$from System 1, $\dot{Q}_{in_1}$ is equal to Equation 23, and $\dot{Q}_{out_2}$ is equal to Equation 24.

$$\dot{Q}_{in_1} = k_i \frac{T_{i-1} - T_i}{\Delta x} A_c \tag{23}$$

$$\dot{Q}_{out_2} = k_{i+1} \frac{T_i - T_{i+1}}{\Delta x} A_c \tag{24}$$

Where k is the thermal conductivity, A_c is the cross-sectional area of the tube, T is temperature, and Δx is segment length. Subbing Equations 20, 23, and 24 into Equation 22 and solving for $\dot{S}_{gen}$ yields the function for the total entropy generation in the wall-fluid system. This is shown in Equation 25.

$$\dot{S}_{gen} = \frac{T_i - T_{i+1}}{\Delta x} \frac{k_{i+1} A_c}{T_{o_3}} - \frac{T_{i-1} - T_i}{\Delta x} \frac{k_i A_c}{T_{o_2}} - \frac{\dot{m}(h_{i+1} - h_i)}{T_{o_1}} + \dot{m}(s_{i+1} - s_i) \tag{25}$$

The entropy generated in each section is summed to get the total entropy generated in the heat exchanger. The heat transferred from the fluid stream into the wall, the third term on the right-hand side of Equation 25, makes the largest contribution to entropy generation in the system. To minimize this contribution, the temperature gradient between Systems 1 and 2 must be

decreased. The first and second terms in Equation 25 are highly reliant on the thermal conductivity and cross-sectional area. To minimize variation in these terms, when the thermal conductivity decreases as the temperature lowers the cross-sectional area must be increased.

3.3.4 Energy Balance

To determine the temperature profiles along Systems 1 and 2 in Figure 17 energy balances are conducted. The energy balance for System 2, the wall, is shown in Equation 26.

$$\dot{q}_{w,x} + \dot{q}_{wh} = \dot{q}_{w,x+dx} \tag{26}$$

Where $\dot{q}$ is the rate of heat transfer, w indicates a position along the wall, wh indicates the location where the wall and hydrogen stream are in contact, and dx is an incremental length. Expanding Equation 26 and doing a Taylor series expansion of the x+dx term yields Equation 27.

$$\dot{q}_{w,x} + \dot{q}_{wh} = \dot{q}_{w,x} + \left(\frac{d\dot{q}}{dx}\right) dx \tag{27}$$

The $\dot{q}_{w,x}$ terms on each side cancel. The equations for $\dot{q}_{wh}$ and $\dot{q}$ are shown in Equations 28 and 29 respectively.

$$\dot{q}_{wh} = h_{conv} A_s (T_H - T_w) \tag{28}$$

$$\dot{q} = -k_w A_c \frac{dT}{dx} \tag{29}$$

Where h_{conv} is the coefficient of convective heat transfer, A_s is the surface area, and k is the thermal conductivity. Substituting Equations 28 and 29 in Equation 27 and solving for d^2T/dx^2 yields Equation 30.

$$\frac{d^2T}{dx^2} = \frac{4h_{conv} ID (T_{wx} - T_{Hx})}{k_w (OD^2 - ID^2)} \tag{30}$$

Where ID is the inner diameter of the tube, and OD is the outer diameter of the tube. Equation 30 represents the curvature of the temperature profile of the wall. Increasing the coefficient of heat

transfer, the inner diameter, and the temperature gradient between the fluid and wall increase the curvature. Increasing the thermal conductivity or the cross-sectional area decrease the curvature. The energy balance for System 1, the fluid flow, is shown in Equation 31.

$$\dot{q}_{H,x} = \dot{q}_{H,x+dx} + \dot{q}_{wH} \tag{31}$$

Where H indicates a position along the hydrogen stream. The equations for $\dot{q}_{H,x}$ and $\dot{q}_{H,x+dx}$ are shown in Equations 32 and 33.

$$\dot{q}_{H,x} = \dot{m}i_i \tag{32}$$

$$\dot{q}_{H,x+dx} = \dot{m}i_i + \dot{m}\frac{di}{dx}dx = \dot{m}i_i + \dot{m}c_p\frac{dT}{dx}dx \tag{33}$$

Where i is enthalpy and c_p is heat capacity at constant pressure. Substituting Equations 28, 32, and 33 into Equation 31, cancelling terms, and solving for dT/dx, the temperature profile of the fluid stream, yields Equation 34.

$$\frac{dT}{dx} = \frac{-h_{conv}A_s(T_{H,x} - T_{w,x})}{\dot{m}C\Delta x} \tag{34}$$

Equation 34 represents the slope of the temperature profile of the fluid stream. It predicts how quickly the temperature of will change. Increasing the coefficient of heat transfer, the surface area, or the temperature gradient between the fluid stream and the wall increase the slope, and result in rapid temperature change. Increasing the mass flow rate, heat capacity of the fluid, or interval decrease the slope, representing a slower change in temperature.

3.3.5 Numerical Integration

Both the wall and hydrogen stream temperature profiles are solved for using Crank-Nicolson integration. The Crank-Nicolson method is a semi-implicit finite difference method used to numerically solve differential equations. It calculates the next value in a function by averaging the current and predicted curvatures or slopes and then multiplying the average over half of the

defined interval. The result is then added to the current value. The method mimics the trapezoidal rule used in calculus. The standard equations used for integration are shown in Equations 35-36.

$$T_{i+1} = T_i + \left[\frac{dT}{dx_i} + \frac{dT}{dx_{i+1}}\right]\frac{\Delta x}{2} \tag{35}$$

$$\frac{dT}{dx_{i+1}} = \frac{dT}{dx_i} + \left[\frac{d^2T}{dx^2_i} + \frac{d^2T}{dx^2_{i+1}}\right]\frac{\Delta x}{2} \tag{36}$$

Where T is temperature and i denotes a position along the length. Equation 36 determines the slope, and Equation 35 determines the value. Only Equation 35 is necessary to solve for the temperature profile along the hydrogen stream. Equations 35 and 36 are both necessary to determine the temperature profile along the wall. There is also interdependency between both profiles. A sensitivity analysis is conducted to determine the appropriate number of nodes for the system. This value is determined to be 50 nodes per branch.

3.3.6 Boundary Conditions

Three boundary conditions are required to solve the system for the hydrogen and wall temperature profiles. The first boundary conditions is the inlet temperature of the hydrogen. The inlet gas is assumed to be room temperature at 293 K. The second boundary condition is the assumption that the wall inlet is adiabatic: $dTw/dx_1 = 0$. The third boundary condition is the heat draw from the Gifford-McMahon cryocooler. It is assumed that each stage only pulls heat from the portion of the heat exchanger prior. This boundary condition is shown in Equation 37.

$$\dot{q}_{cryo} = \frac{T_{w,N-1} - T_N}{R_{cond}} \tag{37}$$

Where $\dot{q}_{cryo}$ is the heat flux from the Gifford-McMahon cryocooler and R_{cond} is the resistance from axial conduction.

3.4 Varying Wall Thickness

The wall thickness is increased along the length of the heat exchanger. This is done for two reasons. The first reason is that as the temperature decreases, so does the thermal conductivity of the wall. Therefore, the wall thickness must be increased to prevent the resistance to conduction from increasing along the length and limiting heat transfer. The second reason is that heat accumulates along the length of the tube, and the resistance must decrease to allow the accumulated heat to effectively travel to a flange, where is can be removed by the Gifford-McMahon cryocooler. After experimentation it is found that an exponentially increasing wall thickness results in a linear temperature profile, which is optimum for maximizing system efficiency. The thickness is varied according to the exponential function shown in Equation 38.

$$th = x[i]^x + y \tag{38}$$

Where th is the wall thickness, x[i] is the position along the length and y is the initial thickness. y is adjusted to achieve continuity in the temperature profile. Table 10 shows how entropy generation and the final wall and fluid stream temperatures relate to the exponent used. The data shown is for a 0.1 m long Al 6061 tube with an inner diameter of 0.003175 m. The heat removed by the upper stage of the Gifford-McMahon cryocooler at the bottom of the tube is 110 W.

Table 10: Varying exponential function and resulting entropy generation and outlet temperature.

x	y	Total Entropy Generation (W/K)	Hydrogen Outlet Temperature (K)	Wall Outlet Temperature (K)
3	0.003	0.2283	246.4	178.5
2	0.003	0.06269	274.6	260.1
1.5	0.0032	0.03101	286.6	283.6
1.3	0.0032	0.01449	288.8	287.2
1.1	0.0033	0.04193	290.4	289.6
0.9	0.0033	0.1221	291.2	290.9

0.7	0.0028	0.3265	291.5	291.3
0.5	0.0026	0.8385	291.6	291.4
0.3	0.0026	2.116	291.6	291.4

A plot of the outlet temperatures as a function of the exponent is shown in Figure 18. Both the hydrogen and wall outlet temperatures decrease as the exponent is increased. The difference between the hydrogen and wall outlet temperatures also increase with the increasing exponent.

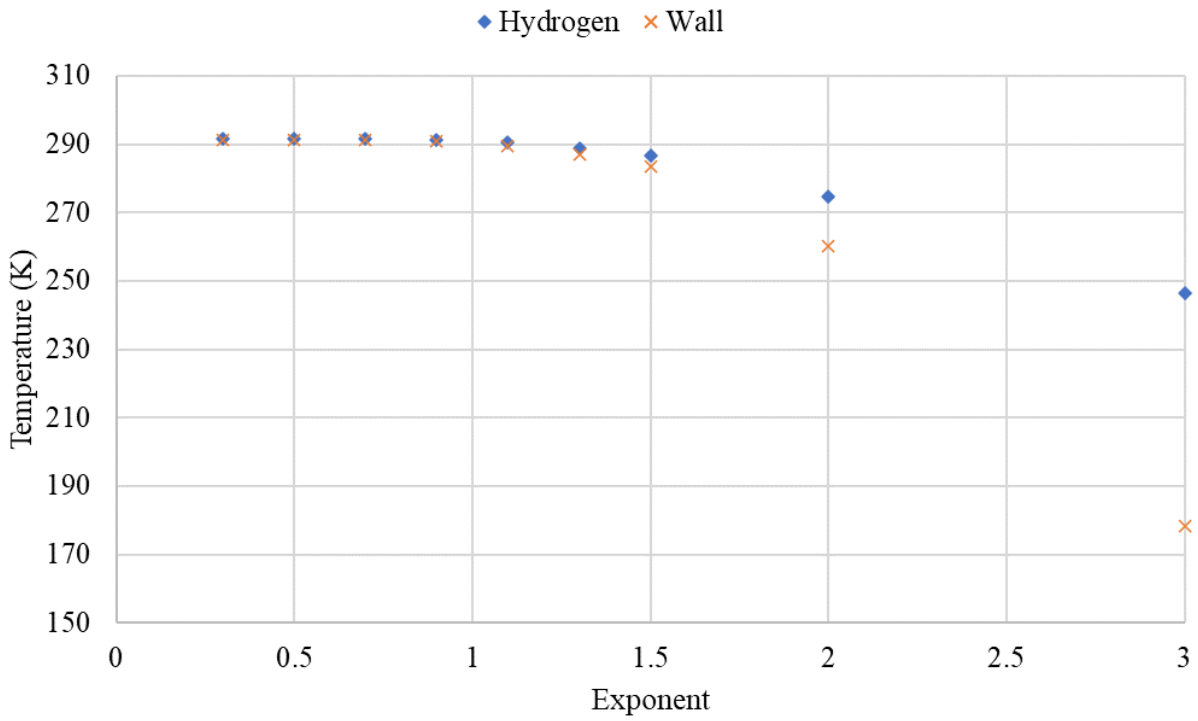

Figure 18: Outlet temperatures of the wall and hydrogen streams as a function of the wall thickness function exponent.

A plot of the entropy generation as a function of the exponent is shown in Figure 19. The minimum entropy generation, 0.01449 W/K, occurs with an exponent of 1.3. When the exponent

is below 1.3 the resistance to axial conduction is higher than ideal, and when the exponent is above 1.3 the resistance to axial conduction is lower than ideal.

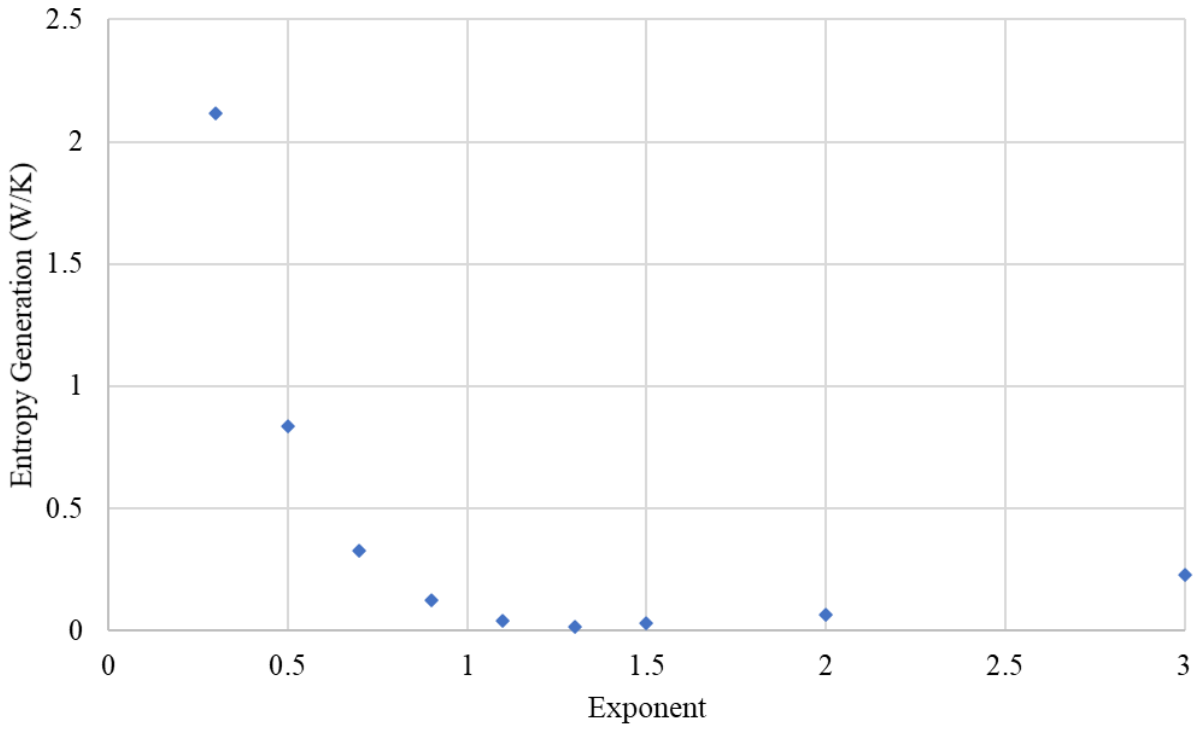

Figure 19: Entropy generation as a function of the wall thickness function exponent.

An exponent of 1.3 causes both temperature profiles to become linear, therefore decreasing entropy generation by minimizing temperature gradients. The temperature profiles are shown in Figure 20.

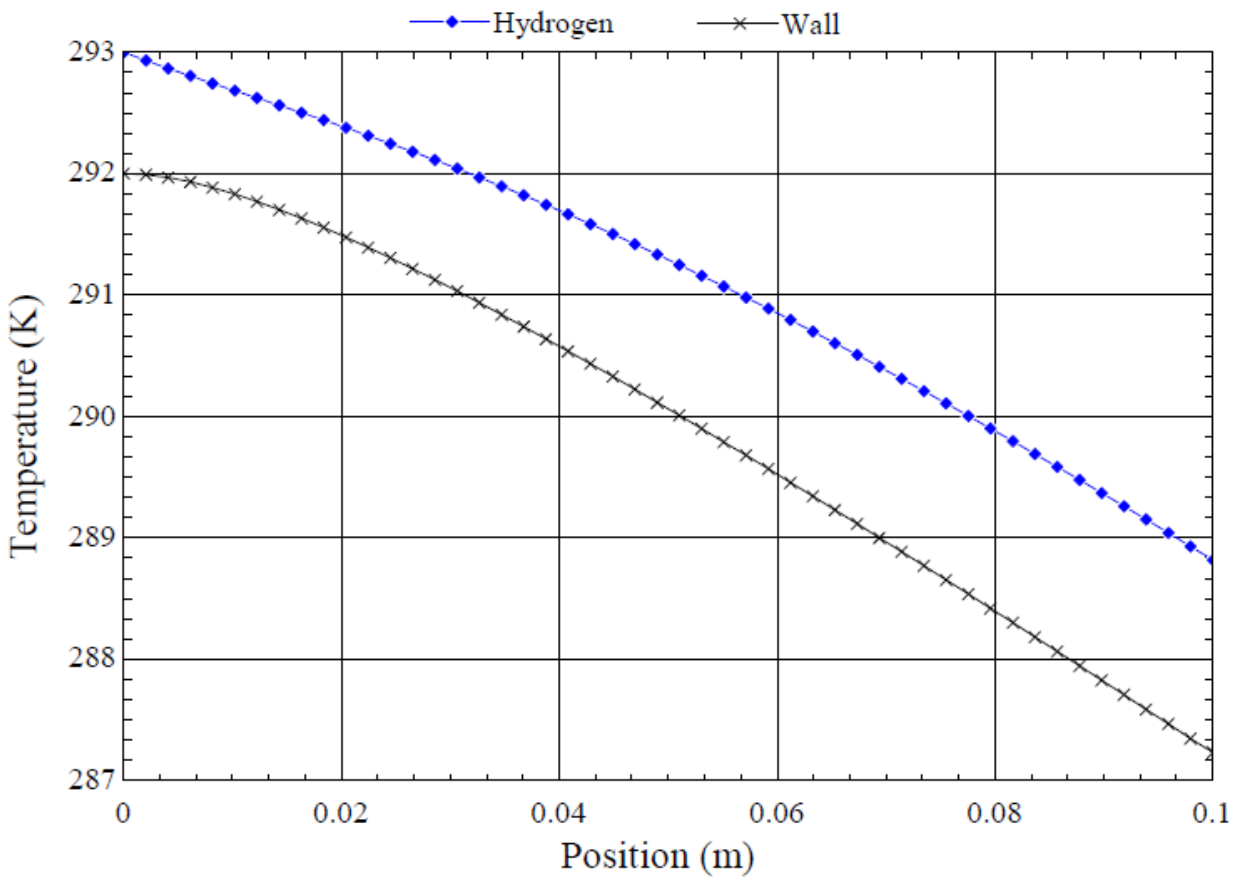

Figure 20: Temperature profiles of the wall and hydrogen streams with a wall thickness function exponent of 1.3.

Increasing the exponent above 1.3 produces a concave curve as shown in Figure 21. When the exponent is larger than 1.3 the resistance to axial conduction is lower than ideal. This results in large temperature differentials between the hydrogen stream and the wall. In turn, this yields a higher rate of entropy generation.

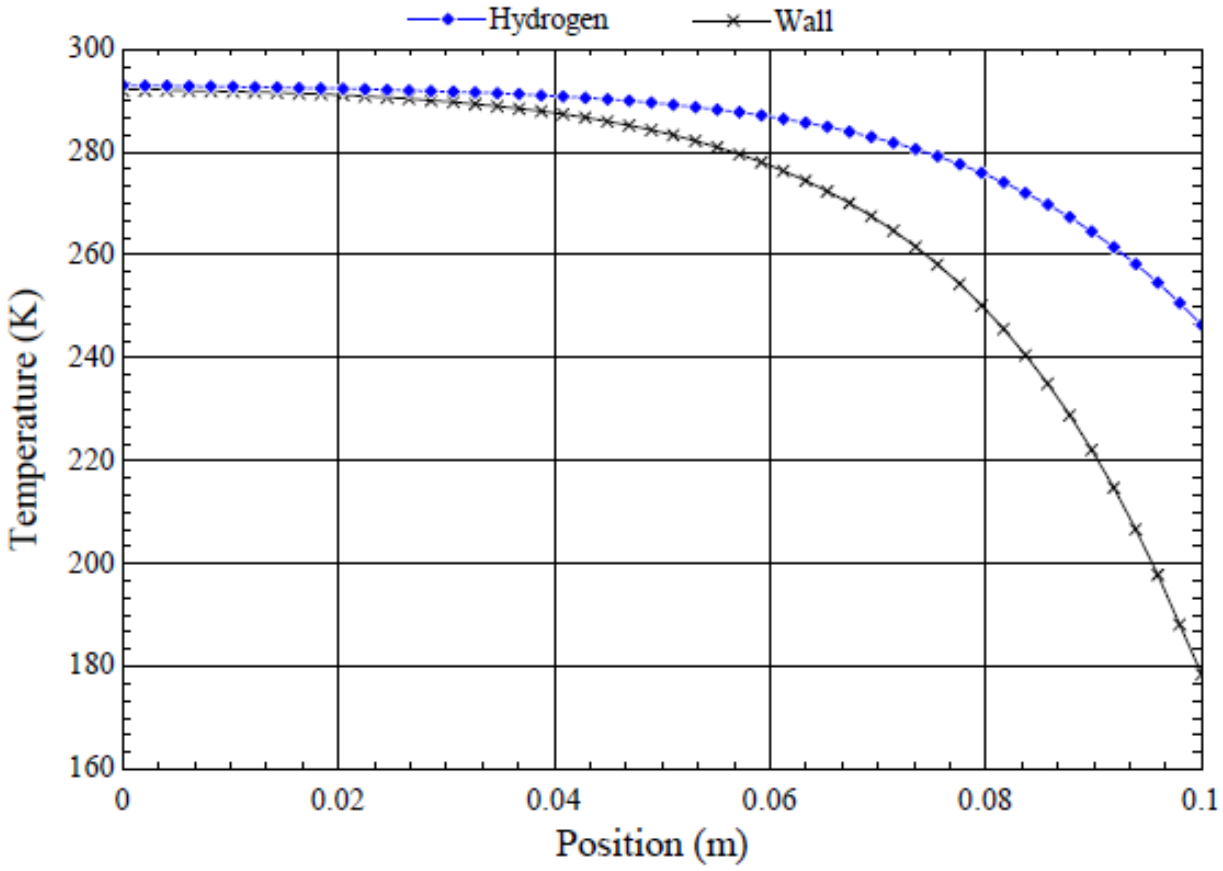

Figure 21: Temperature profiles of the wall and hydrogen streams with a wall thickness function exponent of 3.

Decreasing the exponent below 1.3 produces a convex curve as shown in Figure 22. When the exponent is lower than 1.3 the resistance to axial conduction is higher than ideal. This limits the heat transfer that can occur and results in larger temperature gradients than the ideal scenario, therefore yielding higher rates of entropy generation.

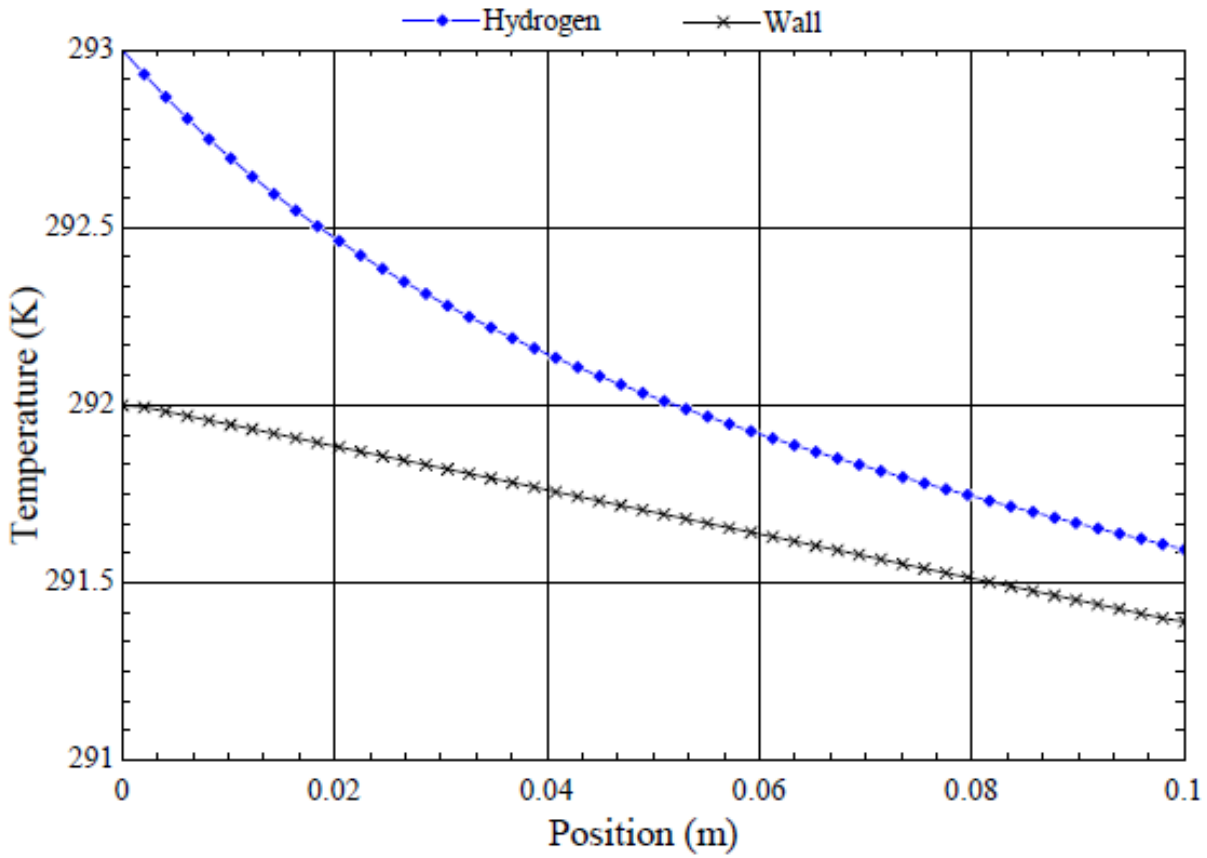

Figure 22: Temperature profiles of the wall and hydrogen streams with a wall thickness function exponent of 0.5.

In a fluid flow scenario, increasing mass flow rate, increasing length, and decreasing the inner diameter to or below 0.003175 m causes significant increases in entropy generation and pressure drop. At diameters above 0.003175 m, changes in entropy generation and pressure drop resulting from varying system parameters are small. Entropy is generated from pressure drops and heat transfer. In a given scenario, there is an optimum length that will yield minimum entropy generation. Branching when this minimum is reached increases system efficiency by decreasing entropy generation.

In a tube without a wall, increasing the number of layers decreases the entropy generation. This is true when the wall condition is either isothermal or a linear gradient. These scenarios represent tubes with high and low values of the axial conduction parameter. The resulting geometry is not consistent with the Hess-Murray rule because the fluid properties are not similar to those of water, and they are not constant through the temperature range.

In a tube with a wall, resistance to radial conduction is negligible, the axial conduction parameter is likely high, and the pressure drop from branching is negligible. Varying the wall thickness according to an exponential function yields a minimum entropy scenario when the wall thickness function exponent is 1.3. The increasing wall thickness accounts for decreasing thermal conductivity with decreasing temperature and heat accumulation along the length traveling toward a Gifford-McMahon cryocooler flange.

In Chapter 4, the numerical model derived for a tube with a wall is implemented to design a heat exchanger that mounts to a Sumitomo RDK-415D Gifford-McMahon cryocooler. Experimental constraints are evaluated, and then multiple design scenarios are considered. Finally, the branching heat exchanger is compared to a single tube heat exchanger, and installation instructions are given.

CHAPTER FOUR: EXPERIMENTAL DESIGN

This chapter details the final heat exchanger design and the expected performance. It begins by explaining experimental constraints, such as the minimum wall thickness, allowable lengths and diameters, and the maximum mass flow rate. Next, the final design is presented, as well as the expected performance assuming equilibrium hydrogen. Iterations are then run to predict system performance with normal hydrogen, ideal wall thickness, and different wall material. Finally, the branching heat exchanger design is compared to a single tube design, and installation instructions are given.

4.1 Experimental Constraints

The heat exchanger must attach to a Sumitomo RDK-415D Gifford-McMahon cryocooler. The material chosen for the heat exchanger construction is an aluminum composite, due to the low thermal mass and high conductivity. The hydrogen is assumed to be equilibrium at all points, representing the minimum mass flow rate case. There are a series of constraints placed on the system such as allowable diameters and wall thicknesses.

4.1.1 Mass Flow Rate

The mass flow rate is bounded by the maximum output of the electrolyzer and the total load capacity of the Gifford-McMahon cryocooler. The upper and lower stages of the Gifford-McMahon cryocooler reside at set temperatures reached during steady state operation. The higher the temperatures the more heat the system can remove and the larger the mass flow rate can be. The load capacity of the Gifford-McMahon cryocooler as a function of temperature is shown in Figure 23.

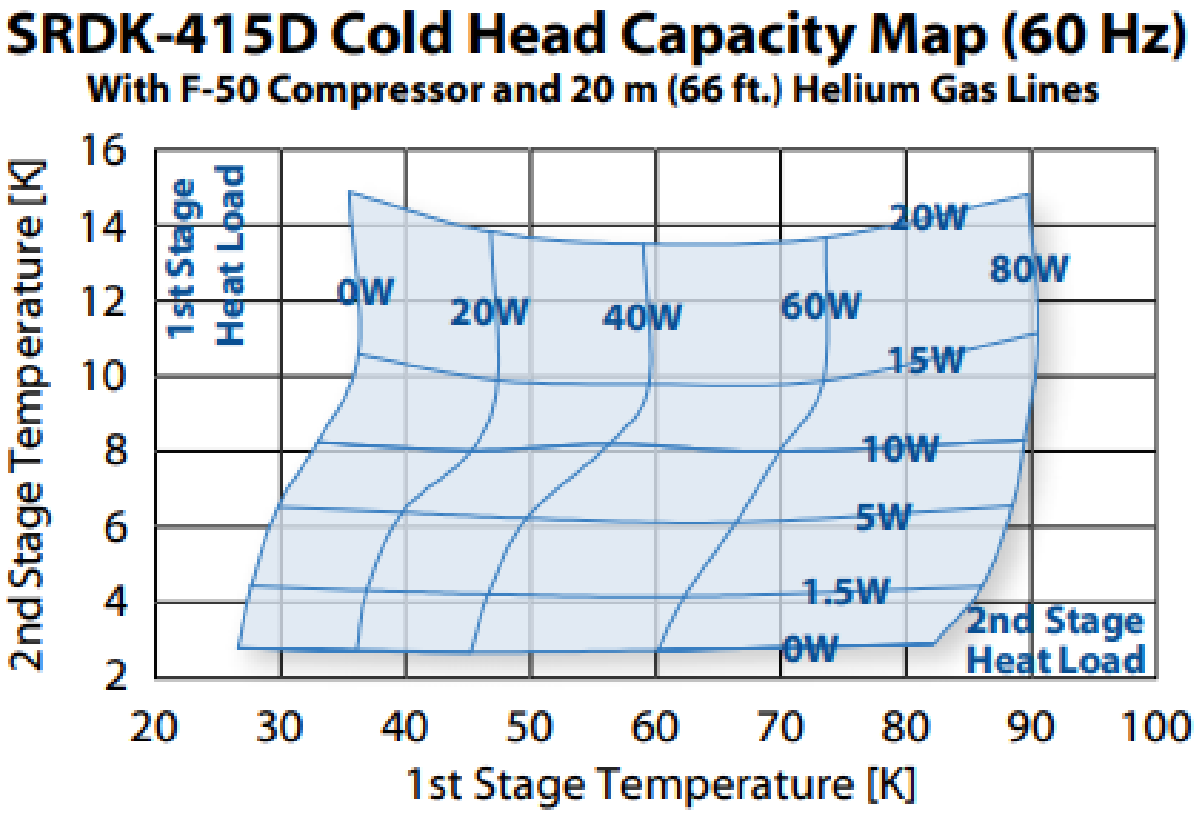

Figure 23: Heat load capacity of Sumitomo RDK-415D Gifford-McMahon cryocooler at 60 Hz [60].

The Gifford-McMahon cryocooler must cool incoming gaseous hydrogen from room temperature (293 K) to the saturation temperature at 652.93 kPa (28.1 K), cool the aluminum walls of the heat exchanger from 293 K to 25 K, and account for full ortho-para conversion. The lower stage of the Gifford-McMahon cryocooler resides at 25 K and pulls an estimated 30 W. The upper stage temperature is unknown. Therefore, the total load capacity of the Gifford-McMahon cryocooler is unknown as well as the allowable mass flow rate.

The maximum hydrogen output from the electrolyzer is 18.8 SLPM. This is equivalent to a mass flow rate of 0.02614 g/s. As the only known mass flow rate, this is the maximum flow rate used to bound design.

4.1.2 Allowable Lengths and Diameters

The part is being 3D printed; therefore, the dimensions are bounded by the printer size. The Gifford-McMahon cryocooler dimensions are listed in Table 11.

Table 11: Relevant Sumitomo RDK-415D dimensions [61].

	Length
Bottom of the top plate to the top of the first stage	0.142 m
Thickness of the first stage	0.065 m
Bottom of the first stage to the top of the second stage	0.223 m
Thickness of the second stage	0.06 m

The part is designed for a printer with a maximum print height is 0.325 m. Therefore, 0.0525 m of the total length cannot be printed. The portion of the heat exchanger extending between the stages is 0.239 m, and it is assumed that 0.01 m extends below the lower stage. These dimensions cannot be changed, therefore the portion of the heat exchanger above the upper stage must be modified to fit the printer. With the given dimensions, the portion of the heat exchanger above the top stage is 0.0795 m.

The maximum allowable inner diameter is 0.009525 m. At larger diameters the heat transfer coefficient associated with internal convection is not high enough to induce significant heat transfer. The minimum allowable inner diameter is 0.003175 m. This is the minimum diameter at which powder can be removed from the system after printing.

4.1.3 Resistance from Indium Foil

Indium foil is used as a thermal interface material between the heat exchanger and the Gifford-McMahon cryocooler flanges. The resistance of indium foil is related to the temperature and the applied pressure. Figure 24 shows how the thermal conductance of a variety of solid-solid joints depend on temperature and either pressure or contact area.

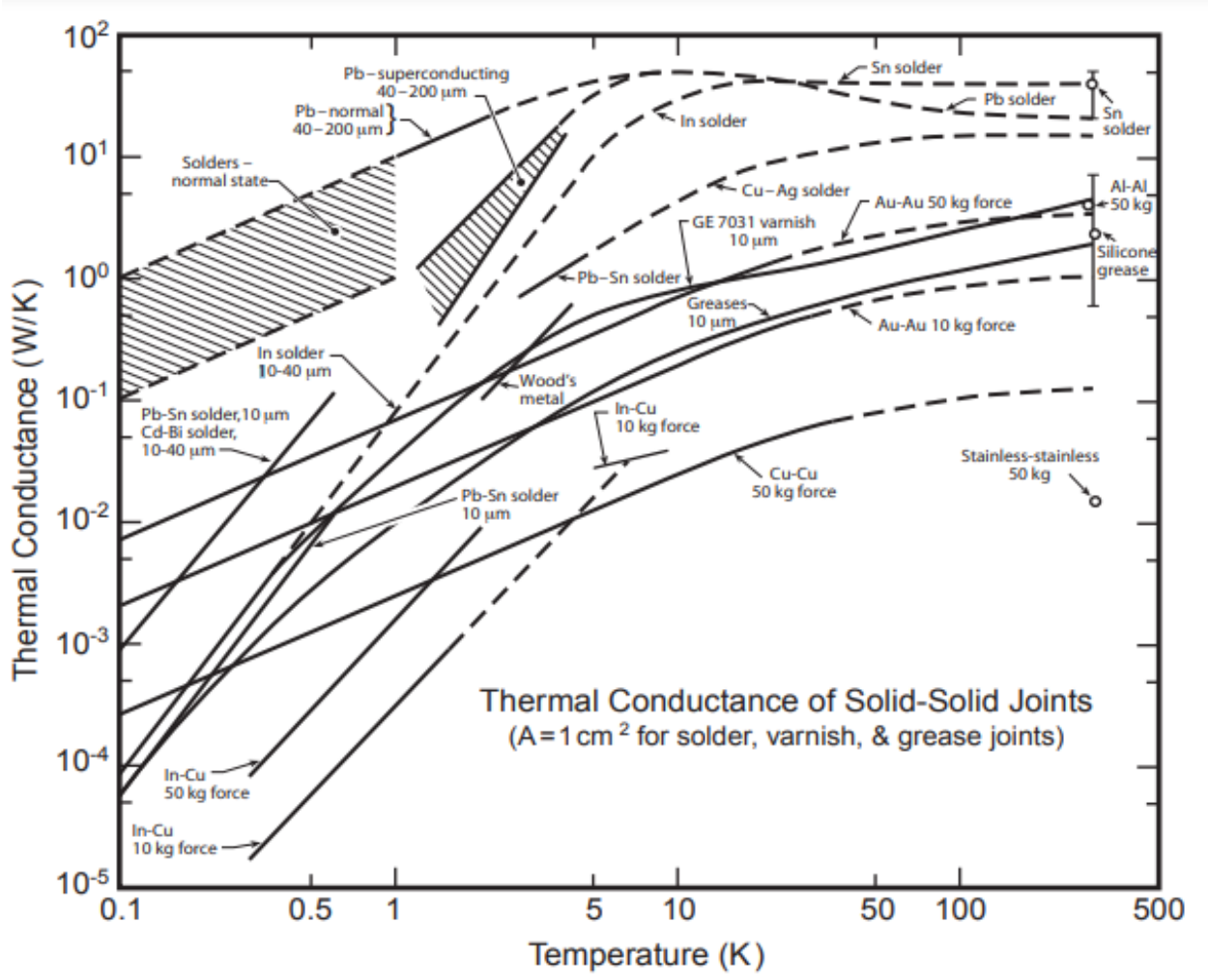

Figure 24: Thermal conductance versus temperature for solid-solid joints [62].

The thermal conductance of the indium foil is estimated by assuming an indium-copper interface with 10 kg of force. The thermal conductance for this type of joint is only known for 0.3-5 K. Assuming an average temperature of 100 K, the thermal conductance can be extrapolated and estimated at 20 W/K. For simplicity, this is assumed constant during modeling.

4.1.4 Minimum Wall Thickness

There is a minimum wall thickness associated with the inlet pressure to prevent bursting. Equation 39 is used to calculate this thickness.

$$th = \frac{P\ F\ ID}{2(S - P\ F)} \tag{39}$$

Where P is pressure, th is thickness, ID is the inner diameter, S is yield strength of the material, and F is the factor of safety. The minimum allowable inner diameter is 0.003175 m, the assumed factor of safety is 1.5, P, the maximum pressure in the system, is 652.93 kPa, and S is the tensile yield strength of the material. For aluminum 6061 the tensile yield strength is 276 MPa. Using these values, the calculated minimum wall thickness is 5.653 μm. This is the minimum allowable wall thickness within the system to prevent bursting.

4.1.5 Thermal Contraction

The heat exchanger is aluminum, and it is mounted onto copper flanges attached to a stainless-steel column. During use, the aluminum will contract more than the stainless steel. The stainless steel is much stronger than the aluminum, therefore, there is a risk that the heat exchanger will crack due to an inability to fully contract. The total contraction of 316 stainless steel and 6061 aluminum are estimated for a temperature drop from 293 K to 25 K using the linear expansion coefficient at 25 K. The difference in length is found to be 0.462 mm. This means that the aluminum will contract 0.462 mm more than the stainless steel. To account for this difference, the heat exchanger tubes must be curved, so that they can straighten slightly as the heat

exchanger contracts and alleviate stress. All physical property data used is determined via data compiled by NIST, as implemented in the 64-bit professional version of EES [54, 63, 64]

4.2 Final Heat Exchanger Design

The experimental constraints outlined in Section 4.1 and the theoretical model derived in Section 3.3 are implemented to design a manufacturable heat exchanger. The resulting design is detailed in the following sections.

4.2.1 Upper Stage to Lower Stage Design

The lower portion of the heat exchanger is designed to maximize the inlet temperature of the section, therefore increasing the outlet temperature of the upper section. This increases the heat lift at the upper stage of the Gifford-McMahon cryocooler, therefore increasing the allowable mass flow rate for the system. This is achieved by maximizing contact between the heat exchanger and the lower flange of the Gifford-McMahon cryocooler, as well as maximizing the number of tubes. The outlet temperature of the hydrogen must be about 25 K to achieve liquefaction, which corresponds to a heat load of 30 W.

The maximum number of tubes that can fit around the lower stage without touching is determined as follows. A wall thickness of 0.01 m and an inner diameter of 0.003175 m are assumed. These assumptions yield an outer tube diameter of 0.023175 m. The outer diameter of the lower stage of the Gifford-McMahon cryocooler is 0.068 m which corresponds to a circumference of 0.2136 m. The maximum number of tubes is determined to be eight. It is assumed that there is no branching in the lower portion of the heat exchanger so that contact with the upper flange of the heat exchanger is also maximized. The length is the total length of the segment, 0.239 m. The optimized inner diameter is 0.003175 m. The resulting lower section of the heat exchanger is shown in Figure 25.

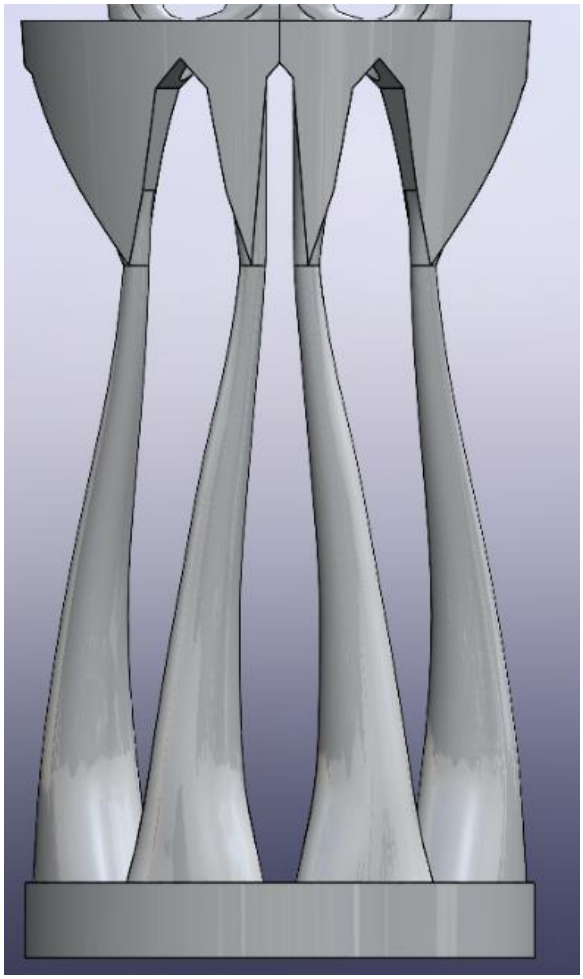

Figure 25: CAD rendering of the lower portion of the heat exchanger. Only half of the tubes can be seen in this image because the other four tubes are a reflection.

Using the predetermined dimensions, the inlet temperatures is modified to achieve an outlet temperature of the hydrogen of about 25 K. The inlet pressure is assumed to be the same as the system inlet pressure, 652.93 kPa. A temperature difference between the wall and the hydrogen of 5 K is assumed, with the wall being colder. The mass flow rate is also adjusted to achieve a balance between the maximum mas flow rate and the maximum upper stage

temperature. The exponent for the wall thickness is increased away from ideal as much as is necessary to achieve the desired temperature profiles. The wall thickness equation is scaled by a constant to prevent the wall thickness at the end of the tube from being on the order of centimeters, which would prevent the desired outlet temperature from being reached. The final values are listed in Table 12.

Table 12: Values of upper to lower stage final design parameters.

Parameter	Value
Hydrogen Inlet Temperature	100 K
Wall Inlet Temperature	95 K
Mass Flow Rate	0.008 g/s
Hydrogen Outlet Temperature	24.39 K
Wall Outlet Temperature	20.18 K
Wall Thickness Equation	th[i] = 0.3*x[i]^2.1 + 0.0009
Inner Diameter	0.003175 m
Length	0.239
Rate of Entropy Generation	0.7087 W/K

The temperature profiles and the ortho-hydrogen concentration, assuming full conversion, are shown in Figure 26 and Figure 27 respectively. The temperature profiles are concave, and both the wall and hydrogen reach an outlet temperature below 25 K. Full conversion from ortho- to para-hydrogen is assumed. Therefore, the ortho-hydrogen profile represents the equilibrium concentration over the temperature range. About two-thirds of the ortho-para conversions take place in the lower section of the heat exchanger.

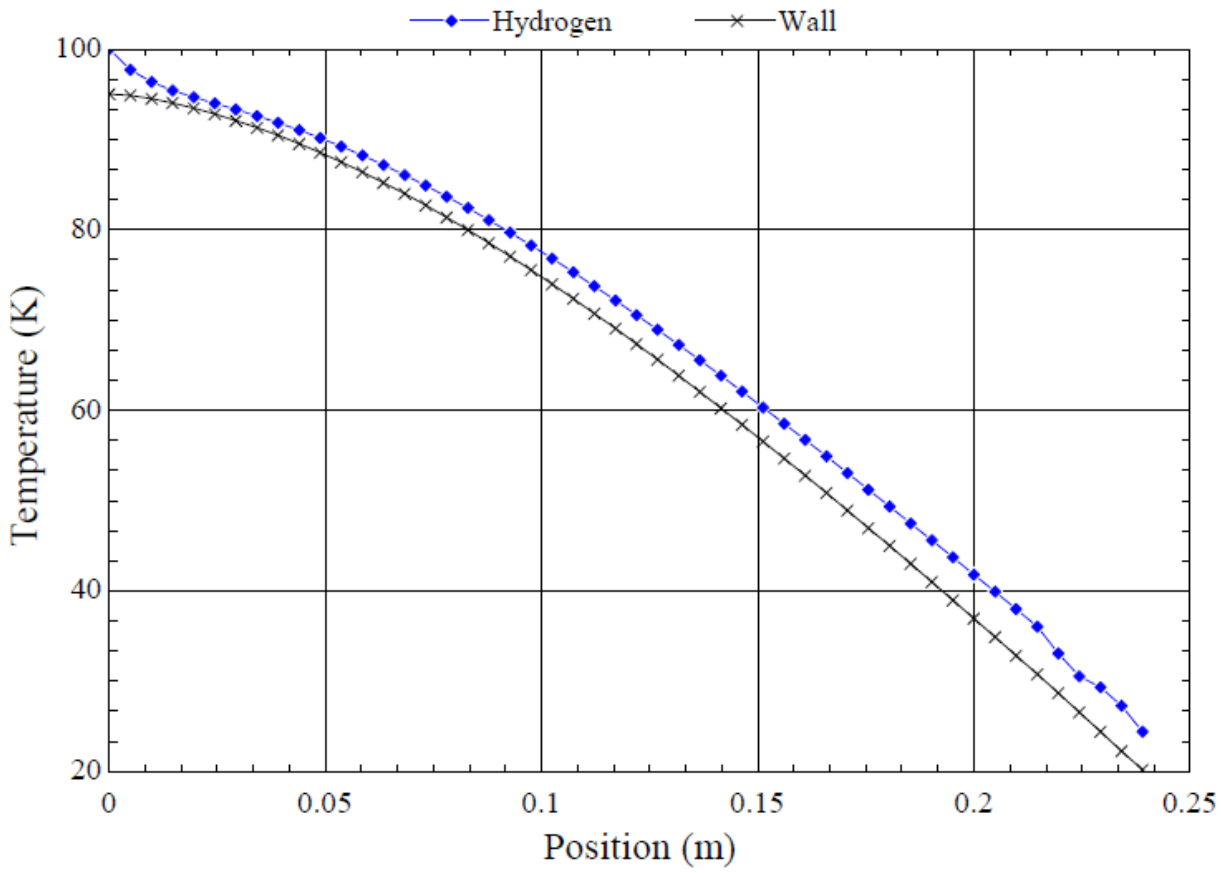

Figure 26: Temperature profiles of the wall and hydrogen stream in the lower portion of the heat exchanger.

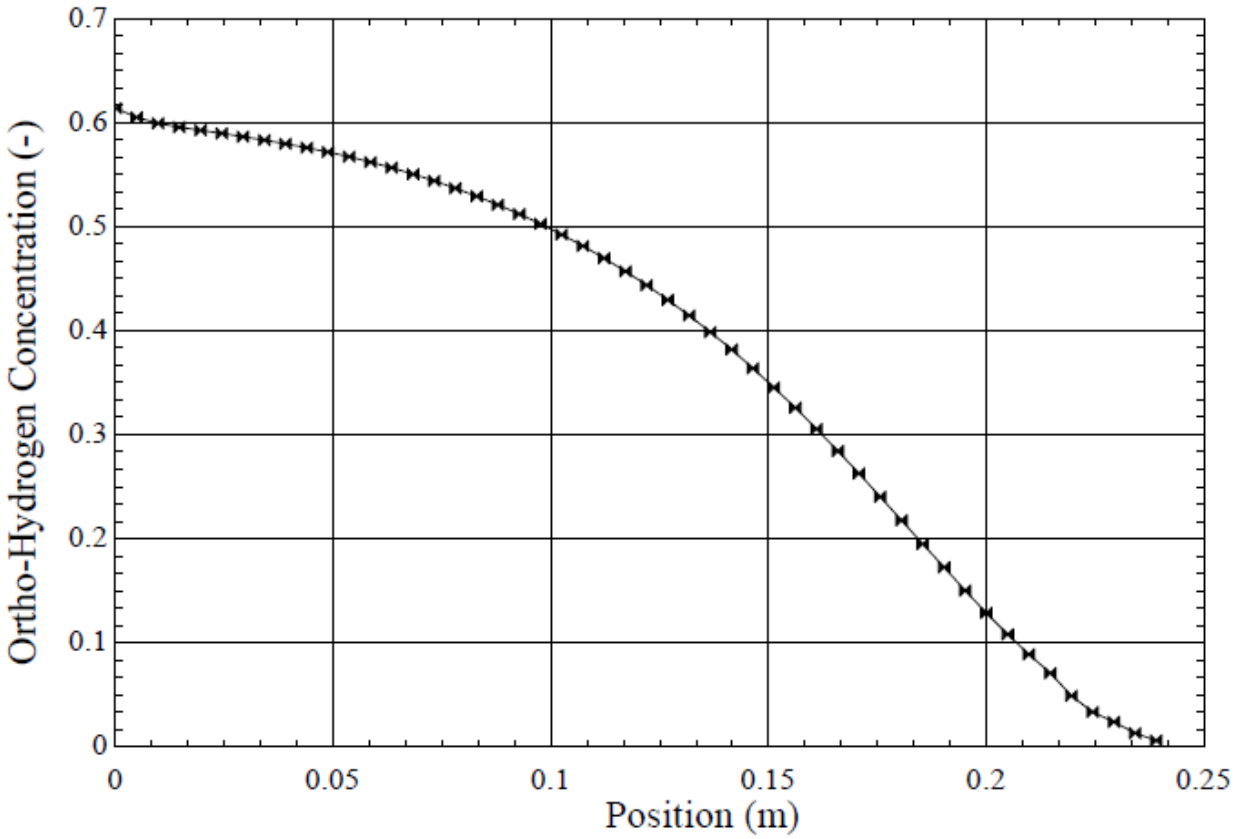

Figure 27: Ortho-hydrogen concentration over the lower portion of the heat exchanger.

4.2.2 Top Plate to Upper Stage Design

The upper portion of the heat exchanger receives gaseous hydrogen at 293 K. The maximum inlet temperature reached by the lower portion is 95 K, therefore the upper stage of the Gifford-McMahon cryocooler is estimated to pull 90 W. The outlet temperature of the upper portion must be 95 K, and the system must include four layers. The geometry is determined using the code of a tube with no wall, and a linear temperature gradient from 293 – 95 K. The final geometry is shown in Table 13. The lengths and diameters of all except the last layer are the minimum values provided. The minimum allowable diameter is not small enough to facilitate entropy generation from the pressure drop on the same order of magnitude as that of the entropy generation from

heat transfer. Therefore, a minimum generated by the intersection of the possible modes of entropy generation is not reached. As a result, the optimum geometry is one that maximizes heat transfer, and this is done by maximizing the length and number of tubes within the system. All lengths are 0.01 m, except that of the final layer. All diameters are the minimum value, 0.003175 m.

Table 13: Lengths and diameters of the upper portion of the heat exchanger.

	Layer 1	Layer 2	Layer 3	Layer 4
Length (m)	0.01	0.01	0.01	0.0495
Diameter (m)	0.003175	0.003175	0.003175	0.003175

A CAD rendering of the upper portion of the heat exchanger is shown in Figure 28.

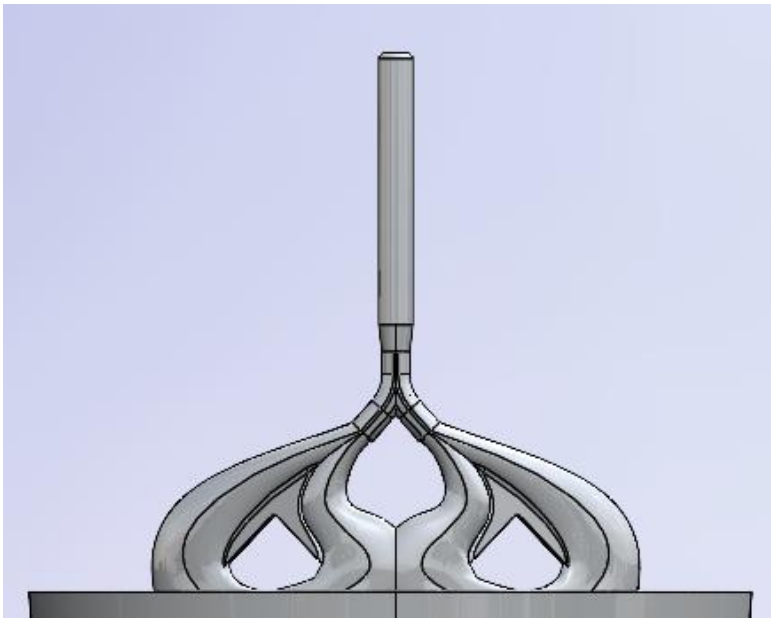

Figure 28: CAD rendering of the upper portion of the heat exchanger. Only half of the tubes are shown because the other tubes are a reflection.

The resulting parameters for the upper portion of the heat exchanger are shown in Table 14.

Table 14: Values of top plate to upper stage final design parameters.

Parameter	Value
Hydrogen Inlet Temperature	293 K
Wall Inlet Temperature	292 K
Mass Flow Rate	0.008 g/s
Hydrogen Outlet Temperature	102 K
Wall Outlet Temperature	84.63 K
Wall Thickness Equation	th[i] = x[i]^2.15 + 0.00043
Rate of Entropy Generation	0.6886 W/K

The temperature profiles and the ortho-hydrogen concentration, assuming full conversion, are shown in Figure 29 and Figure 30 respectively. The temperature profiles are concave, and both have outlet temperatures below 102 K. Full ortho- to para-hydrogen conversion is assumed, therefore the ortho-hydrogen profile reflects the equilibrium concentration over the temperature range.

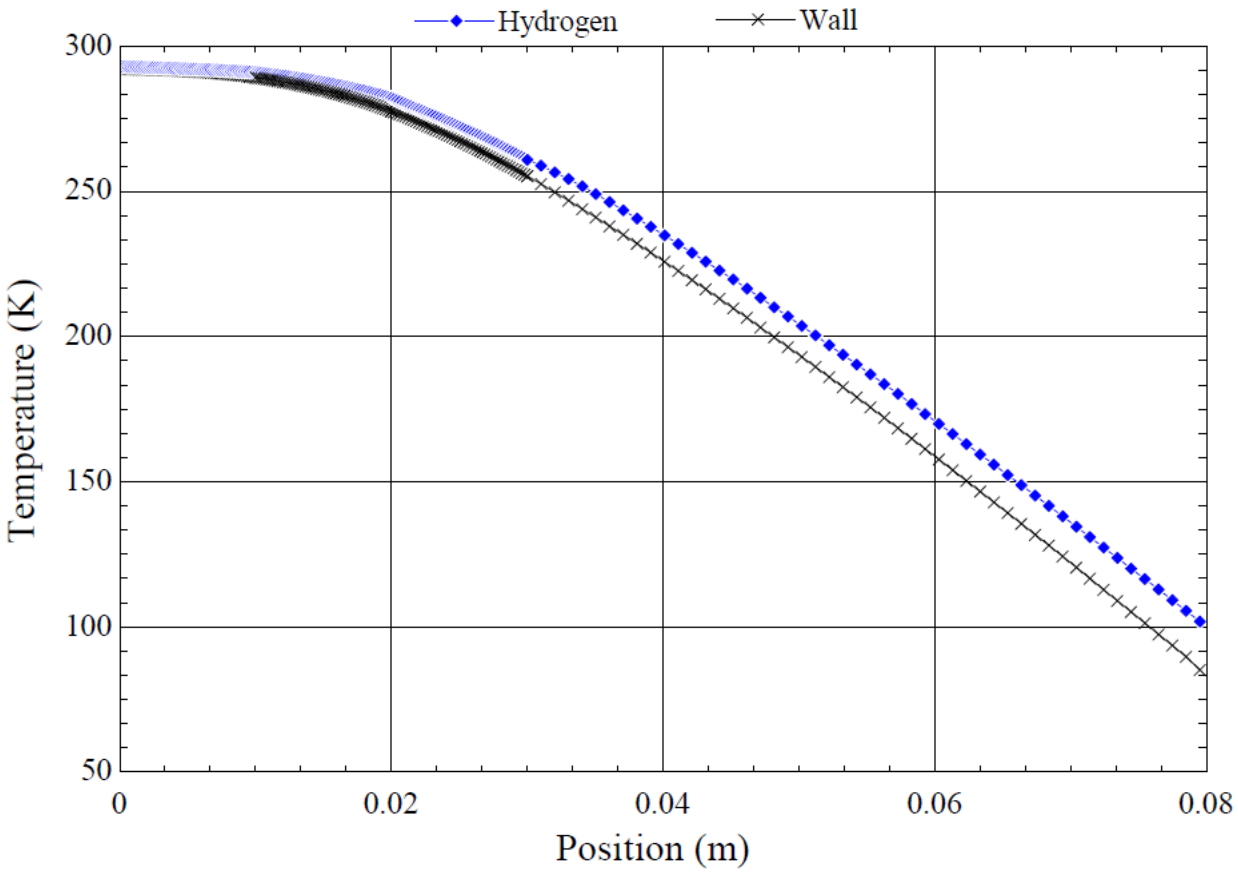

Figure 29: Temperature profiles of the wall and hydrogen stream in the upper portion of the heat exchanger.

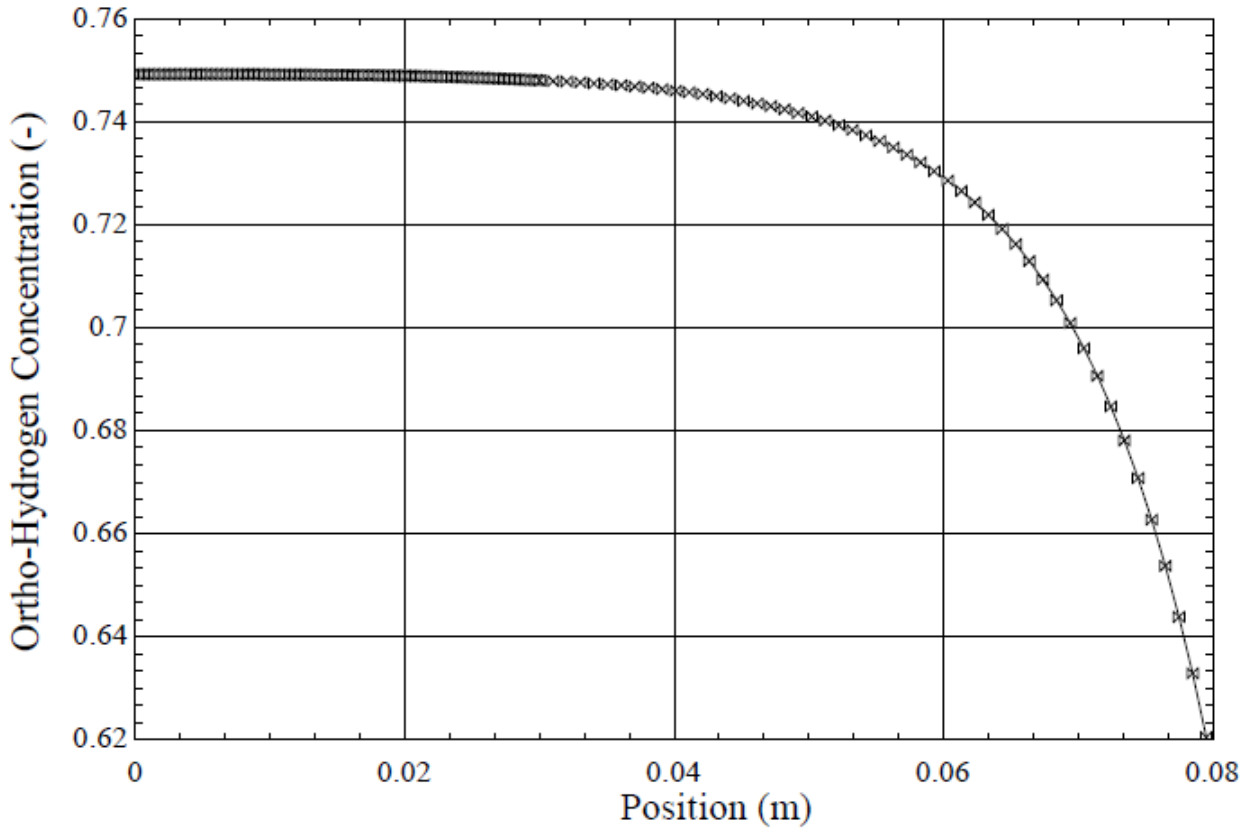

Figure 30: Ortho-hydrogen concentration throughout the upper portion of the heat exchanger.

4.2.3 Quantifying Performance

The final heat exchanger design has an upper stage temperature of 100 K and a lower stage of 25 K. The upper portion of the heat exchanger has four layers while the lower portion has one. Traditionally, the log mean temperature difference or the effectiveness-NTU method is used to quantify heat exchanger performance. Both methods rely on known temperature changes of a hot and a cold fluid in a system with contained flow in a known configuration. In this system, the two fluids are the hydrogen in the heat exchanger and the helium in the cryogenic refrigerator. The temperature profile of the helium is unknown. As a result, it is not possible to define variables as required to use the standard methods to quantify performance. Therefore, a new

metric is defined. The metric used to quantify the heat exchanger performance is shown in Equation 40.

$$\mu = \frac{\dot{Q}_{ideal}}{\dot{Q}_{real}} \tag{40}$$

Where μ is the efficiency metric, Q_{ideal} is the amount of heat that would have to be removed to achieve the final state assuming no losses, and Q_{real} is the actual amount of heat that was removed to reach the final state. In the ideal scenario, μ equals one because the process is reversible, and the real system matches the ideal. Q_{ideal} is calculated by summing the heat needed to be removed from the fluid stream, the heat needed to be removed from the heat exchanger walls, and the heat from the ortho-para reaction to move from the initial to the final state, as shown in Equation 41.

$$\dot{Q}_{ideal} = \dot{Q}_{H2} + \dot{Q}_{HEX} + \dot{Q}_{OP} \tag{41}$$

Where Q_{H2} is the heat removed from the hydrogen stream, Q_{HEX} is the heat removed from the heat exchanger material, and Q_{OP} is the heat from the ortho-para conversion. The equations for Q_{H2}, Q_{HEX}, and Q_{OP} are shown in Equations 42-44.

$$\dot{Q}_{H2} = \dot{m}(h_i - h_f) \tag{42}$$

$$\dot{Q}_{HEX} = \frac{mC_p(T_i - T_f)}{t} \tag{43}$$

$$\dot{Q}_{OP} = \dot{m}h_c f \tag{44}$$

Where $\dot{m}$ is the mass flow rate of the fluid, h_i is the enthalpy of the fluid at the inlet, h_f is the enthalpy of the fluid at the outlet, m is the mass of the heat exchanger material, C_p is the heat capacity of the heat exchanger material at constant pressure, T_i is the initial temperature of the material, T_f is the final temperature of the material, t is the time that is takes the system to reach

steady state, h_c is the heat of conversion (702 kJ/kg), and f is the fraction of the fluid stream converting. The actual amount of heat removed, Q_{real}, is calculated using Equation 46.

$$\dot{Q}_{real} = \dot{S}_{gen} T_f + \dot{Q}_{ideal} \tag{46}$$

Where S_{gen} is the rate of entropy generation in the system. In the final heat exchanger design, assuming three quarters of the fluid stream undergoes conversion and the heat exchanger weighs 2.19 kg, the value of μ is 0.6645.

4.2.4 Heat Exchanger Flange Thickness

The resistance of the heat exchanger flanges must be either equal in the radial and axial directions or favor the radial direction to promote heat transfer towards the Gifford-McMahon cryocooler flange so that heat can be removed from the system effectively. The material properties are constant throughout the flange; therefore, the required flange thickness is a function of the ratio of the cross-sectional areas of the tubes and the flange itself.

There are eight tubes in contact with the upper flange of the heat exchanger, with a total cross-sectional area of 10.10 cm^2. The cross-sectional area of the upper flange is 59.10 cm^2. The flange cross-sectional area is about six times larger than the tubes, therefore there is more resistance to heat transfer axially than radially. Inward heat transfer is favored, which promotes movement towards the Gifford-McMahon cryocooler and is preferable. The resistances do not need to be equalized; therefore, a width of 1 cm is used for ease of manufacturing.

There are eight tubes in contact with the lower flange of the heat exchanger, with a total cross-sectional area of 68.26 cm^2. The cross-sectional area of the lower flange is 36.30 cm^2. The tube area is about twice that of the flange, therefore there is less resistance for heat flow axially than radially. The flange must be 2 cm thick to promote equal resistance in all directions.

4.3 Final Heat Exchanger with Optimum Wall Thickness

To achieve the desired temperature gradients along the length of the heat exchanger, a non-optimum exponent for the wall thickness is used. Increasing the exponent above the optimum results in larger temperature gradients. If the optimum exponent is used, the length of each section must be increased to achieve the gradients. The optimum exponent case also represents a more optimized heat exchanger. The code is run with optimum exponent trends and the lengths are modified so that the temperature gradients are maintained within each section. The diameters are consistent with those in the final design, and the length ratios are maintained between layers. The inlet temperatures to each section, and the mass flow rate, are consistent with those in the final design. The lengths are modified to achieve the same final temperatures as the non-optimum design. The resulting geometries and values are shown in Table 15.

Table 15: Values of final design parameters for heat exchanger with the optimum wall thickness.

Parameter	Value	
	Top Plate to Upper Stage	Upper Stage to Lower Stage
Hydrogen Outlet Temperature	105.3 K	30.94 K
Wall Outlet Temperature	95.92 K	27.99 K
Wall Thickness Equation	th = 0.09 * x[i]^1.3 + 0.000678	th = 0.09 * x[i]^1.3 + 0.00085
Total Length	0.17 m	0.35 m
Rate of Entropy Generation	0.5836 W/K	0.4938 W/K

The total rate of entropy generation is about 30% less than that of the final design. The total length is about one and a half that of the final design. There is a tradeoff between form factor and efficiency. The resulting temperature profiles for the upper and lower portions of the heat exchanger are shown in Figure 31 and Figure 32.

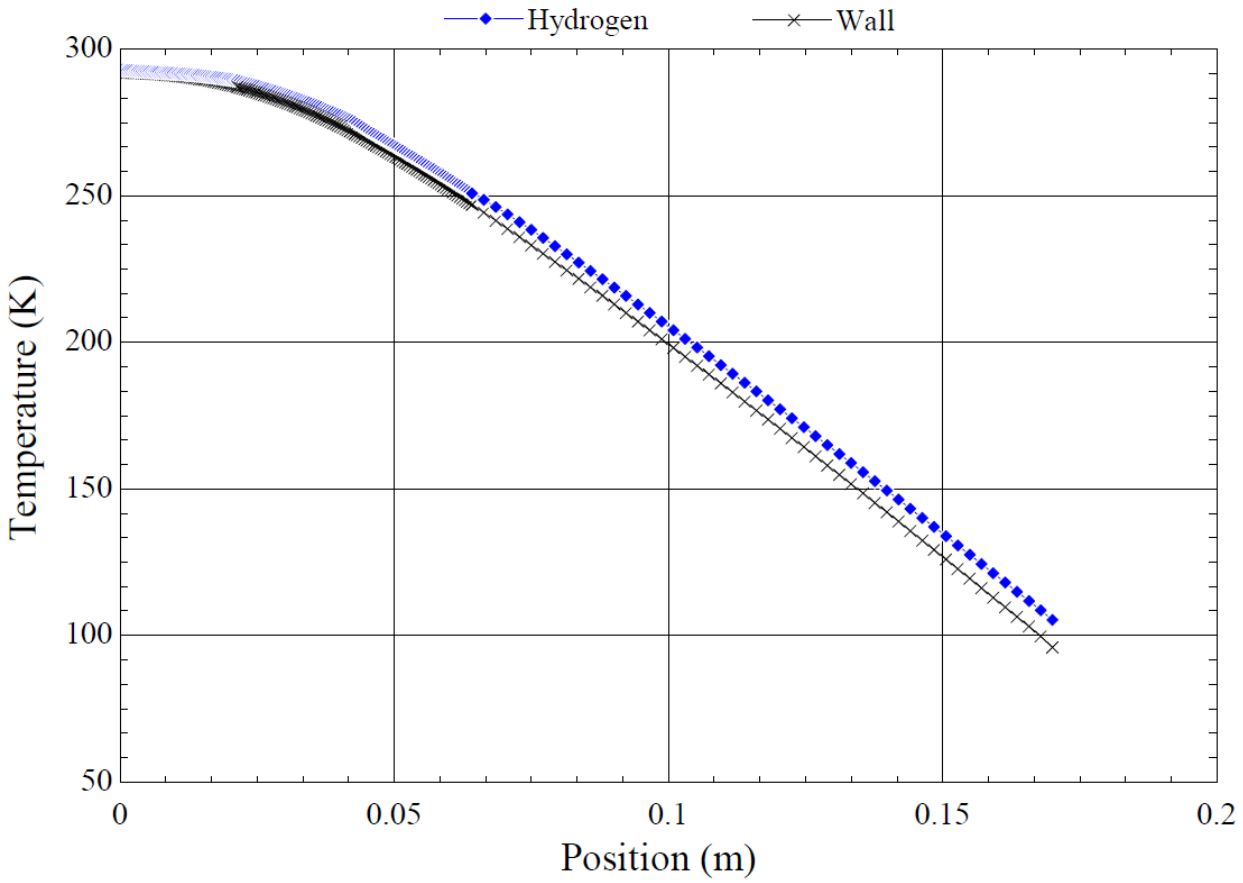

Figure 31: Temperature profiles of the wall and hydrogen stream in the upper portion of the heat exchanger with optimum wall thickness.

The beginning of the temperature profile in the upper portion is slightly concave, but becomes linear after about 0.04 m. The temperature differentials between the curves are smaller than those in the non-optimum design.

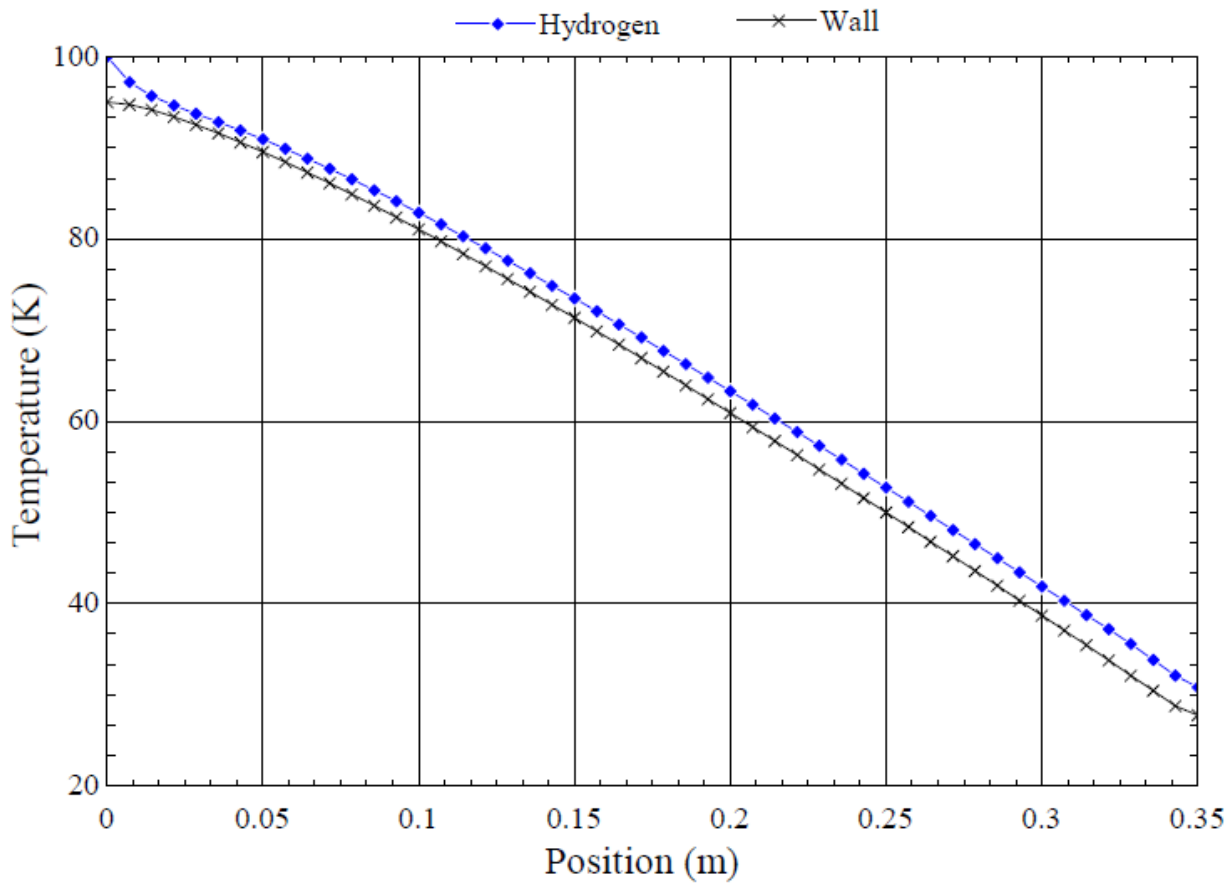

Figure 32: Temperature profiles of the wall and hydrogen stream in the lower portion of the heat exchnager with optimum wall thickness.

The temperature profiles in the lower portion of the heat exchnager are almost linear and the temperature differential between the streams is smaller than that in the non-optimum design. The value of μ with the optimum wall thickness is 0.7506. To determine the mass of the system the mass of the final design was scaled based on tube length, assuming the flanges way 1 kg combined. The value of μ of the final design is about 13% less than that of the design with optimal wall thickness.

4.4 Final Heat Exchanger with Normal Hydrogen

The final heat exchanger is designed assuming the hydrogen is equilibrium at all points, which means that the full conversion is achieved. This represents the minimum flow case, because the heat exchanger must handle the heat required to cool the hydrogen stream, as well as the heat from the exothermic ortho to para hydrogen reaction. It is unlikely that full conversion will be achieved. Therefore, the code is run with normal hydrogen to determine bounds of operation. All of the geometry and system parameters are consistent with the final design in Section 4.2. The resulting outlet temperatures and entropy generation are shown in Table 16.

Table 16: Values of final design parameters for heat exchanger with normal hydrogen and non-optimum design.

Parameter	Value	
	Top Plate to Upper Stage	Upper Stage to Lower Stage
Hydrogen Outlet Temperature	101.6 K	29.40 K
Wall Outlet Temperature	84.68 K	24.43 K
Rate of Entropy Generation	0.6897 W/K	0.2973 W/K

There is minimal change in the outlet temperatures, although there is a slight discontinuity that cannot be resolved without modifying the wall thickness. If this issue were resolved it is expected that the outlet temperature would decrease.

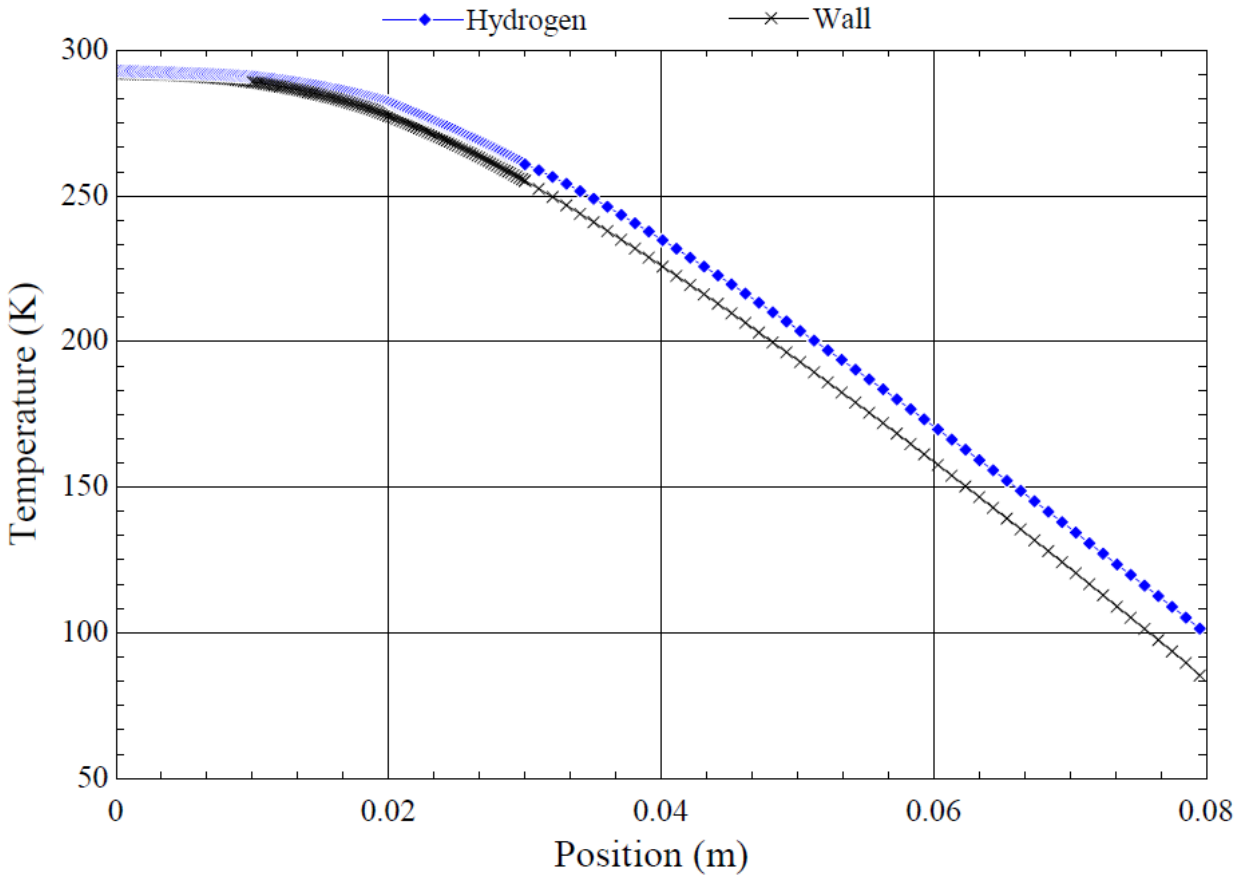

Figure 33: Temperature profiles of the wall and hydrogen stream in the upper portion of the non-optimum heat exchanger with normal hydrogen.

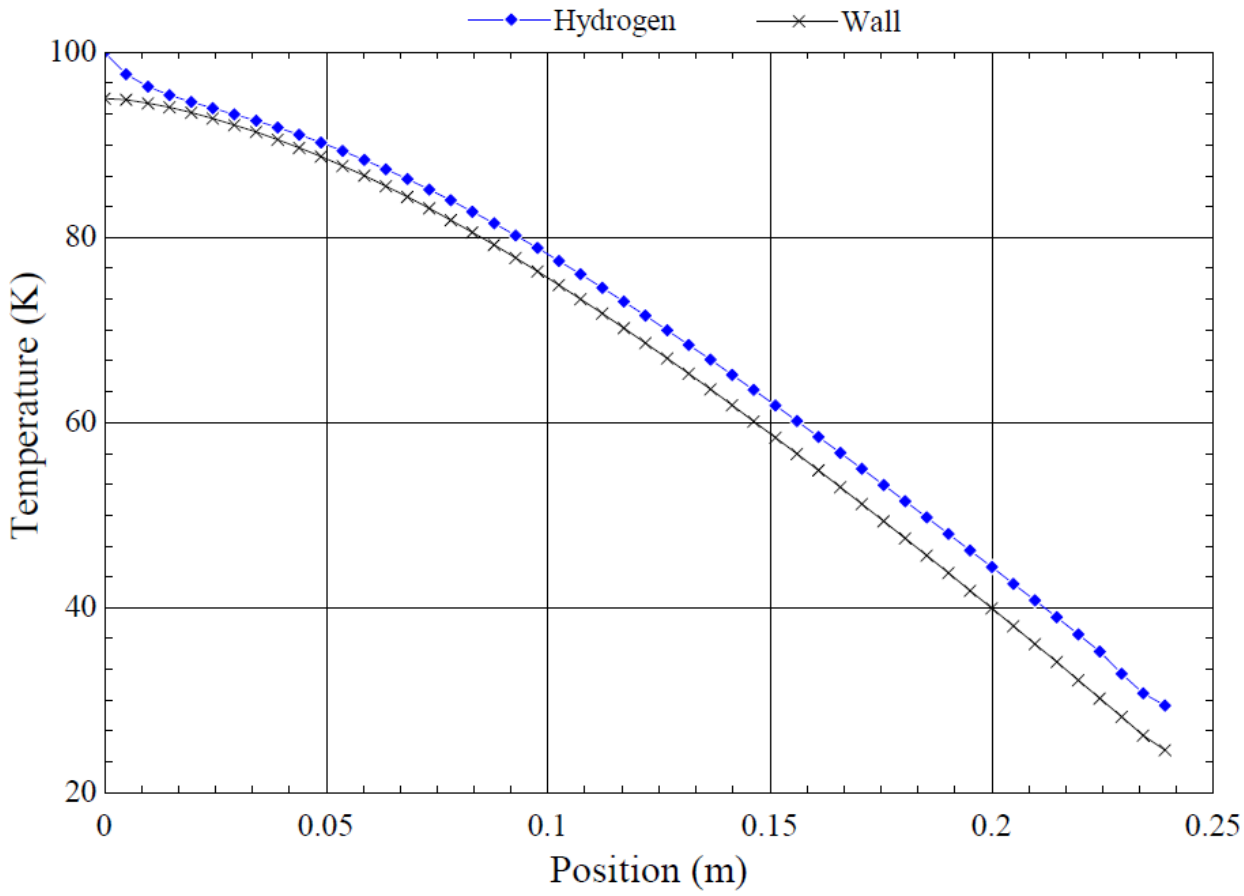

Figure 34: Temperature profiles of the wall and hydrogen stream in the lower portion of the non-optimum heat exchanger with normal hydrogen.

The value of μ for this configuration is 0.7247. This is comparable to the value of μ for the heat exchanger with the optimum wall thickness, which is only 3.5% larger, despite taking into account the complete ortho- to para- conversion of the hydrogen stream.

4.5 Assessing Heat Exchanger Robustness

The heat exchanger code represents an optimum scenario. There will likely be deviations between the ideal and real scenarios. The code is too optimized for convenient parametric analysis; however, the effect of varying variables can be estimated. Table 17 shows the variables

most likely to deviate from ideal, and the predicted results. The variables of concern will generally not cause runaway events. The system is self-limiting, and a new steady state should be achieved.

Table 17: Possible deviations in the system, the effect on the system performance, and whether or not the effect is a concern.

Variable	Deviation	Effect	Concern?
Mass Flow Rate	Higher	The hydrogen outlet temperature will increase, and the heat load of the Gifford-McMahon cryocooler will increase. The heat exchanger could be surrounded with hot hydrogen which would also need to be cooled, representing a parasitic heat load.	Yes, this could decrease the system performance.
	Lower	The hydrogen outlet temperature will decrease, and the heat load of the Gifford-McMahon cryocooler will decrease.	No, the system performance will be maintained.
Thermal Conductivity	Higher	The heat exchanger will be able to transfer heat to the Gifford-McMahon cryocooler flanges more effectively, and the hydrogen outlet temperature will decrease. If not monitored, the mass flow rate will increase.	No, this will cause an increase in performance.
	Lower	The hydrogen outlet temperature will increase, the Gifford-McMahon cryocooler load will increase, and if not monitored the mass flow rate will decrease.	Yes, this will decrease the system performance.
Gifford-McMahon cryocooler Heat Load	Higher	The hydrogen outlet temperature will decrease, and if not monitored the mass flow rate will increase.	No, this will increase system performance.
	Lower	The hydrogen outlet temperature will increase, and if not monitored the mass flow rate will decrease.	Yes, this will decrease system performance.

Hydrogen Purity	Higher or Lower	There will be an unknown change in the heat capacity of the gas stream which will change the outlet temperature and, if not monitored, the mass flow rate.	Yes, this will cause an unknown variation in system performance depending on the contaminant. If the contaminant is water, the heat exchanger passageways could freeze shut, preventing hydrogen flow.
Wall Thickness	Higher	The resistance to axial conduction will decrease, and the efficiency of heat transfer from the heat exchanger to the Gifford-McMahon cryocooler flanges will increase. The hydrogen outlet temperature will decrease, and if not monitored the mass flow rate will increase.	No, this will increase system performance.
	Lower	The resistance to axial conduction will increase, and the efficiency of heat transfer from the heat exchanger to the Gifford-McMahon cryocooler flanges will decrease. The hydrogen outlet temperature will increase, and if not monitored the mass flow rate will decrease.	Yes, this will decrease system performance.
Tube Length	Higher	The resistance to axial conduction will increase, and the efficiency of heat transfer from the heat exchanger to the Gifford-McMahon cryocooler flanges will decrease. The hydrogen outlet temperature will increase, and if not monitored the mass flow rate will decrease.	Yes, this will decrease system performance.
	Lower	The resistance to axial conduction will decrease, and the efficiency of heat transfer from the heat exchanger to the Gifford-McMahon cryocooler flanges will increase. The hydrogen outlet temperature will decrease, and if not monitored the mass flow rate will increase.	No, this will increase system performance.

4.6 Heat Exchanger Made from AlSi10Mg

The heat exchanger is designed to be 3D printed in aluminum 6061, however, despite having the capability to print in this material no company is comfortable printing the part due to the novelty of this new capability. Despite being common in industrial practices, aluminum 6061 is a newer metal for sintering and the geometry of the part is deemed too complex. Instead, the part is printed in AlSi10Mg, an aluminum composite common to printing. The thermal conductivity of AlSi10Mg is known from 323.15 – 773.15 K [65]. The heat exchanger model cannot predict the expected outlet temperatures when a material other than aluminum 6061 is used, however, the trend of the outlet temperatures can be postulated given the relative thermal conductivities. Figure 35 shows the thermal conductivities of aluminum composites common to industry, as well as known values for AlSi10Mg in the x-y and z planes. The thermal conductivity of AlSi10Mg is lower than that of industry accepted composites at all temperatures.

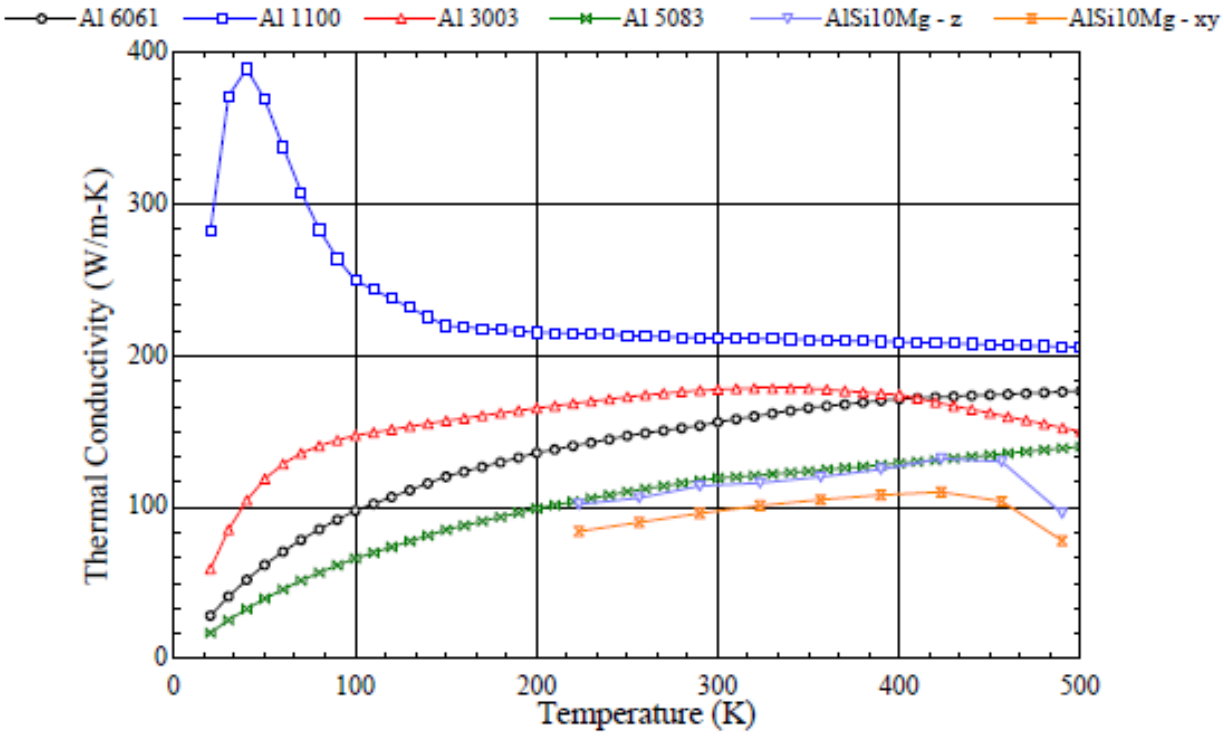

Figure 35: Thermal conductivities of common aluminum composites and AlSi10Mg as a function of temperature.

The thermal conductivity of AlSi10Mg in the x-y plane is the lowest in Figure 35. In the heat exchanger heat travels in the z plane. The thermal conductivity of AlSi10Mg in the z plane is comparable to that of Al 5083. The thermal conductivity is lower than that of Al 6061, so there is more resistance in the axial direction in the 3D printed heat exchanger than is predicted by the model. This indicates that the hydrogen outlet temperature will be higher than theoretically predicted. Thermal conductivity can be approximated as linear, and the thermal conductivity of AlSi10Mg is about 30% less than that of Al 6061. Therefore, it can be assumed that the heat transfer in the printed model will be about 30% less than that of the theoretical model, and the mass flow rate will also decrease by 30%. To achieve the performance predicted in the model

using 6061 aluminum, the cross-sectional tube area would have to be increased to achieve similar values for axial conduction.

Modifications are made to the original heat exchanger design in order to make it printable. Material is added between the tops of the tubes below the upper flange, as well as between the tubes at the beginning of the upper section. Everywhere that the wall thickness is below 1 mm it is increased to the minimum. The lengths are also modified slightly to allow for curvature. All changes result in increased thermal mass and are predicted to increase the outlet temperature of the hydrogen stream. The final heat exchanger CAD rendering is shown in Figure 36-Figure 38. The printed part is shown in Figure 39.

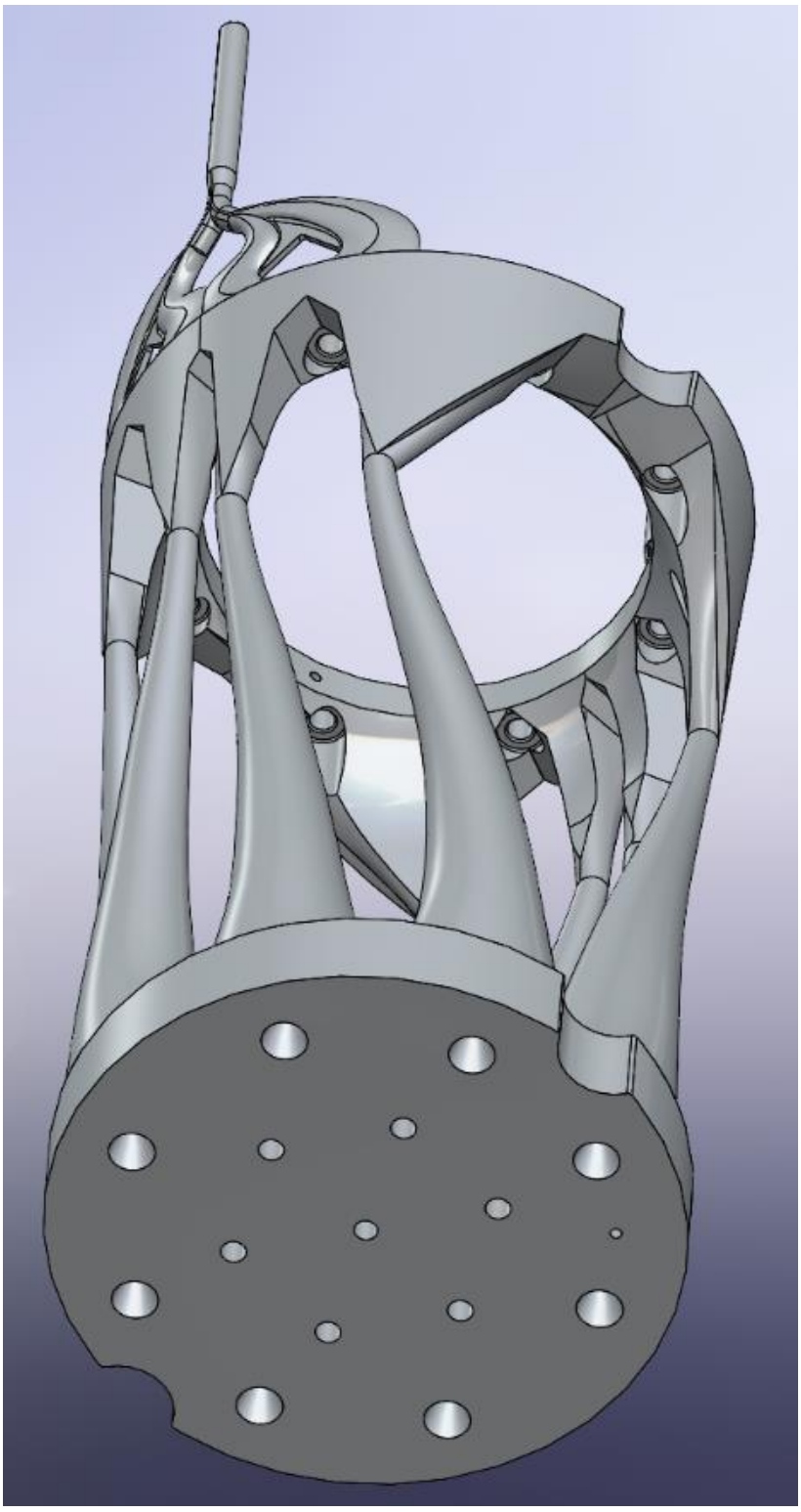

Figure 36: View of the final heat exchanger design from a bottom-up angled view.

Figure 37: View of the final heat exchanger design from a top-down angled view.

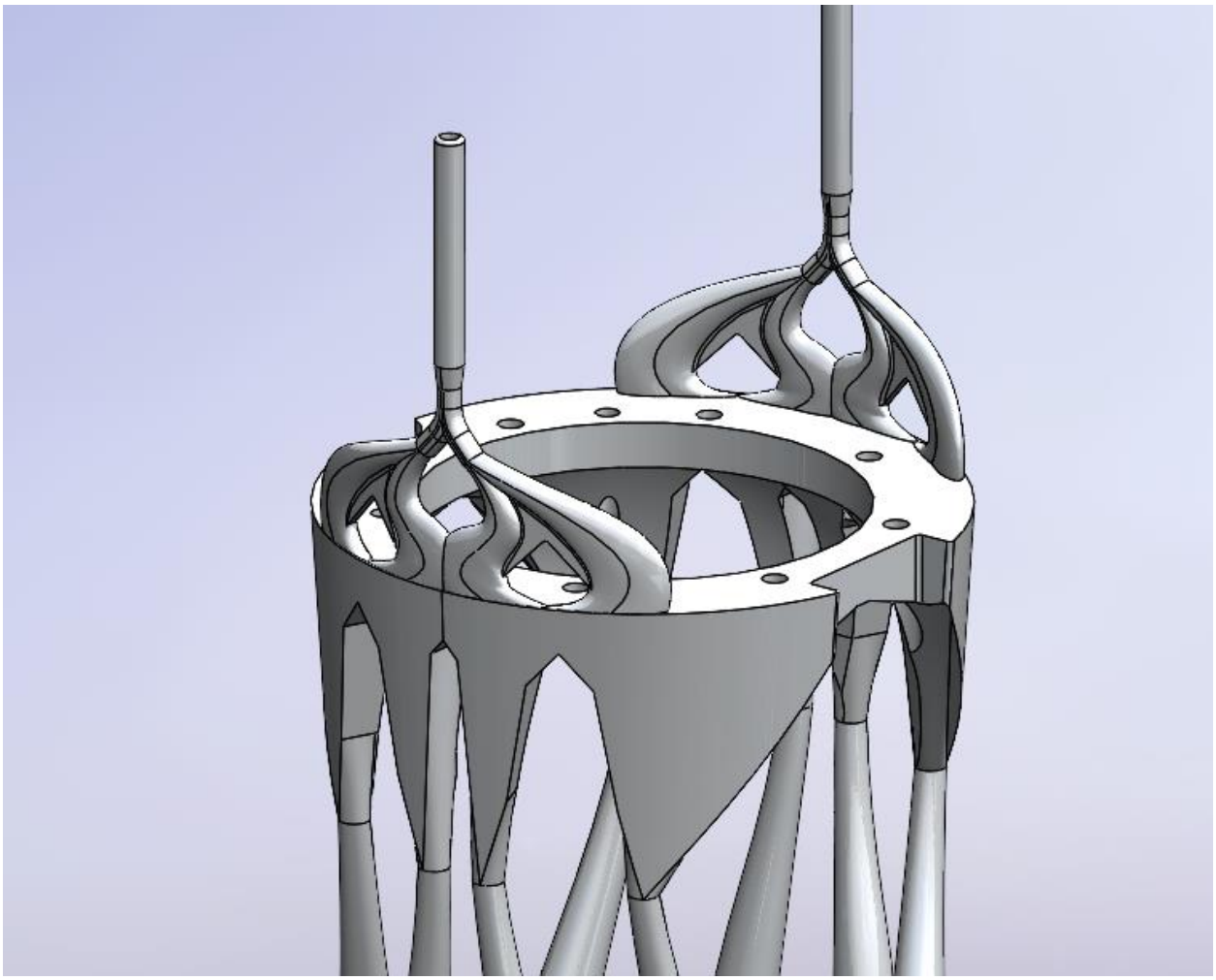

Figure 38: Top half of the heat exchanger, showing the added support material.

Figure 39: Printed part.

4.7 Single Tube Heat Exchanger

A single tube heat exchanger was built for the first iteration of the system. The purposes of the design are speed of manufacturing and guaranteeing effectiveness. The resulting system is a single copper tube wrapped around two 6061 aluminum collars, one of which is attached to the upper stage of a Sumitomo RDK-408D2 Gifford-McMahon cryocooler, and the other to the lower. This is shown in Figure 40.

Figure 40: Single tube heat exchanger mounted on a Sumitomo RDK-408D2 Gifford-McMahon cryocooler.

The copper tube size is 1/8 and has a wall thickness of 0.0008128 m. The length of tubing wrapped around the upper block is 2.26 m and the length around the lower is 1.44 m. Operating the system shows that the upper stage resides at 110 K and the lower at 25 K. The system contains a packed bed catalyst, so the hydrogen is assumed to be equilibrium at all points. The catalyst is Ionex and is 300 μm in diameter. The mass flow rate is determined to be 0.01087 g/s. The temperature gradient along the collars is determined by calculating the heat that needs to be removed from the hydrogen stream to achieve the upper and lower stage temperatures, and then depositing all of the heat into the top of the respective collar and determining the temperature at the far end. The heat that needs to be removed from the hydrogen is calculated using Equation 46.

$$\dot{Q} = \dot{m} c_{int_{avg}} (T_{high} - T_{low}) \tag{46}$$

Where $\dot{Q}$ is the heat to be removed, T_{high} is the inlet temperature of the hydrogen, and T_{low} is the outlet temperature of the hydrogen. It is assumed that all heat travels axially through the collar. The upper collar is an extruded ring, and the lower is an extruded disk. The resistances of the upper and lower collars are calculated using Equations 47 and 48, respectively.

$$R_{upper} = \frac{L_{upper}}{k_{upper} \frac{\pi}{4} (OD_{upper}^2 - ID_{upper}^2)} \tag{47}$$

$$R_{lower} = \frac{L_{lower}}{k_{lower} \frac{\pi}{4} D_{lower}^2} \tag{48}$$

Where R is the resistance and L is the axial length. The temperature at the bottom of the collar is calculated using Equation 49.

$$\dot{Q} = \frac{T_{top} - T_{bottom}}{R} \tag{49}$$

Where T_{top} is the temperature at the top of the collar, T_{bottom} is the temperature at the bottom of the collar, and R is the resistance of the collar. The upper collar has an outer diameter of 0.1281 m, an inner diameter of 0.09 m, and a length of 0.127 m. The lower collar has a diameter of 0.0762 m and a length of 0.1016 m. The hydrogen inlet temperature at the upper stage is 293 K and the outlet temperature is 110 K. The hydrogen inlet temperature at the lower stage is 110 K and the outlet temperature is 25 K. The temperature at the top of each collar is assumed to be the average of the hydrogen inlet and outlet temperatures. Using these values, the temperature gradient across the top collar is found to be 3.905 K and the gradient across the lower collar is found to be 3.381 K. The gradient is small enough that both collars are assumed to be isothermal.

Code iterations are run using isothermal wall conditions, and the established geometry. The outlet temperatures of the wall and hydrogen stream are 110 K at the upper portion and 25 K at the lower portion. The entropy generation in the upper and lower portions of the heat exchanger are determined to be 0.6882 W/K and 1.649 W/K respectively. This yields a total entropy generation of 2.3372 W/K, and the resulting value of μ is 0.5392, assuming a seven hour cool down.

4.7.1 Comparing Single Tube Heat Exchanger to Branching Heat Exchanger

The main variables of interest in a heat exchanger are the mass flow rate, rate of entropy generation, cost, and thermal mass. The value of μ for the single tube heat exchanger is 0.5392. This value of μ is 23.23% smaller than that of the final heat exchanger design and 39.21% smaller than that of the heat exchanger design with the optimum wall thickness. The single tube heat exchanger cost about $4,200, whereas the branching heat exchanger cost $8,633, or twice as much. However, the single tube heat exchanger weighs about 3.15 kg, compared to the branching structure which weighs 2.19 kg. The thermal mass of the single tube design can be estimated at

2002 J/K, whereas that of the branching design is 1392 J/K, or 43.82% less. This is assuming an integrated average heat capacity from 25-293 K of 635.5 J/kg-K for both heat exchangers. Both are modeled as aluminum 6061 because in the single tube design the mass of copper is negligible compared to the mass of aluminum, and the heat capacity for AlSi10Mg over the temperature range is unknown. The drastic decrease in thermal mass of the optimized design increases overall system performance by decreasing cooldown time. In addition, the total length of the final design is only 8.61% the length of the single tube design.

4.8 Mounting the Heat Exchanger to the Gifford-McMahon cryocooler and Applying Catalyst

The heat exchanger is mounted to the Gifford-McMahon cryocooler with 316 stainless steel M5 socket headed cap screws and Belleville washers on the upper and lower flanges. At each flange, 1 mm thick indium foil is placed between the heat exchanger and Gifford-McMahon cryocooler. The indium is thicker than ideal to fill the gap between the upper flange of the heat exchanger and the upper stage of the cryocooler. The screws are tightened as much as possible to minimize resistance from the indium. The two inlets of the heat exchanger are connected to 122 copper tubing, which is joined with a brass Swagelok t-fitting that leads to the top plate. A 316 stainless steel set screw is added to the bottom of both flanges of the Gifford-McMahon cryocooler to aid with future removal of the heat exchanger, after the indium foil diffuses into the Gifford-McMahon cryocooler and heat exchanger. To monitor the temperature profile of the heat exchanger, Lakeshore XDT-670-CU-1.4L temperature sensors are mounted to both flanges of the heat exchanger using 316 stainless steel M3 socket headed cap screws and Belleville washers. A third temperature sensor is mounted on a nylon bracket attached to the thermocouple rake so that the sensor is held in the outlet fluid flow. Ruthenium(iii) chloride is applied to the

inside of the heat exchanger tubes to aid in the ortho- para-hydrogen conversion. Seven layers are added, following the procedures outlined by Jow et al [66]. Weighing the heat exchanger before and after application suggests that 1.13 g of catalyst was deposited. The mounted heat exchanger is shown in Figure 41. A 6061 aluminum spacer was added between the upper flanges of the heat exchanger and the Gifford-McMahon cryocooler because the printed part was shorter than anticipated. Indium foil was laid on both sides of the spacer.

Figure 41: Printed heat exchanger mounted on Sumitomo RDK-415D Gifford-McMahon cryocooler.

A thermocouple rake and two superconducting wires are attached to the bottom of the heat exchanger to determine the liquid level in the dewar, which can be used to help predict the liquefaction rate. A heater block is also added to force boil off when necessary. The thermocouple rake consists of four 6061 aluminum plates mounted on 316 stainless steel rods. On each plate is a temperature sensor identical to those on the heat exchanger, mounted with 316 stainless steel M3 screws, Belleville washers, and lock nuts. There are two MgB_2 superconducting wires, both clad in stainless steel, as a second mode for determining liquid level. The resistance of the wire is correlated to the percentage submerged. The heater block is C110 copper and contains a 50 W heater cartridge that is turned on to force boil off when necessary. All components below the heat exchanger are shown in Figure 42.

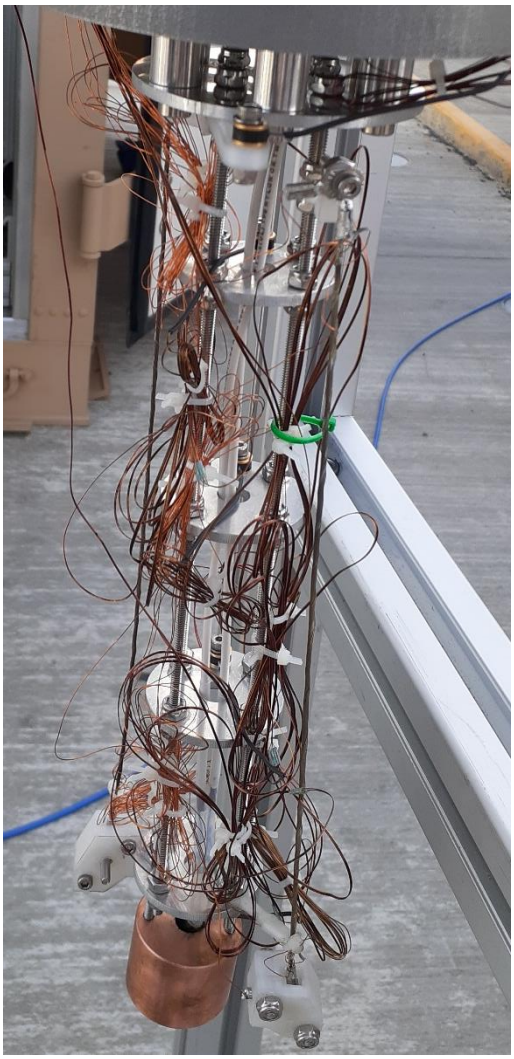

Figure 42: Thermocouple rake, superconducting wires, and heater block suspended below heat exchanger.

The full liquefaction system, which includes everything within the dewar, is shown in Figure 43.

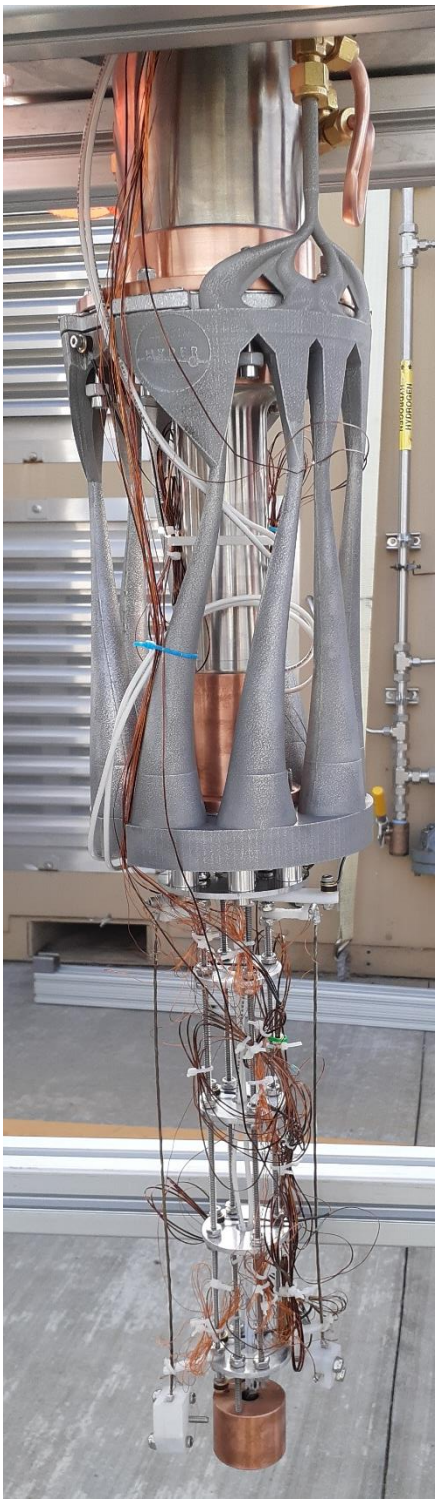

Figure 43: Complete assembly including heat exchanger and all attachments.

The system mounted in the dewar is shown in Figure 44.

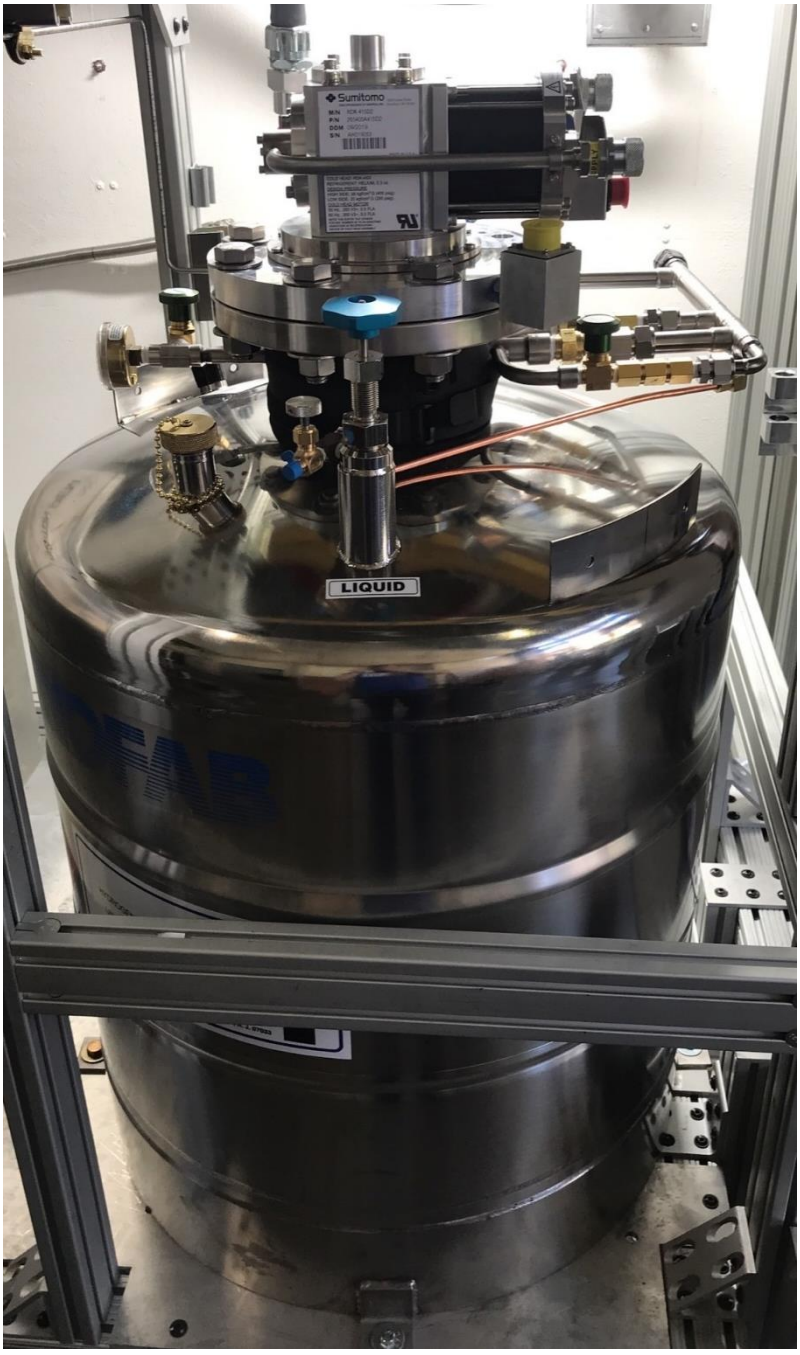

Figure 44: Assembled system mounted in dewar.

The final heat exchanger design has a μ value of 0.6645, the final heat exchanger design with optimal wall thickness has a μ value of 0.7516, and the μ value of a single tube design is 0.5392. μ is a representation of system efficiency, with values closer to one representing a more ideal system. The value of μ for the single tube design is 23.23% smaller than that of the final heat exchanger design and 39.21% smaller than that of the heat exchanger design with the optimum wall thickness. This suggests that the branching heat exchanger, will have vastly improved performance compared to the standard, single tube design.

The heat exchanger with optimal wall thickness and the single tube design require more length to reach the desired outlet temperature. The final design represents a smaller form factor. The thermal mass of the final design is 43.82% less than that of the single tube design, which will further increase system efficiency by requiring less energy for cooldown and maintaining temperature. Outlet temperatures are expected to increase and mass flow rate is expected to decrease as a result of printing the heat exchanger in AlSi10Mg, which has lower thermal conductivity than aluminum 6061 which was used during modeling.

Chapter 5 presents experimental results for the system and draws conclusions about overall performance. The results are discussed, and suggestions for improvements and future work are given.

CHAPTER FIVE: RESULTS AND DISCUSSION

This chapter details the system performance and gives suggestions for future work. It begins by quantifying the system performance using measured liquefaction rates, comparing the outlet stream temperature to that of the lower flange of the heat exchanger, and comparing the predicted temperature profile of the heat exchanger with the measured profile. Next, the results are discussed. Impacts of the system performance are considered and options are given as explanations for the measured results. Finally, system improvements for future work are detailed.

5.1 Quantifying System Performance

The system performance is assessed by comparing the assumed cryocooler capacity from the manufacturer with the measured mass flow rate and the measured temperature profile along the heat exchanger. The mass flow rate is determined by monitoring the pressure drop in a buffer tank, and the temperature profile is estimated using three temperature measurements. A sensor is mounted on each flange, as well as in the outlet flow, and the inlet temperature is assumed to be ambient.

5.1.1 Mass Flow Rate

One of the parameters used to quantify the system performance is the liquefaction rate. The liquefaction rate is equivalent to the mass flow rate because condensation is used to draw mass into the system. To determine the mass flow rate, a buffer tank is installed between the electrolyzer and the inlet to the heat exchanger. The pressure drop within the buffer tank over recorded time intervals is used to determine the rate of liquefaction. Nine data points were recorded, and the buffer tank was recharged twice. The collected data are shown in Table 18. The average temperature during data collection was 292 K and the buffer tank was a t-sized

bottle with an internal volume of 0.0490 m^3. The uncertainty associated with the pressure readings is ±344.74 Pa.

Table 18: Buffer tank and dewar pressure over time.

	Time	Buffer Tank Pressure (kPa)	Dewar Pressure (kPa)
Charge 1	9:00	1354.82	409.55
	9:40	1129.36	410.93
	11:01	668.79	416.44
	11:30	508.83	413.00
Charge 2	13:15	1295.52	413.00
	14:00	1068.69	413.00
	15:00	752.91	415.75
	15:35	575.02	417.13
Charge 3	16:15	1441.69	418.51
	17:24	1121.78	414.37

The mass flow rate can be quantified as the change in mass of gas in the buffer tank over time. Equation 50 is used to calculate the mass of hydrogen in the buffer tank at a given time.

$$PV=ZmRT \tag{50}$$

Where P is the buffer tank pressure, V is the internal volume of the buffer tank, Z is the compressibility factor, m is the mass of hydrogen in the buffer tank, R is the ideal gas constant divided by the molecular weight of hydrogen, and T is the temperature. Next, the liquefaction rate is determined by dividing the change in mass of the hydrogen gas by a measured time interval within the same buffer tank charge. This is shown in Equation 51.

$$\dot{L} = \frac{|m_1 - m_2|}{\Delta t} \tag{51}$$

Where $\dot{L}$ is the rate of liquefaction, m_1 and m_2 are two values for the mass of hydrogen, and Δt is a measured time interval. The calculated values for the liquefaction rate are shown in Table 19.

Table 19: Calculated rates of liquefaction.

	Rate of Liquefaction (g/s)
Charge 1	0.003770
	0.003819
	0.003718
Charge 2	0.003374
	0.003534
	0.003433
Charge 3	0.003100

The average rate of liquefaction is 0.003535 g/s and the standard deviation is 0.0002375 g/s. The calculated average value is 44.19% of the value predicted using 6061 aluminum.

5.1.2 Temperature Profile

To assess heat exchanger performance the fluid outlet temperature is compared to the temperature on the lower flange of the heat exchanger. If the temperatures are similar this is indicative of small temperature gradients, and a minimum entropy system. In addition, the measured temperature profile is compared to the predicted. If the measured temperature at a flange on the heat exchanger varies from the predicted this indicates that the heat lift of the cryogenic refrigerator has also changed, which impacts the mass flow rate. The temperatures of both heat exchanger flanges, as well as the outlet fluid stream, during system cool down and liquefaction, are shown in Figure 45. The system begins to cool after about 125 minutes and reaches steady state operation near 750 minutes. Once steady state is reached, the upper flange of the heat exchanger maintains an average temperature of 58.05 K, the lower flange maintains an average temperature of 26.16 K, and the outlet stream maintains an average temperature of 26.39 K. The measurements are accurate within ±12 mK.

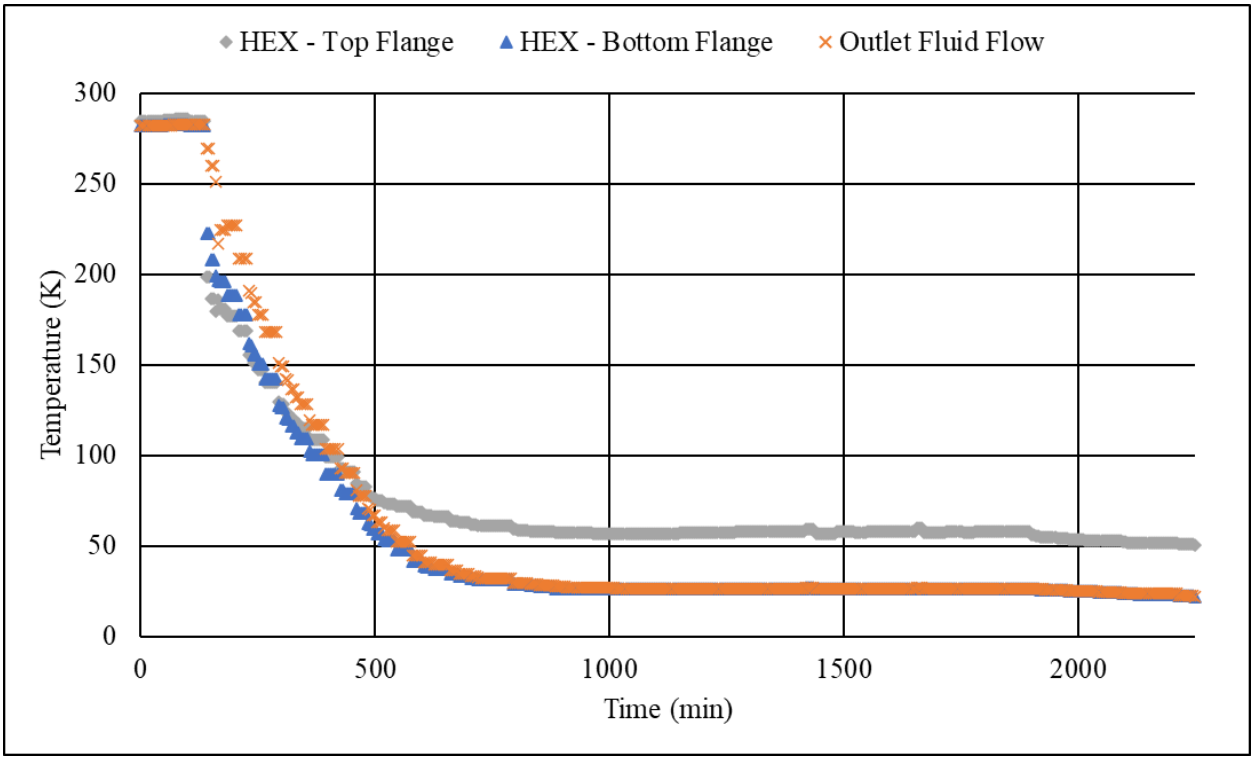

Figure 45: Temperature profiles of the heat exchanger flanges and the outlet stream during cooldown and steady state liquefaction.

At steady state, the difference between the outlet stream temperature and the temperature of the lower flange of the heat exchanger is 0.23 K. This indicates that the temperature profiles of the heat exchanger and the hydrogen flow are likely very similar; therefore, temperature gradients within the system are minimized, as well as the rate of entropy generation.

The measured and predicted temperature profiles of the heat exchanger are shown in Figure 46. In both systems the inlet temperature is assumed to be 293 K. The measured values at each flange are taken as the average values during steady state liquefaction. The curves are spline-fit approximations.

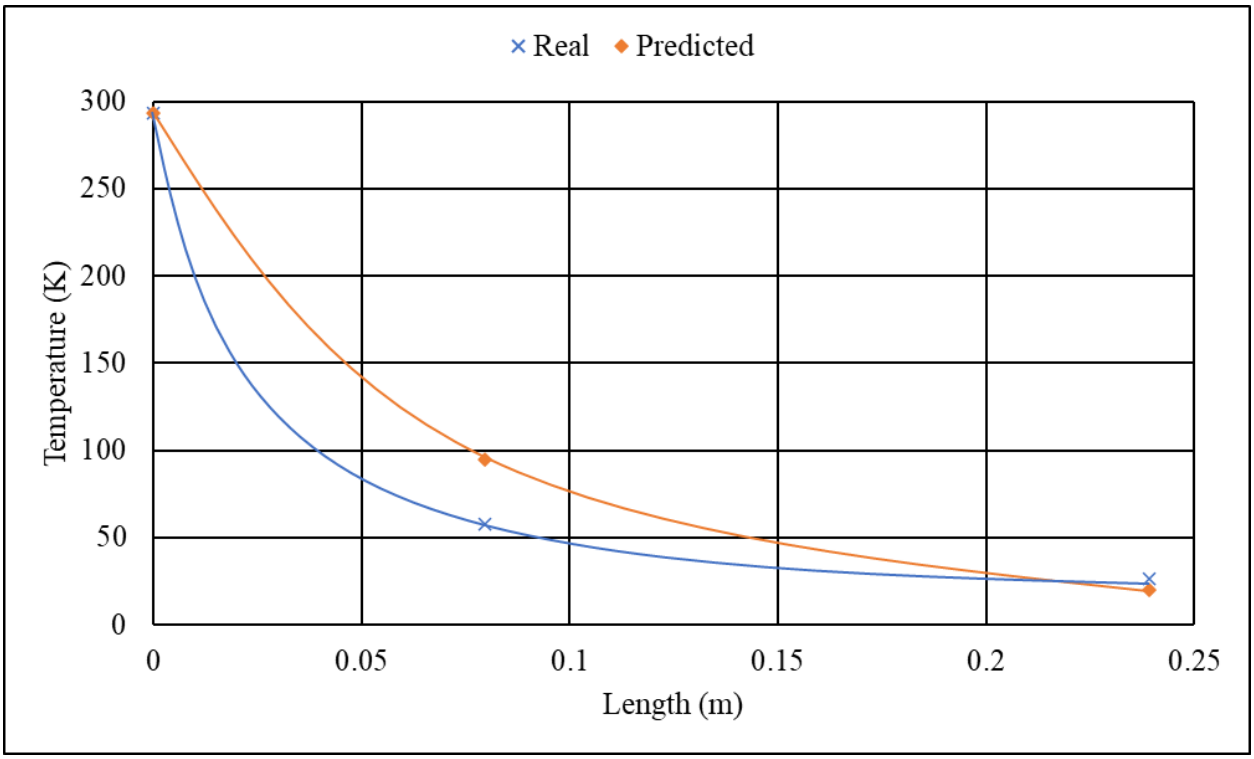

Figure 46: Predicted and measured heat exchanger temperature profiles.

Most of the heat is removed from the system at the upper stage of the cryogenic refrigerator, and the amount of heat that can be lifted is a function of the operating temperature. At higher temperatures, the heat lift increases. The measured temperature at the upper flange of the heat exchanger is about 45 K less than predicted, this corresponds to a lower capacitance temperature of the cryocooler as heat lift correlates with temperature, therefore the cryogenic refrigerator heat lift is lower than expected, and the allowable mass flow rate is decreased. This likely occurred because the lower stage was not able to lift the anticipated 30 W, thermal contraction caused a gap between the upper flange and heat exchanger to reduce heat transfer, or the heat exchanger thermal conductivity was lower than anticipated; all of which would decrease the temperature gradient between the upper and lower stages of the refrigerator. As a result, the temperature

gradient between the top plate and the upper stage would have to increase, lowering the upper stage operating temperature, the associated heat lift, and the allowable mass flow rate.

5.2 Discussion of Results

The mass flow rate and temperature profiles are lower than predicted. The mass flow rate was expected to vary from the predicted results by about 30% due to unknown thermal properties of the material used for construction, and the temperature profile was expected to decrease by an unknown amount. However, the variance is larger than expected, with the mass flow rate less than half of the theoretical value, and the upper stage of the cryogenic refrigerator residing around 58 K rather than 100 K. In addition to unknown thermal properties, the following parameters likely impacted system performance:

- A 6061 aluminum spacer was added between the upper flange of the heat exchanger and the upper stage of the cryogenic refrigerator. The thermal contraction of the spacer was unaccounted for and the shrinkage could have resulted in decreased thermal contact, which would in turn decrease the amount of heat that could be removed from the system. The inclusion of the spacer also necessitated a second indium foil, which would further increase the resistance to heat transfer.
- The ruthenium catalyst has an unknown resistance and thermal conductivity. It is possible that the catalyst forms a strong thermal resistance or has a low conductivity, which would limit the heat transfer that could occur between the heat exchanger and the hydrogen stream.
- The assumption that each stage of the cryocooler only pulls heat from the portion of the heat exchanger prior may have been invalid due to the support material added for part construction. Adding support material decreases axial resistance to heat transfer, which

could allow for communication between the upper and lower stages of the cryogenic refrigerator.

- The lower stage of the cryogenic refrigerator may be lifting less heat than anticipated. This would reduce mass flow rate into the system resulting in a lower upper stage temperature, which would in turn decrease the amount of heat that could be lifted at the upper stage leading to a lower rate of liquefaction.
- There may not be adequate pressure applied to the indium foil, resulting in increased resistance and decreasing the amount of heat that can be lifted by the cryogenic refrigerator.

All of the above reasons may be impacting system performance. The most likely contributing factors are the low thermal conductivity of the heat exchanger material and poor thermal contact at the upper stage of the cryogenic refrigerator due to the addition of the spacer plate.

The effectiveness metric cannot be calculated using the experimental data to compare to the theoretical values. The value of $\dot{Q}_{ideal}$ can be found because the mass flow rate and the mass of the heat exchanger are known. However, $\dot{Q}_{real}$ cannot be calculated because $\dot{S}_{gen}$ is unknown. To calculate $\dot{S}_{gen}$ the temperature profiles of the hydrogen stream and the heat exchanger must be known along the entire length, as well as the pressure profile along the hydrogen stream. When these are known, $\dot{S}_{gen}$ can be calculated using the gradients. In this scenario, the profiles are unknown. Therefore, this metric is not useful for quantifying real results, only theoretical.

5.3 Suggested Improvements for Future Work

In this system, the most significant factors impacting performance are the thermal properties of the heat exchanger and the resistance between the cryogenic refrigerator stages and the heat

exchanger flanges. Therefore, these areas have the most room for improvement. The material used to construct the heat exchanger, AlSi10Mg, has largely unknown thermal properties, and the added spacer likely resulted in decreased thermal contact, and decreased heat lift. The following are suggested improvements:

- Remove support material when possible. This will decrease thermal mass and the possibility of communication between the upper and lower stages of the cryogenic refrigerator.
- Construct the heat exchanger out of a more optimal material, such as aluminum 6061. The ideal material has a high thermal conductivity, a low heat capacity, and a low density. This will maximize heat transfer between the heat exchanger and the hydrogen stream while minimizing the cool down time of the system.
- Investigate the amount of contraction that occurs during printing to determine how the height of the physical part will differ from the height on the model. This should negate the need for a spacer plate and a second indium foil, which will decrease resistance to heat transfer on the upper stage of the cryogenic refrigerator and maximize heat lift. This will also remove the risk of excessive thermal contraction of the spacer plate, guaranteeing adequate pressure on the indium foil.
- Characterize the resistance and thermal properties of ruthenium oxide. It needs to be determined whether or not the catalyst is impacting system performance.
- Quantify the communication between the upper and lower stages of the cryogenic refrigerator to assess the assumption that each stage only pulls heat from the portion of the heat exchanger prior.

- Decrease the lower bound of the inner diameter below 0.003175 m. This will yield a more optimum geometry and turbulent flow, which will increase heat transfer and catalytic activity.

There is much room for improvement in this design, and many future opportunities. Much of this technology depends on material selection and is therefore dependent on advances in the additive manufacturing industry.

The designed heat exchanger, manufactured out of AlSi10Mg, achieves a liquefaction rate of 0.003535 g/s. This is 44.19% of the value predicted using 6061 aluminum. The temperature of the upper flange of the heat exchanger is significantly lower than predicted, which is likely due to poor thermal properties of the heat exchanger, and results in decreased heat lift, lowering the allowable rate of liquefaction. The possibilities for this technology are vast, and highly dependent on material selection and thermal contact between the flanges of the heat exchanger and the upper and lower stages of the cryogenic refrigerator. An opportunity is presented to optimize a notoriously inefficient liquefaction component, increasing overall system efficiency and making small-scale liquefaction economically viable.

Figure 47: Two years in the making, done.

REFERENCES

[1] Biosphere T M A f H a t 2019 When Fossil Fuels Run Out, What Then? : (Stanford)

[2] Runkevicius D 2020 As Tesla Booms, Lithium is Running Out. In: *Forbes,* (Forbes.com)

[3] Power P 2020 Plug Power To Source 100% Renewable Energy From Brookfield Renewable To Fully Power One Of North America's First 'Green' Hydrogen Production Facilities. (plugpower.com: Plug Power, Inc.)

[4] Power P 2021 Plug Power To Build North America's Largest Green Hydrogen Production Facility In Western New York. (plugpower.com: Plug Power, Inc.) p 4

[5] Power P 2021 Plug Power And Sk Group Complete $1.6 Billion Capital Investment To Build Hydrogen Economy In Asian Markets. (plugpower.com: Plug Power, Inc.)

[6] Cooper R K 2021 Plug Power hauls in record $2 billion in stock sale. In: *Albany Business Review,*

[7] 2019 The Future of Hydrogen. ed I E Agency (Paris

[8] California Fuel Cell Partnership 2020 FCEV Sales, FCEB, & Hydrogen Station Data.

[9] Kyodo 2020 Hydrogen to fuel 2020 Olympic flame. In: *the japan times,*

[10] Miftakhov V 2020 Aviation Is The Driving Force Of Hydrogen. In: *Forbes,*

[11] Airbus 2020 Airbus reveals new zero-emission concept aircraft. (Airbus.com

[12] Rezaie H, Ziabasharhagh M and Mafi M A review of hydrogen liquefaction, current situation and its future

[13] Alternative Fuels Data Center 2020 Hydrogen Fueling Station Locations. U.S. Department of Energy)

[14] 2019 Air Liquide committed to producing renewable hydrogen for the West Coast mobility market with new liquid hydrogen plant. In: *Air Liquide,* (airliquide.com

[15] Schwartz J 2011 Advanced Hydrogen Liquefaction Process. ed D o Energy p 4

[16] Elizabeth Conelly M P, Amgad Elgowainy, Chad Hunter 2019 DOE Hydrogen and Fuel Cells Program Record. ed D o Energy p 10

[17] Chen T 2008 Final Report Hydrogen Delivery Infrastructure Options Analysis *DOE award number: DE-FG36–05GO15032*

[18] Baker C and Shaner R 1978 A study of the efficiency of hydrogen liquefaction *International Journal of Hydrogen Energy* **3** 321-34

[19] Krasae-in S, Stang J H and Neksa P 2010 Development of large-scale hydrogen liquefaction processes from 1898 to 2009 *International journal of hydrogen energy* **35** 4524-33

[20] Radebaugh R 2015 The Role of Cryogenics in the U.S. Hydrogen Bomb Program and Vise Versa. (National Institute of Standards and Technology)

[21] Ronquillo R Understanding Heat Exchangers. (Thomasnet.com)

[22] Timmerhaus K and Schoenhals R 1995 *Advances in Cryogenic Engineering*: (Springer) pp 445-62

[23] Lerou P, Veenstra T, Burger J F, ter Brake H J and Rogalla H 2005 Optimization of counterflow heat exchanger geometry through minimization of entropy generation *Cryogenics* **45** 659-69

[24] Ordóñez J C and Bejan A 2000 Entropy generation minimization in parallel-plates counterflow heat exchangers *International Journal of Energy Research* **24** 843-64

[25] Ogulata R and Doba F 1998 Experiments and entropy generation minimization analysis of a cross-flow heat exchanger *International journal of heat and mass transfer* **41** 373-81

[26] Guo J, Cheng L and Xu M 2010 Multi-objective optimization of heat exchanger design by entropy generation minimization *Journal of heat transfer* **132**

[27] Guo J, Cheng L and Xu M 2009 Optimization design of shell-and-tube heat exchanger by entropy generation minimization and genetic algorithm *Applied Thermal Engineering* **29** 2954-60

[28] Farzaneh-Gord M, Ameri H and Arabkoohsar A 2016 Tube-in-tube helical heat exchangers performance optimization by entropy generation minimization approach *Applied Thermal Engineering* **108** 1279-87

[29] Popov D, Fikiin K, Stankov B, Alvarez G, Youbi-Idrissi M, Damas A, Evans J and Brown T 2019 Cryogenic heat exchangers for process cooling and renewable energy storage: A review *Applied Thermal Engineering* **153** 275-90

[30] Ahmadi P, Hajabdollahi H and Dincer I 2011 Cost and entropy generation minimization of a cross-flow plate fin heat exchanger using multi-objective genetic algorithm *Journal of heat transfer* **133**

[31] Babaelahi M, Sadri S and Sayyaadi H 2014 Multi-Objective Optimization of a Cross-Flow Plate Heat Exchanger Using Entropy Generation Minimization *Chemical Engineering & Technology* **37** 87-94

[32] Sahiti N, Krasniqi F, Fejzullahu X, Bunjaku J and Muriqi A 2008 Entropy generation minimization of a double-pipe pin fin heat exchanger *Applied Thermal Engineering* **28** 2337-44

[33] Zhou Y, Zhu L, Yu J and Li Y 2014 Optimization of plate-fin heat exchangers by minimizing specific entropy generation rate *International Journal of Heat and Mass Transfer* **78** 942-6

[34] Xie G, Song Y, Asadi M and Lorenzini G 2015 Optimization of pin-fins for a heat exchanger by entropy generation minimization and constructal law *Journal of Heat Transfer* **137**

[35] Industries C Brazed Aluminum Heat Exchangers. (ChartIndustries.com: Chart Industries)

[36] Berstad D O, Stang J H and Nekså P 2010 Large-scale hydrogen liquefier utilising mixed-refrigerant pre-cooling *International journal of hydrogen energy* **35** 4512-23

[37] Kanoglu M, Yilmaz C and Abusoglu A 2016 Geothermal energy use in absorption precooling for Claude hydrogen liquefaction cycle *international journal of hydrogen energy* **41** 11185-200

[38] Krasae-In S, Stang J H and Neksa P 2010 Exergy analysis on the simulation of a small-scale hydrogen liquefaction test rig with a multi-component refrigerant refrigeration system *International journal of hydrogen energy* **35** 8030-42

[39] Quack H 2002 Conceptual design of a high efficiency large capacity hydrogen liquefier. In: *AIP Conference Proceedings*: American Institute of Physics) pp 255-63

[40] Cardella U, Decker L, Sundberg J and Klein H 2017 Process optimization for large-scale hydrogen liquefaction *International Journal of Hydrogen Energy* **42** 12339-54

[41] Greenspan J 1932 The Preservation and Determination of Sodium Sulfocyanate *Journal of the American Chemical Society* **54** 2850-

[42] Dawson V P 2004 *Taming liquid hydrogen: the Centaur upper stage rocket, 1958-2002* vol 4230: National Aeronautics and Space Administration, Office of External Relations)

[43] Farkas A 1935 *Orthohydrogen, parahydrogen and heavy hydrogen*: CUP Archive)

[44] Truhlar D G 1976 Interpretation of ortho–para hydrogen conversion *The Journal of Chemical Physics* **65** 1008-10

[45] Larsen A, Simon F and Swenson C 1948 The Rate of Evaporation of Liquid Hydrogen Due to the Ortho-Para Hydrogen Conversion *Review of Scientific Instruments* **19** 266-9

[46] Hutchinson H L 1966 Analysis of catalytic ortho-parahydrogen reaction mechanisms

[47] Pepe V R, Rocha L A and Miguel A F 2017 Optimal branching structure of fluidic networks with permeable walls *BioMed research international* **2017**

[48] Bejan A 2016 *Advanced engineering thermodynamics*: John Wiley & Sons)

[49] Bejan A 1997 Constructal tree network for fluid flow between a finite-size volume and one source or sink *Revue generale de thermique* **36** 592-604

[50] Klein G F N a S A 2009 *Heat Transfer*: Cambridge University Press)

[51] J. Leachman R J, S. Penoncello, E. Lemmon 2009 Fundamental Equations of State for Parahydrogen, Normal Hydrogen, and Orthohydrogen.

[52] Muzny C D, Huber M L and Kazakov A F 2013 Correlation for the viscosity of normal hydrogen obtained from symbolic regression *Journal of Chemical & Engineering Data* **58** 969-79

[53] Assael M J, Assael J-A, Huber M L, Perkins R A and Takata Y 2011 Correlation of the Thermal Conductivity of Normal and Parahydrogen from the Triple Point to 1000 K and up to 100 MPa *Journal of Physical and Chemical Reference Data* **40** 033101

[54] 2019 Engineering Equation Solver.

[55] Group S C RDK-415D 4K Cryocooler Series.

[56] Mann D 1977 LNG Materials and Fluids. ed C D National Bureau of Standards

[57] Veres H Thermal Properties Database for Materials at Cryogenic Temperatures.

[58] Touloukian Y 1965 Recommended values of the Thermophysical Properties of eight Alloys, Major Constituents and their Oxides. ed P University

[59] 2020 In: *Pressure Loss From Fittings - Excess Head (K) Method*, (Neutrium.net: Native Dynamics)

[60] Group S C 2019 SRDK-415D Cold Head Capacity Map (60 Hz). ed RDK-415D_Capacity_Map.pdf

[61] Group S C 2012 RDK-415D Cold Head Outline Drawing.

[62] Ekin J 2006 Thermal Conductance of Solid-Solid Joints. ed F wcap (Experimental Techniques in Low Temperature Measurements: Oxford University Press)

[63] Material Properties: 6061-T6 Aluminum (UNS A96061). ed NIST

[64] Material Properties: 316 Stainless. ed N I o S a Technology

[65] Yang P, Stefan D K, Rodriguez M A, Bradley D R, Griego J, Deibler L A, Rodelas J, Carroll J and Jared B H 2016 Thermal Characterization of AlSi10Mg Alloy Fabricated by Selective Laser Melting. Sandia National Lab.(SNL-NM), Albuquerque, NM (United States))

[66] T. Jow J-P S 1997 Amorphous Thin Film Electrode Materials from Hydrous Metal Oxides. ed T U S o America (The United States of America p 10

[67] i3Dmfg EOS Aluminum AlSi10Mg Material Data Sheet.

APPENDIX

7.1 AlSi10Mg Composition [67]

Material	Weight Percentage
Aluminum (Al)	Balance
Silicon (Si)	9 – 11
Iron (Fe)	0.55
Copper (Cu)	0.05
Manganese (Mn)	0.45
Magnesium (Mg)	0.2 – 0.45
Nickel (Ni)	0.05
Zinc (Zn)	0.10
Lead (Pb)	0.05
Tin (Sn)	0.05
Titanium (Ti)	0.15

7.2 Code for Isothermal Tube Without a Wall

```
Procedure tempprofile(L,T :T_s)
T_s = -1887*L + 293                    //surface temperature profile
End check

{L2 = 0.01
L3 = 0.01
L4 = 0.01
L5 = 0.01
ID1 = 0.008
ID2 = 0.008
ID3 = 0.008
ID4 = 0.008
ID5 = 0.008}

"Constants"
H$ = 'Hydrogen'                        //fluid
RelRough = 0.01 [-]                    //relative roughness
R = 8.314 [J/kg-K]                     //universal gas constant
B = 4 [-]                              //number of times branching will occur
L_tot = 0.142 [m]                      //total section length
L_tot = L1 + L2 + L3 + L4 + L5         //length components

"Sgen for system"
 S_gen_tot = S_gen_tot1 + S_gen_tot2 + S_gen_tot3 + S_gen_tot4 + S_gen_tot5
    //total entropy generation in the system
```

```
"First Node"                                    //nodes are defined as branch clusters (first
node is one branch)
A_s1 = PI*ID1*delta_x1                          //surface area for heat transfer
A_c1 = (PI/4)*ID1^2                             //cross sectional area

T1[1] = 293 [K]                                 //assumed, room/ambient temp
P1[1] = 94 [psi]*convert(psi,Pa)                //inlet pressure based on electrolyzer output
h1[1] = enthalpy(H$, T=T1[1], P=P1[1])          //initial enthalpy

m_dot[1] = 0.000012 [kg/s]                      //intial mass flow rate, based on electrolyzer
and insitu data
branches[1] = 1 [-]                             //number of branches/segments in first node

"Branches/Segments in each node"
Duplicate i=1, B
branches[i+1] = branches[i]*2                   //number of branches in each layer
End

"Mass Flow Rate in each branch in each node"
Duplicate i=1, B
m_dot[i+1] = m_dot[1]/branches[i+1]             //mass flow rate in each layer
End


"Incremental Network for each segment"          //only looking at one branch within each
node
N = 100 [-]                                     //total number of nodes

    "Create delta x"
    delta_x1 = L1/(N-1)                         //establish nodal network
    x1[1] = 0 [m]
    Duplicate i=1, N-1
    x1[i+1] = x1[i] + delta_x1
    End

Call tempprofile(x1[N], T1[1]: T_s1)            //surface temperature for the layer
Duplicate i=1,N-1

Call pipeflow(H$,T1[i],P1[i],m_dot[1],ID1,L1,RelRough:h_T1[i], h_H1[i] ,DELTAP1[i],
Nusselt_T1[i], f1[i], Re1[i])                   //Find pressure drop and convection
coefficient
P1[i+1] = P1[i] - DELTAP1[i]                    //determine next pressure

Q_dot1[i] = (T_avg1[i] - T_s1)/R1[i]            //heat transfer out of the section
```

```
T_avg1[i] = (T1[i] + T1[i+1])/2                    //average temperature in the section
R1[i] = 1/(h_T1[i] * A_s1)                         //resistance within the system from internal
convection

Q_dot1[i] = m_dot[1]*(DELTA_H1[i])                 //heat transfer from enthalpy difference
    h1[i+1]=h1[i]-DELTA_H1[i]                      //determine next enthalpy
    T1[i+1]=temperature(H$,h=h1[i+1],P=P1[i+1])
    //determine next temperature


del_P1[i] = P1[i] - P1[i+1]                        //pressure difference
S_gen_P1[i] = m_dot[1]*R*(del_P1[i]/P1[i])         //entropy generation from pressure

del_T1[i] = T1[i+1] - T_s1                         //temperature difference
S_gen_T1[i] = m_dot[1]*Cp1[i]*(del_T1[i]/T_s1)     //entropy generation from temperature
difference
Cp1[i] =  ((23.16383-22.2923*ln(T1[i])+8.085544*ln(T1[i])^2-
1.30587*ln(T1[i])^3+0.079239*ln(T1[i])^4)/(1-0.93421*ln(T1[i])+0.328506*ln(T1[i])^2-
0.05149*ln(T1[i])^3+0.00304*ln(T1[i])^4))* (1/molarmass(H$)) * 1000
    //equilibrium heat capacity of hydrogen
End

S_gen_P1 = sum(S_gen_P1[i], i=1,N-1)               //total entropy generation from pressure
S_gen_T1 = sum(S_gen_T1[i], i=1, N-1)              //total entropy generation from temperature

"Sgen total"
S_gen_tot1 = S_gen_P1 + S_gen_T1                   //total entropy generation in the layer
//END NODE 1//

"Second Node"                                      //nodes are defines are branch clusters (first
node is one branch)
A_s2 = PI*ID2*delta_x2                             //surface area for heat transfer -> will
have to be branch
A_c2 = (PI/4)*ID2^2                                //cross sectional area

T2[1] = T1[N]
P2[1] = P1[N]
h2[1] = enthalpy(H$, T=T2[1], P=P2[1])             //initial enthalpy

delta_x2 = L2/(N-1)
x2[1] = L1
Duplicate i=1, N-1
    x2[i+1] = x2[i] + delta_x2
    End
```

***Call* tempprofile**(x2[N], T2[1]: T_s2)
Duplicate i=1,N-1

"Find pressure drop and convection coefficient"
***Call* pipeflow**(H$,T2[i],P2[i],m_dot[2],ID2,L2,RelRough:h_T2[i], h_H2[i] ,DELTAP2[i], Nusselt_T2[i], f2[i], Re2[i])

"Find incremental pressure"
P2[i+1] = P2[i] - DELTAP2[i]

Q_dot2[i] = (T_avg2[i] - T_s2)/R2[i]
T_avg2[i] = (T2[i] + T2[i+1])/2
R2[i] = 1/(h_T2[i] * A_s2)

Q_dot2[i] = m_dot[2]*(DELTA_H2[i])
    h2[i+1]=h2[i]-DELTA_H2[i] //next enthalpy
    T2[i+1]=**temperature**(H$,***h***=h2[i+1],***P***=P2[i+1])

del_P2[i] = P2[i] - P2[i+1]
S_gen_P2[i] = m_dot[2]*R*(del_P2[i]/P2[i])

del_T2[i] = T2[i+1] - T_s2
S_gen_T2[i] = m_dot[2]*Cp2[i]*(del_T2[i]/T_s2)
Cp2[i] = ((23.16383-22.2923***ln**(T2[i])+8.085544***ln**(T2[i])^2-1.30587***ln**(T2[i])^3+0.079239***ln**(T2[i])^4)/(1-0.93421***ln**(T2[i])+0.328506***ln**(T2[i])^2-0.05149***ln**(T2[i])^3+0.00304***ln**(T2[i])^4))* (1/**molarmass**(H$)) * 1000
End

S_gen_P2 = sum(S_gen_P2[i], i=1,N-1) //Sgen from pressure
S_gen_T2 = sum(S_gen_T2[i], i=1, N-1) //Sgen from temp

"Sgen total"
S_gen_tot2 = (S_gen_P2 + S_gen_T2)*branches[2]
//END NODE//

"Third Node" //nodes are defines are branch clusters (first node is one branch)
A_s3 = PI*ID3*delta_x3 **//surface area for heat transfer -> will have to be branch**
A_c3 = (PI/4)*ID3^2 **//cross sectional area**

T3[1] = T2[N]
P3[1] = P2[N]

```
h3[1] = enthalpy(H$, T=T3[1], P=P3[1])              //initial enthalpy


delta_x3 = L3/(N-1)
x3[1] = L1 + L2
Duplicate i=1, N-1
    x3[i+1] = x3[i] + delta_x3
    End

Call tempprofile(x3[N], T3[1]: T_s3)
Duplicate i=1,N-1

"Find pressure drop and convection coefficient"
Call pipeflow(H$,T3[i],P3[i],m_dot[3],ID3,L3,RelRough:h_T3[i], h_H3[i] ,DELTAP3[i],
Nusselt_T3[i], f3[i], Re3[i])

"Find incremental pressure"
P3[i+1] = P3[i] - DELTAP3[i]

Q_dot3[i] = (T_avg3[i] - T_s3)/R3[i]
T_avg3[i] = (T3[i] + T3[i+1])/2
R3[i] = 1/(h_T3[i] * A_s3)

Q_dot3[i] = m_dot[3]*(DELTA_H3[i])
    h3[i+1]=h3[i]-DELTA_H3[i]                       //next enthalpy
    T3[i+1]=temperature(H$,h=h3[i+1],P=P3[i+1])

del_P3[i] = P3[i] - P3[i+1]
S_gen_P3[i] = m_dot[3]*R*(del_P3[i]/P3[i])

del_T3[i] = T3[i+1] - T_s3
S_gen_T3[i] = m_dot[3]*Cp3[i]*(del_T3[i]/T_s3)
Cp3[i] =  ((23.16383-22.2923*ln(T3[i])+8.085544*ln(T3[i])^2-
1.30587*ln(T3[i])^3+0.079239*ln(T3[i])^4)/(1-0.93421*ln(T3[i])+0.328506*ln(T3[i])^2-
0.05149*ln(T3[i])^3+0.00304*ln(T3[i])^4))* (1/molarmass(H$)) * 1000
End

S_gen_P3 = sum(S_gen_P3[i], i=1,N-1)            //Sgen from pressure
S_gen_T3 = sum(S_gen_T3[i], i=1, N-1)           //Sgen from temp

"Sgen total"
S_gen_tot3 = (S_gen_P3 + S_gen_T3)*branches[3]
//END NODE//
```

```
"Fourth Node"                                   //nodes are defines are branch clusters (first
node is one branch)
A_s4 = PI*ID4*delta_x4                          //surface area for heat transfer -> will
have to be branch
A_c4 = (PI/4)*ID4^2                             //cross sectional area

T4[1] = T3[N]
P4[1] = P3[N]
h4[1] = enthalpy(H$, T=T4[1], P=P4[1])          //initial enthalpy


delta_x4 = L4/(N-1)
x4[1] = L1 + L2 + L3
Duplicate i=1, N-1
    x4[i+1] = x4[i] + delta_x4
    End


Call tempprofile(x4[N], T4[1]: T_s4)
Duplicate i=1,N-1

"Find pressure drop and convection coefficient"
Call pipeflow(H$,T4[i],P4[i],m_dot[4],ID4,L4,RelRough:h_T4[i], h_H4[i] ,DELTAP4[i],
Nusselt_T4[i], f4[i], Re4[i])

"Find incremental pressure"
P4[i+1] = P4[i] - DELTAP4[i]

Q_dot4[i] = (T_avg4[i] - T_s4)/R4[i]
T_avg4[i] = (T4[i] + T4[i+1])/2
R4[i] = 1/(h_T4[i] * A_s4)

Q_dot4[i] = m_dot[4]*(DELTA_H4[i])
    h4[i+1]=h4[i]-DELTA_H4[i]                   //next enthalpy
    T4[i+1]=temperature(H$,h=h4[i+1],P=P4[i+1])

del_P4[i] = P4[i] - P4[i+1]
S_gen_P4[i] = m_dot[4]*R*(del_P4[i]/P4[i])

del_T4[i] = T4[i+1] - T_s4
S_gen_T4[i] = m_dot[4]*Cp4[i]*(del_T4[i]/T_s4)
Cp4[i] =  ((23.16383-22.2923*ln(T4[i])+8.085544*ln(T4[i])^2-
1.30587*ln(T4[i])^3+0.079239*ln(T4[i])^4)/(1-0.93421*ln(T4[i])+0.328506*ln(T4[i])^2-
0.05149*ln(T4[i])^3+0.00304*ln(T4[i])^4))* (1/molarmass(H$)) * 1000
End
```

```
S_gen_P4 = sum(S_gen_P4[i], i=1,N-1)          //Sgen from pressure
S_gen_T4 = sum(S_gen_T4[i], i=1, N-1)         //Sgen from temp


"Sgen total"
S_gen_tot4 = (S_gen_P4 + S_gen_T4)*branches[4]
//END NODE//

"Fifth Node"                                  //nodes are defines are branch clusters (first
node is one branch)
A_s5 = PI*ID5*delta_x5                        //surface area for heat transfer -> will
have to be branch
A_c5 = (PI/4)*ID5^2                           //cross sectional area

T5[1] = T4[N]
P5[1] = P4[N]
h5[1] = enthalpy(H$, T=T5[1], P=P5[1])        //initial enthalpy


delta_x5 = L5/(N-1)
x5[1] = L1 + L2 + L3 + L4
Duplicate i=1, N-1
    x5[i+1] = x5[i] + delta_x5
    End


Call tempprofile(x5[N], T5[1]: T_s5)
Duplicate i=1,N-1

"Find pressure drop and convection coefficient"
Call pipeflow(H$,T5[i],P5[i],m_dot[5],ID5,L5,RelRough:h_T5[i], h_H5[i] ,DELTAP5[i],
Nusselt_T5[i], f5[i], Re5[i])

"Find incremental pressure"
P5[i+1] = P5[i] - DELTAP5[i]

Q_dot5[i] = (T_avg5[i] - T_s5)/R5[i]
T_avg5[i] = (T5[i] + T5[i+1])/2
R5[i] = 1/(h_T5[i] * A_s5)

Q_dot5[i] = m_dot[5]*(DELTA_H5[i])
    h5[i+1]=h5[i]-DELTA_H5[i]                 //next enthalpy
    T5[i+1]=temperature(H$,h=h5[i+1],P=P5[i+1])
```

```
del_P5[i] = P5[i] - P5[i+1]
S_gen_P5[i] = m_dot[5]*R*(del_P5[i]/P5[i])

del_T5[i] = T5[i+1] - T_s5
S_gen_T5[i] = m_dot[5]*Cp5[i]*(del_T5[i]/T_s5)
Cp5[i] =  ((23.16383-22.2923*ln(T5[i])+8.085544*ln(T5[i])^2-
1.30587*ln(T5[i])^3+0.079239*ln(T5[i])^4)/(1-0.93421*ln(T5[i])+0.328506*ln(T5[i])^2-
0.05149*ln(T5[i])^3+0.00304*ln(T5[i])^4))* (1/molarmass(H$)) * 1000
End

S_gen_P5 = sum(S_gen_P5[i], i=1,N-1)          //Sgen from pressure
S_gen_T5 = sum(S_gen_T5[i], i=1, N-1)         //Sgen from temp


"Sgen total"
S_gen_tot5 = (S_gen_P5 + S_gen_T5)*branches[5]
//END NODE//
```

7.3 Code for Tube with a Linear Temperature Gradient and Without a Wall

```
Procedure tempprofile(L :T_s)
T_s = -1887*L + 293                           //surface temperature profile
End check


"Constants"
H$ = 'Hydrogen'                               //fluid
RelRough = 0.01 [-]                           //relative roughness
R = 8.314 [J/kg-K]                            //universal gas constant
B = 3 [-]                                     //number of times branching occurs
L_tot = 0.142 [m]                             //total section length
L_tot = L1 + L2 + L3 + L4                     //length components

"Sgen for system"
 S_gen_tot = S_gen_tot1 + S_gen_tot2 + S_gen_tot3 + S_gen_tot4
    //total entropy generation in the system

"First Node"                                  //nodes are defines are branch clusters (first
node is one branch)
A_s1 = PI*ID1*delta_x1                        //surface area for heat transfer
A_c1 = (PI/4)*ID1^2                           //cross sectional area

T1[1] = 293 [K]                               //assumed, room/ambient temp
P1[1] = 94 [psi]*convert(psi,Pa)              //inlet pressure based on electrolyzer
h1[1] = enthalpy(H$, T=T1[1], P=P1[1])        //initial enthalpy
```

```
m_dot[1] = 0.000012 [kg/s]                    //intial mass flow rate
branches[1] = 1 [-]                           //number of branches/segments layer one

"Branches/Segments in each node"
Duplicate i=1, B
branches[i+1] = branches[i]*2                 //number of branches in each layer
End

"Mass Flow Rate in each branch in each node"
Duplicate i=1, B
m_dot[i+1] = m_dot[1]/branches[i+1]           //mass flow rate in each layer
End


"Incremental Network for each segment"        //only looking at one branch within each
node
N = 100 [-]                                   //total number of nodes

    "Create delta x"
    delta_x1 = L1/(N-1)                       //establish nodal network
    x1[1] = 0 [m]
    Duplicate i=1, N-1
    x1[i+1] = x1[i] + delta_x1
    End

Duplicate i=1,N-1
Call tempprofile(x1[i]: T_s1[i])              //determine surface temp in section
Call pipeflow(H$,T1[i],P1[i],m_dot[1],ID1,L1,RelRough:h_T1[i], h_H1[i] ,DELTAP1[i],
Nusselt_T1[i], f1[i], Re1[i])                 //Find pressure drop and convection
coefficient
P1[i+1] = P1[i] - DELTAP1[i]                  //determine pressure in section

Q_dot1[i] = (T_avg1[i] - T_s1[i])/R1[i]       //heat transfer out of section
T_avg1[i] = (T1[i] + T1[i+1])/2               //average temperature in section
R1[i] = 1/(h_T1[i] * A_s1)                    //resistance in section from internal
convection

Q_dot1[i] = m_dot[1]*(DELTA_H1[i])            //heat transfer from enthalpy difference
    h1[i+1]=h1[i]-DELTA_H1[i]                 //determine enthalpy in section
    T1[i+1]=temperature(H$,h=h1[i+1],P=P1[i+1])
    //determine temperature in section


del_P1[i] = P1[i] - P1[i+1]                   //pressure difference in section
```

```
S_gen_P1[i] = m_dot[1]*R*(del_P1[i]/P1[i])          //entropy generation from pressure
difference

del_T1[i] = T1[i+1] - T_s1[i]                       //temperature difference in section
S_gen_T1[i] = m_dot[1]*Cp1[i]*(del_T1[i]/T_s1[i])
    //entropy generation from temperature difference
Cp1[i] =  ((23.16383-22.2923*ln(T1[i])+8.085544*ln(T1[i])^2-
1.30587*ln(T1[i])^3+0.079239*ln(T1[i])^4)/(1-0.93421*ln(T1[i])+0.328506*ln(T1[i])^2-
0.05149*ln(T1[i])^3+0.00304*ln(T1[i])^4))* (1/molarmass(H$)) * 1000
    //equilibrium heat capacity of hydrogen in section
End

S_gen_P1 = sum(S_gen_P1[i], i=1,N-1)                //total entropy generation in layer from
pressure difference
S_gen_T1 = sum(S_gen_T1[i], i=1, N-1)               //total entropy generation in layer from
temperature difference

"Sgen total"
S_gen_tot1 = S_gen_P1 + S_gen_T1                    //total entropy generation in layer
//END NODE 1//

"Second Node"                                       //nodes are defines are branch clusters (first
node is one branch)
A_s2 = PI*ID2*delta_x2                              //surface area for heat transfer -> will
have to be branch
A_c2 = (PI/4)*ID2^2                                 //cross sectional area

T2[1] = T1[N]
P2[1] = P1[N]
h2[1] = enthalpy(H$, T=T2[1], P=P2[1])              //initial enthalpy

delta_x2 = L2/(N-1)
x2[1] = L1
Duplicate i=1, N-1
    x2[i+1] = x2[i] + delta_x2
    End


Duplicate i=1,N-1
 Call tempprofile(x2[i]: T_s2[i])
"Find pressure drop and convection coefficient"
Call pipeflow(H$,T2[i],P2[i],m_dot[2],ID2,L2,RelRough:h_T2[i], h_H2[i] ,DELTAP2[i],
Nusselt_T2[i], f2[i], Re2[i])

"Find incremental pressure"
```

```
P2[i+1] = P2[i] - DELTAP2[i]

Q_dot2[i] = (T_avg2[i] - T_s2[i])/R2[i]
T_avg2[i] = (T2[i] + T2[i+1])/2
R2[i] = 1/(h_T2[i] * A_s2)

Q_dot2[i] = m_dot[2]*(DELTA_H2[i])
    h2[i+1]=h2[i]-DELTA_H2[i]                    //next enthalpy
    T2[i+1]=temperature(H$,h=h2[i+1],P=P2[i+1])


del_P2[i] = P2[i] - P2[i+1]
S_gen_P2[i] = m_dot[2]*R*(del_P2[i]/P2[i])

del_T2[i] = T2[i+1] - T_s2[i]
S_gen_T2[i] = m_dot[2]*Cp2[i]*(del_T2[i]/T_s2[i])
Cp2[i] =  ((23.16383-22.2923*ln(T2[i])+8.085544*ln(T2[i])^2-
1.30587*ln(T2[i])^3+0.079239*ln(T2[i])^4)/(1-0.93421*ln(T2[i])+0.328506*ln(T2[i])^2-
0.05149*ln(T2[i])^3+0.00304*ln(T2[i])^4))* (1/molarmass(H$)) * 1000
End

S_gen_P2 = sum(S_gen_P2[i], i=1,N-1)         //Sgen from pressure
S_gen_T2 = sum(S_gen_T2[i], i=1, N-1)        //Sgen from temp

"Sgen total"
S_gen_tot2 = (S_gen_P2 + S_gen_T2)*branches[2]
//END NODE//


"Third Node"                                 //nodes are defines are branch clusters (first
node is one branch)
A_s3 = PI*ID3*delta_x3                       //surface area for heat transfer -> will
have to be branch
A_c3 = (PI/4)*ID3^2                          //cross sectional area

T3[1] = T2[N]
P3[1] = P2[N]
h3[1] = enthalpy(H$, T=T3[1], P=P3[1])       //initial enthalpy


delta_x3 = L3/(N-1)
x3[1] = L1 + L2
Duplicate i=1, N-1
    x3[i+1] = x3[i] + delta_x3
    End
```

Duplicate i=1,N-1
 Call **tempprofile**(x3[i]: T_s3[i])
"Find pressure drop and convection coefficient"
Call **pipeflow**(H$,T3[i],P3[i],m_dot[3],ID3,L3,RelRough:h_T3[i], h_H3[i] ,DELTAP3[i], Nusselt_T3[i], f3[i], Re3[i])

"Find incremental pressure"
P3[i+1] = P3[i] - DELTAP3[i]

Q_dot3[i] = (T_avg3[i] - T_s3[i])/R3[i]
T_avg3[i] = (T3[i] + T3[i+1])/2
R3[i] = 1/(h_T3[i] * A_s3)

Q_dot3[i] = m_dot[3]*(DELTA_H3[i])
    h3[i+1]=h3[i]-DELTA_H3[i] //next enthalpy
    T3[i+1]=**temperature**(H$,***h***=h3[i+1],***P***=P3[i+1])

del_P3[i] = P3[i] - P3[i+1]
S_gen_P3[i] = m_dot[3]*R*(del_P3[i]/P3[i])

del_T3[i] = T3[i+1] - T_s3[i]
S_gen_T3[i] = m_dot[3]*Cp3[i]*(del_T3[i]/T_s3[i])
Cp3[i] = ((23.16383-22.2923***ln**(T3[i])+8.085544***ln**(T3[i])^2-1.30587***ln**(T3[i])^3+0.079239***ln**(T3[i])^4)/(1-0.93421***ln**(T3[i])+0.328506***ln**(T3[i])^2-0.05149***ln**(T3[i])^3+0.00304***ln**(T3[i])^4))* (1/**molarmass**(H$)) * 1000
End

S_gen_P3 = sum(S_gen_P3[i], i=1,N-1) //Sgen from pressure
S_gen_T3 = sum(S_gen_T3[i], i=1, N-1) //Sgen from temp

"Sgen total"
S_gen_tot3 = (S_gen_P3 + S_gen_T3)*branches[3]
//END NODE//

"Fourth Node" //nodes are defines are branch clusters (first node is one branch)
A_s4 = PI*ID4*delta_x4 **//surface area for heat transfer -> will have to be branch**
A_c4 = (PI/4)*ID4^2 **//cross sectional area**

T4[1] = T3[N]
P4[1] = P3[N]
h4[1] = enthalpy(H$, ***T***=T4[1], ***P***=P4[1]) //initial enthalpy

```
delta_x4 = L4/(N-1)
x4[1] = L1 + L2 + L3
Duplicate i=1, N-1
    x4[i+1] = x4[i] + delta_x4
    End


Duplicate i=1,N-1
 Call tempprofile(x4[i]: T_s4[i])
"Find pressure drop and convection coefficient"
Call pipeflow(H$,T4[i],P4[i],m_dot[4],ID4,L4,RelRough:h_T4[i], h_H4[i] ,DELTAP4[i],
Nusselt_T4[i], f4[i], Re4[i])

"Find incremental pressure"
P4[i+1] = P4[i] - DELTAP4[i]

Q_dot4[i] = (T_avg4[i] - T_s4[i])/R4[i]
T_avg4[i] = (T4[i] + T4[i+1])/2
R4[i] = 1/(h_T4[i] * A_s4)

Q_dot4[i] = m_dot[4]*(DELTA_H4[i])
    h4[i+1]=h4[i]-DELTA_H4[i]                    //next enthalpy
    T4[i+1]=temperature(H$,h=h4[i+1],P=P4[i+1])

del_P4[i] = P4[i] - P4[i+1]
S_gen_P4[i] = m_dot[4]*R*(del_P4[i]/P4[i])

del_T4[i] = T4[i+1] - T_s4[i]
S_gen_T4[i] = m_dot[4]*Cp4[i]*(del_T4[i]/T_s4[i])
Cp4[i] =  ((23.16383-22.2923*ln(T4[i])+8.085544*ln(T4[i])^2-
1.30587*ln(T4[i])^3+0.079239*ln(T4[i])^4)/(1-0.93421*ln(T4[i])+0.328506*ln(T4[i])^2-
0.05149*ln(T4[i])^3+0.00304*ln(T4[i])^4))* (1/molarmass(H$)) * 1000
End

S_gen_P4 = sum(S_gen_P4[i], i=1,N-1)          //Sgen from pressure
S_gen_T4 = sum(S_gen_T4[i], i=1, N-1)         //Sgen from temp


"Sgen total"
S_gen_tot4 = (S_gen_P4 + S_gen_T4)*branches[4]
//END NODE//
```

7.4 Code for Upper Portion of Heat Exchanger with Equilibrium Hydrogen

```
"Assumptions"
//hydrogen is adiabatic at inlet
//all heat is removed through the Gifford-McMahon cryocooler (no environmental losses)

"Constants"
H$ = 'Hydrogen'
    //fluid
O$ = 'OrthoHydrogen'
P$ = 'ParaHydrogen'
A$ = 'Aluminum_6061'
    //wall material
T_in = 293 [K]
    //inlet temp
T_out = 30 [K]
    //outlet temp
P_in = 652933 [Pa]
    //inlet pressure
L_tot = 0.0795 [m]

RelRough = 0.01 [-]
    //relative roughness of wall, guess
P_dewar = 80 [psi]*convert(psi,Pa)
    //pressure within the dewar

T_first = 110 [K]
    //temperature of upper/first stage
T_second = 25 [K]
    //temperature of lower/second stage

m_dot_total = 0.000008 [kg/s]
Q_upper = 90 [W]
    //heat removed in upper stage

Q_lower = 30 [W]
    //heat removed in lower stage

L_tot = L1 + L2 + L3 + L4
S_gen_tot = S_gen_tot1 + S_gen_tot2 + S_gen_tot3 + S_gen_tot4
B = 4 [-]
    //number of sections in the system

N = 50 [-]
    //total number of nodes
```

```
"Number of branches in each section"
branches[1] = 1 [-]
DUPLICATE i=2, B
branches[i] = branches[i-1]*2
END

"Mass flow rate in each branch/section"
m_dot[1] = m_dot_total/branches[1]
DUPLICATE i=2, B
m_dot[i] = m_dot_total/branches[i]
END


"Heat Flux - Upper"
OD_upper1 = 12.5 [cm]*convert(cm,m)
OD_upper2 = 9 [cm]*convert(cm,m)
th_upper = 0.65 [cm]*convert(cm,m)
h_upper = 7.1 [cm]*convert(cm,m)
A_upper = PI * OD_upper2 * (h_upper - th_upper) + PI * OD_upper1 * th_upper + 2* ((PI/4) *
(OD_upper1^2 - OD_upper2^2))
Flux_upper = Q_upper/A_upper

contact_area = (PI/4) * (OD_upper1^2 - OD_upper2^2)
indium_resistance = 20 [W/K]

"Establish Nodal Network"
delta_x1 = L1/(N-1)
x[1] = 0 [m]
Duplicate i = 2, N
x[i] = x[i-1] + delta_x1
End

ID1 = 0.003175 [m]
    //tube inner diameter
A_s1 = PI* ID1 * delta_x1
    //internal surface area of tube

"Varying wall thickness"
x1 =2.15
    //exponential coeff
y1 = 0.00043
    //vertical shift, constant
f=1
                                                    //scaling factor
```

```
DUPLICATE i=1, N
OD1[i] = ID1 + th1[i]
    //varying external diameter
A_c1[i] = (PI/4) * (OD1[i]^2 - ID1^2)
    //varying cross-sectional area
th1[i] = f*x[i]^x1 + y1
    //varying wall thickness
END

"Upper Flange to first stage"
"First Node - Hydrogen"
T_h[1] = T_in
P_h[1] = P_in
Call pipeflow(H$,T_h[1],P_h[1],m_dot[1],ID1,delta_x1,RelRough:h_in_h[1], h_H_h[1],
DELTAP_h[1], Nusselt_T_h[1], f_h[1], Re_h[1])
eq_ortho1[1] = ((-26.339285 + 40.177003 * ln(T_h[1]) -24.070739 * ln(T_h[1])^2 + 7.0854451
* ln(T_h[1])^3 - 1.0266083 * ln(T_h[1])^4 + 0.058838859 * ln(T_h[1])^5) / (1 - 0.71557425 *
ln(T_h[1]) + 0.14395723 * ln(T_h[1])^2 + 0.008041614 * ln(T_h[1])^3 - 0.0056608578 *
ln(T_h[1])^4 + 0.0004869077 * ln(T_h[1])^5)) /100
cp_h[1] = cp(O$, T=T_h[1], P=P_h[1])*eq_ortho1[1] + cp(P$, T=T_h[1], P=P_h[1]) * (1-
eq_ortho1[1])

"Crank-Nicolson - Hydrogen"
Duplicate i=2, N
"Hydrogen"
T_h[i] = T_h[i-1] + (dTdxi_h[i] + dtdxplus_h[i]) * (delta_x1/2)
dTdxi_h[i] = (-h_in_h[i-1]*A_s1*(T_h[i-1]-T_a[i-1]))/(m_dot[1]*cp_h[i-1]*delta_x1)
dTdxplus_h[i] = (-h_in_h[i]*A_s1*(T_h[i]-T_a[i]))/(m_dot[1]*cp_h[i]*delta_x1)

P_h[i] = P_h[i-1] - DELTAP_h[i-1]

Call pipeflow(H$,T_h[i],P_h[i],m_dot[1],ID1,delta_x1,RelRough:h_in_h[i], h_H_h[i],
DELTAP_h[i], Nusselt_T_h[i], f_h[i], Re_h[i])

eq_ortho1[i] = ((-26.339285 + 40.177003 * ln(T_h[i]) -24.070739 * ln(T_h[i])^2 + 7.0854451 *
ln(T_h[i])^3 - 1.0266083 * ln(T_h[i])^4 + 0.058838859 * ln(T_h[i])^5) / (1 - 0.71557425 *
ln(T_h[i]) + 0.14395723 * ln(T_h[i])^2 + 0.008041614 * ln(T_h[i])^3 - 0.0056608578 *
ln(T_h[i])^4 + 0.0004869077 * ln(T_h[i])^5)) /100
cp_h[i] = cp(O$, T=T_h[i], P=P_h[i])*eq_ortho1[i] + cp(P$, T=T_h[i], P=P_h[i]) * (1-
eq_ortho1[i])
End

"First Node - Wall (Al)"
T_a[1] = T_in-1 [K]
dTdx_a[1] = 0
```

```
d2Tdx2_a[1] = (4*ID1*h_in_h[1]*(T_a[1]-T_h[1]))/(k_a[1]*(OD1[1]^2-ID1^2))

k_a[1] = conductivity(A$, T=T_a[1])

"Crank-Nicolson - Wall"
Duplicate i=2, N
T_a[i] = T_a[i-1] + (dTdx_a[i-1] + dTdx_a[i]) * (delta_x1/2)
dTdx_a[i] = dTdx_a[i-1] + (d2Tdx2_a[i-1] + d2Tdx2_a[i]) * (delta_x1/2)
d2Tdx2_a[i] =  (4*ID1*h_in_h[i]*(T_a[i]-T_h[i]))/(k_a[i]*(OD1[i]^2-ID1^2))

k_a[i] = conductivity(A$, T=T_a[i-1])
End

"Last Node - Wall (Al)"
//Flux_upper * contact_area  = (T_a[N-1] - T_a[N]) / ((delta_x1/(k_a[N]*A_c1[N])) +
1/indium_resistance)
//k_a[N] = conductivity(A$, T=T_a[N])


"Entropy in H2 stream"
DUPLICATE i=1,N
s_h[i] = entropy (O$, T=T_h[i], P=P_h[i])*eq_ortho1[i] + entropy (P$, T=T_h[i], P=P_h[i])*(1-
eq_ortho1[i])
END

DUPLICATE i=1, N-1
 Q_h_out[i] = m_dot[1] * (enthalpy(H$, T=T_h[i+1], P=P_h[i+1])  - enthalpy(H$, T=T_h[i],
P=P_h[i]))

//Q_h_out[i] = m_dot[1] * (enthalpy(O$, T=T_h[i+1], P=P_h[i+1]) *eq_ortho[i] + enthalpy(P$,
T=T_h[i+1], P=P_h[i+1]) *(1-eq_ortho[i]) - enthalpy(O$, T=T_h[i], P=P_h[i])*eq_ortho[i]
+enthalpy(P$, T=T_h[i], P=P_h[i])*(1-eq_ortho[i]))

m_dot[1] * s_h[i] + S_gen_h[i] = m_dot[1] * s_h[i+1] + Q_h_out[i] / ((T_a[i] + T_a[i+1])/2)
END

S_gen_h = abs( SUM(S_gen_h[i], i=1, N-1))

"Entropy in wall"
"Node 1"
Q_a_out[1] = k_a[1] * A_c1[1] * ((T_a[1] + T_a[2])/2 - T_a[2]) / delta_x1
Q_h_out[1] / ((T_a[1] + T_a[2]) / 2) + S_gen_a[1] = Q_a_out[1] / T_a[2]
"Middle Nodes"
DUPLICATE i = 2, N-1
Q_a_in[i] = k_a[i] * A_c1[i] * (T_a[i] - (T_a[i+1]+T_a[i])/2) / delta_x1
```

```
Q_a_out[i] = k_a[i] * A_c1[i] * ((T_a[i+1]+T_a[i])/2 - T_a[i+1]) / delta_x1

Q_a_in[i] / T_a[i] + Q_h_out[i] / ((T_a[i] + T_a[i+1])/2) + S_gen_a[i] = Q_a_out[i] / T_a[i+1]
END

"Node N"
//Q_a_in[N-1] = k_a[N-1] * A_c1[N-1] * (T_a[N-1] - (T_a[N]+T_a[N-1])/2) / delta_x1
//Q_a_in[N-1] / T_a[N-1] + Q_h_out[N-1] / ((T_a[N-1] + T_a[N])/2) + S_gen_a[N-1] =
(Flux_upper*A_c1[N])/T_a[N]

S_gen_a = abs (SUM(S_gen_a[i], i=1,N-1))

S_gen_tot1 = (S_gen_a + S_gen_h)*branches[1]

"Node 2"
"Establish Nodal Network"
delta_x2 = L2/(N-1)
x2[1] = x[N]
Duplicate i = 2, N
x2[i] = x2[i-1] + delta_x2
End

L2 = 0.01 [m]
ID2 = 0.003175 [m]
    //tube inner diameter
A_s2 = PI* ID2 * delta_x2
    //internal surface area of tube

"Varying wall thickness"
x2 = x1
    //exponential coeff
y2 =y1
    //vertical shift, constant
DUPLICATE i=1, N
OD2[i] = ID2 + th2[i]
    //varying external diameter
A_c2[i] = (PI/4) * (OD2[i]^2 - ID2^2)
    //varying cross-sectional area
th2[i] = f*x2[i]^x2 + y2
    //varying wall thickness
END

"Upper Flange to first stage"
"First Node - Hydrogen"
T_h2[1] = T_h[N]
```

P_h2[1] = P_h[N]
Call pipeflow(H$,T_h2[1],P_h2[1],m_dot[2],ID2,delta_x2,RelRough:h_in_h2[1], h_H_h2[1], DELTAP_h2[1], Nusselt_T_h2[1], f_h2[1], Re_h2[1])
eq_ortho2[1] = ((-26.339285 + 40.177003 * ln(T_h2[1]) -24.070739 * ln(T_h2[1])^2 + 7.0854451 * ln(T_h2[1])^3 - 1.0266083 * ln(T_h2[1])^4 + 0.058838859 * ln(T_h2[1])^5) / (1 - 0.71557425 * ln(T_h2[1]) + 0.14395723 * ln(T_h2[1])^2 + 0.008041614 * ln(T_h2[1])^3 - 0.0056608578 * ln(T_h2[1])^4 + 0.0004869077 * ln(T_h2[1])^5)) /100
cp_h2[1] = cp(O$, T=T_h2[1], P=P_h2[1])*eq_ortho2[1] + cp(P$, T=T_h2[1], P=P_h2[1]) * (1-eq_ortho2[1])

"Crank-Nicolson - Hydrogen"
Duplicate i=2, N
"Hydrogen"
T_h2[i] = T_h2[i-1] + (dTdxi_h2[i] + dtdxplus_h2[i]) * (delta_x2/2)
dTdxi_h2[i] = (-h_in_h2[i-1]*A_s2*(T_h2[i-1]-T_a2[i-1]))/(m_dot[2]*cp_h2[i-1]*delta_x2)

dTdxplus_h2[i] = (-h_in_h2[i]*A_s2*(T_h2[i]-T_a2[i]))/(m_dot[2]*cp_h2[i]*delta_x2)

P_h2[i] = P_h2[i-1] - DELTAP_h2[i-1]

Call pipeflow(H$,T_h2[i],P_h2[i],m_dot[2],ID2,delta_x2,RelRough:h_in_h2[i], h_H_h2[i], DELTAP_h2[i], Nusselt_T_h2[i], f_h2[i], Re_h2[i])

eq_ortho2[i] = ((-26.339285 + 40.177003 * ln(T_h2[i]) -24.070739 * ln(T_h2[i])^2 + 7.0854451 * ln(T_h2[i])^3 - 1.0266083 * ln(T_h2[i])^4 + 0.058838859 * ln(T_h2[i])^5) / (1 - 0.71557425 * ln(T_h2[i]) + 0.14395723 * ln(T_h2[i])^2 + 0.008041614 * ln(T_h2[i])^3 - 0.0056608578 * ln(T_h2[i])^4 + 0.0004869077 * ln(T_h2[i])^5)) /100
cp_h2[i] = cp(O$, T=T_h2[i], P=P_h2[i])*eq_ortho2[i] + cp(P$, T=T_h2[i], P=P_h2[i]) * (1-eq_ortho2[i])
End

"First Node - Wall (Al)"
T_a2[1] = T_a[N]
dTdx_a2[1] = dTdx_a[N] + (d2Tdx2_a[N] + d2Tdx2_a2[1])*(delta_x2/2)
d2Tdx2_a2[1] = (4*ID2*h_in_h2[1]*(T_a2[1]-T_h2[1]))/(k_a2[1]*(OD2[1]^2-ID2^2))

k_a2[1] = conductivity(A$, T=T_a2[1])

"Crank-Nicolson - Wall"
Duplicate i=2, N
T_a2[i] = T_a2[i-1] + (dTdx_a2[i-1] + dTdx_a2[i]) * (delta_x2/2)
dTdx_a2[i] = dTdx_a2[i-1] + (d2Tdx2_a2[i-1] + d2Tdx2_a2[i]) * (delta_x2/2)

```
d2Tdx2_a2[i] =  (4*ID2*h_in_h2[i]*(T_a2[i]-T_h2[i]))/(k_a2[i]*(OD2[i]^2-ID2^2))


k_a2[i] = conductivity(A$, T=T_a2[i-1])
End

"Last Node - Wall (Al)"
//Flux_upper * contact_area  = (T_a2[N-1] - T_a2[N]) / ((delta_x2/(k_a2[N]*A_c2[N])) +
1/indium_resistance)
//k_a2[N] = conductivity(A$, T=T_a2[N])


"Entropy in H2 stream"
DUPLICATE i=1,N
s_h2[i] = entropy (O$, T=T_h2[i], P=P_h2[i])*eq_ortho2[i] + entropy (P$, T=T_h2[i],
P=P_h2[i])*(1-eq_ortho2[i])
END

DUPLICATE i=1, N-1
Q_h_out2[i] = m_dot[2] * (enthalpy(H$, T=T_h2[i+1], P=P_h2[i+1])  - enthalpy(H$, T=T_h2[i],
P=P_h2[i]))
m_dot[2] * s_h2[i] + S_gen_h2[i] = m_dot[2] * s_h2[i+1] + Q_h_out2[i] / ((T_a2[i] +
T_a2[i+1])/2)
END

S_gen_h2 = abs( SUM(S_gen_h2[i], i=1, N-1))

"Entropy in wall"
"Node 1"
Q_a_out2[1] = k_a2[1] * A_c2[1] * ((T_a2[1] + T_a2[2])/2 - T_a2[2]) / delta_x2
Q_h_out2[1] / ((T_a2[1] + T_a2[2]) / 2) + S_gen_a2[1] = Q_a_out2[1] / T_a2[2]

"Middle Nodes"
DUPLICATE i = 2, N-1
Q_a_in2[i] = k_a2[i] * A_c2[i] * (T_a2[i] - (T_a2[i+1]+T_a2[i])/2) / delta_x2
Q_a_out2[i] = k_a2[i] * A_c2[i] * ((T_a2[i+1]+T_a2[i])/2 - T_a2[i+1]) / delta_x2

Q_a_in2[i] / T_a2[i] + Q_h_out2[i] / ((T_a2[i] + T_a2[i+1])/2) + S_gen_a2[i] = Q_a_out2[i] /
T_a2[i+1]
END

"Node N"
//Q_a_in2[N-1] = k_a2[N-1] * A_c2[N-1] * (T_a2[N-1] - (T_a2[N]+T_a2[N-1])/2) / delta_x2
//Q_a_in2[N-1] / T_a2[N-1] + Q_h_out2[N-1] / ((T_a2[N-1] + T_a2[N])/2) + S_gen_a2[N-1] =
(Flux_upper*A_c2[N])/T_a2[N]
```

```
S_gen_a2 = abs (SUM(S_gen_a2[i], i=1,N-1))

S_gen_tot2 = (S_gen_a2 + S_gen_h2)*branches[2]

"Node 3"
"Establish Nodal Network"
delta_x3 = L3/(N-1)
x3[1] = x2[N]
Duplicate i = 2, N
x3[i] = x3[i-1] + delta_x3
End

L3 = 0.01 [m]
ID3 = 0.003175 [m]
    //tube inner diameter
A_s3 = PI* ID3 * delta_x3
    //internal surface area of tube

"Varying wall thickness"
x3 = x1
    //exponential coeff
y3 = y1
    //vertical shift, constant
DUPLICATE i=1, N
OD3[i] = ID3 + th3[i]
    //varying external diameter
A_c3[i] = (PI/4) * (OD3[i]^2 - ID3^2)
    //varying cross-sectional area
th3[i] = f*x3[i]^x3 + y3
    //varying wall thickness
END

"Upper Flange to first stage"
"First Node - Hydrogen"
T_h3[1] = T_h2[N]
P_h3[1] = P_h2[N]
Call pipeflow(H$,T_h3[1],P_h3[1],m_dot[3],ID3,delta_x3,RelRough:h_in_h3[1], h_H_h3[1],
DELTAP_h3[1], Nusselt_T_h3[1], f_h3[1], Re_h3[1])
eq_ortho3[1] = ((-26.339285 + 40.177003 * ln(T_h3[1]) -24.070739 * ln(T_h3[1])^2 +
7.0854451 * ln(T_h3[1])^3 - 1.0266083 * ln(T_h3[1])^4 + 0.058838859 * ln(T_h3[1])^5) / (1 -
0.71557425 * ln(T_h3[1]) + 0.14395723 * ln(T_h3[1])^2 + 0.008041614 * ln(T_h3[1])^3 -
0.0056608578 * ln(T_h3[1])^4 + 0.0004869077 * ln(T_h3[1])^5)) /100
cp_h3[1] = cp(O$, T=T_h3[1], P=P_h3[1])*eq_ortho3[1] + cp(P$, T=T_h3[1], P=P_h3[1]) * (1-
eq_ortho3[1])
```

"Crank-Nicolson - Hydrogen"
Duplicate i=2, N
"Hydrogen"
T_h3[i] = T_h3[i-1] + (dTdxi_h3[i] + dtdxplus_h3[i]) * (delta_x3/2)
dTdxi_h3[i] = (-h_in_h3[i-1]*A_s3*(T_h3[i-1]-T_a3[i-1]))/(m_dot[3]*cp_h3[i-1]*delta_x3)

dTdxplus_h3[i] = (-h_in_h3[i]*A_s3*(T_h3[i]-T_a3[i]))/(m_dot[3]*cp_h3[i]*delta_x3)

P_h3[i] = P_h3[i-1] - DELTAP_h3[i-1]

Call pipeflow(H$,T_h3[i],P_h3[i],m_dot[3],ID3,delta_x3,RelRough:h_in_h3[i], h_H_h3[i], DELTAP_h3[i], Nusselt_T_h3[i], f_h3[i], Re_h3[i])

eq_ortho3[i] = ((-26.339285 + 40.177003 * ln(T_h3[i]) -24.070739 * ln(T_h3[i])^2 + 7.0854451 * ln(T_h3[i])^3 - 1.0266083 * ln(T_h3[i])^4 + 0.058838859 * ln(T_h3[i])^5) / (1 - 0.71557425 * ln(T_h3[i]) + 0.14395723 * ln(T_h3[i])^2 + 0.008041614 * ln(T_h3[i])^3 - 0.0056608578 * ln(T_h3[i])^4 + 0.0004869077 * ln(T_h3[i])^5)) /100
cp_h3[i] = cp(O$, T=T_h3[i], P=P_h3[i])*eq_ortho3[i] + cp(P$, T=T_h3[i], P=P_h3[i]) * (1-eq_ortho3[i])
End

"First Node - Wall (Al)"
T_a3[1] = T_a2[N]
dTdx_a3[1] = dTdx_a2[N] + (d2Tdx2_a2[N] + d2Tdx2_a3[1])*(delta_x3/2)
d2Tdx2_a3[1] = (4*ID3*h_in_h3[1]*(T_a3[1]-T_h3[1]))/(k_a3[1]*(OD3[1]^2-ID3^2))

k_a3[1] = conductivity(A$, T=T_a3[1])

"Crank-Nicolson - Wall"
Duplicate i=2, N
T_a3[i] = T_a3[i-1] + (dTdx_a3[i-1] + dTdx_a3[i]) * (delta_x3/2)
dTdx_a3[i] = dTdx_a3[i-1] + (d2Tdx2_a3[i-1] + d2Tdx2_a3[i]) * (delta_x3/2)
d2Tdx2_a3[i] = (4*ID3*h_in_h3[i]*(T_a3[i]-T_h3[i]))/(k_a3[i]*(OD3[i]^2-ID3^2))

k_a3[i] = conductivity(A$, T=T_a3[i-1])
End

"Last Node - Wall (Al)"
//Flux_upper * contact_area = (T_a3[N-1] - T_a3[N]) / ((delta_x3/(k_a3[N]*A_c3[N])) + 1/indium_resistance)
//k_a3[N] = conductivity(A$, T=T_a3[N])

"Entropy in H2 stream"
DUPLICATE i=1,N
s_h3[i] = entropy (O$, T=T_h3[i], P=P_h3[i])*eq_ortho3[i] + entropy (P$, T=T_h3[i], P=P_h3[i])*(1-eq_ortho3[i])
END

DUPLICATE i=1, N-1
Q_h_out3[i] = m_dot[3] * (enthalpy(H$, T=T_h3[i+1], P=P_h3[i+1]) - enthalpy(H$, T=T_h3[i], P=P_h3[i]))
m_dot[3] * s_h3[i] + S_gen_h3[i] = m_dot[3] * s_h3[i+1] + Q_h_out3[i] / ((T_a3[i] + T_a3[i+1])/2)
END

S_gen_h3 = abs(SUM(S_gen_h3[i], i=1, N-1))

"Entropy in wall"
"Node 1"
Q_a_out3[1] = k_a3[1] * A_c3[1] * ((T_a3[1] + T_a3[2])/2 - T_a3[2]) / delta_x3
Q_h_out3[1] / ((T_a3[1] + T_a3[2]) / 2) + S_gen_a3[1] = Q_a_out3[1] / T_a3[2]

"Middle Nodes"
DUPLICATE i = 2, N-1
Q_a_in3[i] = k_a3[i] * A_c3[i] * (T_a3[i] - (T_a3[i+1]+T_a3[i])/2) / delta_x3
Q_a_out3[i] = k_a3[i] * A_c3[i] * ((T_a3[i+1]+T_a3[i])/2 - T_a3[i+1]) / delta_x3

Q_a_in3[i] / T_a3[i] + Q_h_out3[i] / ((T_a3[i] + T_a3[i+1])/2) + S_gen_a3[i] = Q_a_out3[i] / T_a3[i+1]
END

"Node N"
//Q_a_in3[N-1] = k_a3[N-1] * A_c3[N-1] * (T_a3[N-1] - (T_a3[N]+T_a3[N-1])/2) / delta_x3
//Q_a_in3[N-1] / T_a3[N-1] + Q_h_out3[N-1] / ((T_a3[N-1] + T_a3[N])/2) + S_gen_a3[N-1] = (Flux_upper*A_c3[N])/T_a3[N]

S_gen_a3 = abs (SUM(S_gen_a3[i], i=1,N-1))

S_gen_tot3 = (S_gen_a3 + S_gen_h3)*branches[3]

"Node 4"
"Establish Nodal Network"
delta_x4 = L4/(N-1)
x4[1] = x3[N]
Duplicate i = 2, N

```
x4[i] = x4[i-1] + delta_x4
End

L4 = 0.0495 [m]
ID4 = 0.003175 [m]
    //tube inner diameter
A_s4 = PI* ID4 * delta_x4
    //internal surface area of tube

"Varying wall thickness"
x4 = x1
    //exponential coeff
y4 = y1
    //vertical shift, constant
DUPLICATE i=1, N
OD4[i] = ID4 + th4[i]
    //varying external diameter
A_c4[i] = (PI/4) * (OD4[i]^2 - ID4^2)
    //varying cross-sectional area
th4[i] = f*x4[i]^x4 + y4
    //varying wall thickness
END

"Upper Flange to first stage"
"First Node - Hydrogen"
T_h4[1] = T_h3[N]
P_h4[1] = P_h3[N]
Call pipeflow(H$,T_h4[1],P_h4[1],m_dot[4],ID4,delta_x4,RelRough:h_in_h4[1], h_H_h4[1],
DELTAP_h4[1], Nusselt_T_h4[1], f_h4[1], Re_h4[1])
eq_ortho4[1] = ((-26.339285 + 40.177003 * ln(T_h4[1]) -24.070739 * ln(T_h4[1])^2 +
7.0854451 * ln(T_h4[1])^3 - 1.0266083 * ln(T_h4[1])^4 + 0.058838859 * ln(T_h4[1])^5) / (1 -
0.71557425 * ln(T_h4[1]) + 0.14395723 * ln(T_h4[1])^2 + 0.008041614 * ln(T_h4[1])^3 -
0.0056608578 * ln(T_h4[1])^4 + 0.0004869077 * ln(T_h4[1])^5)) /100
cp_h4[1] = cp(O$, T=T_h4[1], P=P_h4[1])*eq_ortho4[1] + cp(P$, T=T_h4[1], P=P_h4[1]) * (1-
eq_ortho4[1])

"Crank-Nicolson - Hydrogen"
Duplicate i=2, N
"Hydrogen"
T_h4[i] = T_h4[i-1] + (dTdxi_h4[i] + dtdxplus_h4[i]) * (delta_x4/2)
dTdxi_h4[i] = (-h_in_h4[i-1]*A_s4*(T_h4[i-1]-T_a4[i-1]))/(m_dot[4]*cp_h4[i-1]*delta_x4)

dTdxplus_h4[i] = (-h_in_h4[i]*A_s4*(T_h4[i]-T_a4[i]))/(m_dot[4]*cp_h4[i]*delta_x4)
```

```
P_h4[i] = P_h4[i-1] - DELTAP_h4[i-1]

Call pipeflow(H$,T_h4[i],P_h4[i],m_dot[4],ID4,delta_x4,RelRough:h_in_h4[i], h_H_h4[i],
DELTAP_h4[i], Nusselt_T_h4[i], f_h4[i], Re_h4[i])

eq_ortho4[i] = ((-26.339285 + 40.177003 * ln(T_h4[i]) -24.070739 * ln(T_h4[i])^2 + 7.0854451
* ln(T_h4[i])^3 - 1.0266083 * ln(T_h4[i])^4 + 0.058838859 * ln(T_h4[i])^5) / (1 - 0.71557425 *
ln(T_h4[i]) + 0.14395723 * ln(T_h4[i])^2 + 0.008041614 * ln(T_h4[i])^3 - 0.0056608578 *
ln(T_h4[i])^4 + 0.0004869077 * ln(T_h4[i])^5)) /100
cp_h4[i] = cp(O$, T=T_h4[i], P=P_h4[i])*eq_ortho4[i] + cp(P$, T=T_h4[i], P=P_h4[i]) * (1-
eq_ortho4[i])
End

"First Node - Wall (Al)"
T_a4[1] = T_a3[N]
dTdx_a4[1] = dTdx_a3[N] + (d2Tdx2_a3[N] + d2Tdx2_a4[1])*(delta_x4/2)
d2Tdx2_a4[1] = (4*ID4*h_in_h4[1]*(T_a4[1]-T_h4[1]))/(k_a4[1]*(OD4[1]^2-ID4^2))


k_a4[1] = conductivity(A$, T=T_a4[1])

"Crank-Nicolson - Wall"
Duplicate i=2, N-1
T_a4[i] = T_a4[i-1] + (dTdx_a4[i-1] + dTdx_a4[i]) * (delta_x4/2)
dTdx_a4[i] = dTdx_a4[i-1] + (d2Tdx2_a4[i-1] + d2Tdx2_a4[i]) * (delta_x4/2)
d2Tdx2_a4[i] =  (4*ID4*h_in_h4[i]*(T_a4[i]-T_h4[i]))/(k_a4[i]*(OD4[i]^2-ID4^2))


k_a4[i] = conductivity(A$, T=T_a4[i-1])
End

"Last Node - Wall (Al)"
Flux_upper * contact_area  = (T_a4[N-1] - T_a4[N]) / ((delta_x4/(k_a4[N]*A_c4[N])) +
1/indium_resistance)
k_a4[N] = conductivity(A$, T=T_a4[N])


"Entropy in H2 stream"
DUPLICATE i=1,N
s_h4[i] = entropy (O$, T=T_h4[i], P=P_h4[i])*eq_ortho4[i] + entropy (P$, T=T_h4[i],
P=P_h4[i])*(1-eq_ortho4[i])
END

DUPLICATE i=1, N-1
```

```
Q_h_out4[i] = m_dot[4] * (enthalpy(H$, T=T_h4[i+1], P=P_h4[i+1])  - enthalpy(H$, T=T_h4[i], P=P_h4[i]))
m_dot[4] * s_h4[i] + S_gen_h4[i] = m_dot[4] * s_h4[i+1] + Q_h_out4[i] / ((T_a4[i] + T_a4[i+1])/2)
END

S_gen_h4 = abs( SUM(S_gen_h4[i], i=1, N-1))

"Entropy in wall"
"Node 1"
Q_a_out4[1] = k_a4[1] * A_c4[1] * ((T_a4[1] + T_a4[2])/2 - T_a4[2]) / delta_x4
Q_h_out4[1] / ((T_a4[1] + T_a4[2]) / 2) + S_gen_a4[1] = Q_a_out4[1] / T_a4[2]

"Middle Nodes"
DUPLICATE i = 2, N-2
Q_a_in4[i] = k_a4[i] * A_c4[i] * (T_a4[i] - (T_a4[i+1]+T_a4[i])/2) / delta_x4
Q_a_out4[i] = k_a4[i] * A_c4[i] * ((T_a4[i+1]+T_a4[i])/2 - T_a4[i+1]) / delta_x4

Q_a_in4[i] / T_a4[i] + Q_h_out4[i] / ((T_a4[i] + T_a4[i+1])/2) + S_gen_a4[i] = Q_a_out4[i] / T_a4[i+1]
END

"Node N"
Q_a_in4[N-1] = k_a4[N-1] * A_c4[N-1] * (T_a4[N-1] - (T_a4[N]+T_a4[N-1])/2) / delta_x4
Q_a_in4[N-1] / T_a4[N-1] + Q_h_out4[N-1] / ((T_a4[N-1] + T_a4[N])/2) + S_gen_a4[N-1] = (Flux_upper*A_c4[N])/T_a4[N]

S_gen_a4 = abs (SUM(S_gen_a4[i], i=1,N-1))

S_gen_tot4 = (S_gen_a4 + S_gen_h4)*branches[4]
```

7.5 Code for Lower Portion of Heat Exchanger with Equilibrium Hydrogen

```
"Assumptions"
//hydrogen is adiabatic at inlet
//all heat is removed through the Gifford-McMahon cryocooler (no environmental losses)

"Constants"
H$ = 'Hydrogen'
    //fluid
O$ = 'OrthoHydrogen'
P$ = 'ParaHydrogen'
A$ = 'Aluminum_6061'
    //wall material
```

```
T_in = 100 [K]
    //inlet temp
T_out = 20 [K]
    //outlet temp
P_in = 652933 [Pa]
    //inlet pressure
L_tot = 0.239 [m]

RelRough = 0.01 [-]
    //relative roughness of wall, guess
P_dewar = 80 [psi]*convert(psi,Pa)
    //pressure within the dewar

T_first = 110 [K]
    //temperature of upper/first stage
T_second = 25 [K]
    //temperature of lower/second stage

m_dot_total = 0.000008 [kg/s]
Q_upper = 110 [W]
    //heat removed in upper stage

Q_lower = 30 [W]
    //heat removed in lower stage

L_tot = L1
S_gen_tot = S_gen_tot1
B = 1 [-]
    //number of sections in the system

N = 50 [-]
    //total number of nodes

"Number of branches in each section"
branches[1] = 8 [-]
DUPLICATE i=2, B
branches[i] = branches[i-1]*2
END

"Mass flow rate in each branch/section"
m_dot[1] = m_dot_total/branches[1]
DUPLICATE i=2, B
m_dot[i] = m_dot_total/branches[i]
END
```

```
"Heat Flux - Lower"
OD_lower1 = 6.8 [cm]*convert(cm,m)
OD_lower2 = 5 [cm]*convert(cm,m)
th_lower = 0.6 [cm]*convert(cm,m)
h_lower = 6.2 [cm]*convert(cm,m)
A_lower = PI*h_lower*OD_lower2 + (PI/4)*(OD_lower1^2-OD_lower2^2) +
PI*OD_lower1*th_lower + (PI/4) * OD_lower1^2
Flux_lower = Q_lower/A_lower

contact_area = (PI/4) * (OD_lower1^2 - OD_lower2^2)
indium_resistance = 20 [W/K]

"Establish Nodal Network"
delta_x1 = L1/(N-1)
x[1] = 0 [m]
Duplicate i = 2, N
x[i] = x[i-1] + delta_x1
End

ID1 = 0.003175 [m]
    //tube inner diameter
A_s1 = PI* ID1 * delta_x1
    //internal surface area of tube

"Varying wall thickness"
x1 =2.1
    //exponential coeff
y1 = 0.0009
f = 0.3
    //vertical shift, constant
DUPLICATE i=1, N
OD1[i] = ID1 + th1[i]
    //varying external diameter
A_c1[i] = (PI/4) * (OD1[i]^2 - ID1^2)
    //varying cross-sectional area
th1[i] =  f*x[i]^x1 + y1
    //varying wall thickness
END

"Upper Flange to first stage"
"First Node - Hydrogen"
T_h[1] = T_in
P_h[1] = P_in
```

```
Call pipeflow(H$,T_h[1],P_h[1],m_dot[1],ID1,delta_x1,RelRough:h_in_h[1], h_H_h[1],
DELTAP_h[1], Nusselt_T_h[1], f_h[1], Re_h[1])
eq_ortho1[1] = ((-26.339285 + 40.177003 * ln(T_h[1]) -24.070739 * ln(T_h[1])^2 + 7.0854451
* ln(T_h[1])^3 - 1.0266083 * ln(T_h[1])^4 + 0.058838859 * ln(T_h[1])^5) / (1 - 0.71557425 *
ln(T_h[1]) + 0.14395723 * ln(T_h[1])^2 + 0.008041614 * ln(T_h[1])^3 - 0.0056608578 *
ln(T_h[1])^4 + 0.0004869077 * ln(T_h[1])^5)) /100
cp_h[1] = cp(O$, T=T_h[1], P=P_h[1])*eq_ortho1[1] + cp(P$, T=T_h[1], P=P_h[1]) * (1-
eq_ortho1[1])
"Crank-Nicolson - Hydrogen"
Duplicate i=2, N
"Hydrogen"
T_h[i] = T_h[i-1] + (dTdxi_h[i] + dtdxplus_h[i]) * (delta_x1/2)
dTdxi_h[i] = (-h_in_h[i-1]*A_s1*(T_h[i-1]-T_a[i-1]))/(m_dot[1]*cp_h[i-1]*delta_x1)
dTdxplus_h[i] = (-h_in_h[i]*A_s1*(T_h[i]-T_a[i]))/(m_dot[1]*cp_h[i]*delta_x1)

P_h[i] = P_h[i-1] - DELTAP_h[i-1]

Call pipeflow(H$,T_h[i],P_h[i],m_dot[1],ID1,delta_x1,RelRough:h_in_h[i], h_H_h[i],
DELTAP_h[i], Nusselt_T_h[i], f_h[i], Re_h[i])

eq_ortho1[i] = ((-26.339285 + 40.177003 * ln(T_h[i]) -24.070739 * ln(T_h[i])^2 + 7.0854451 *
ln(T_h[i])^3 - 1.0266083 * ln(T_h[i])^4 + 0.058838859 * ln(T_h[i])^5) / (1 - 0.71557425 *
ln(T_h[i]) + 0.14395723 * ln(T_h[i])^2 + 0.008041614 * ln(T_h[i])^3 - 0.0056608578 *
ln(T_h[i])^4 + 0.0004869077 * ln(T_h[i])^5)) /100
cp_h[i] = cp(O$, T=T_h[i], P=P_h[i])*eq_ortho1[i] + cp(P$, T=T_h[i], P=P_h[i]) * (1-
eq_ortho1[i])
End

"First Node - Wall (Al)"
T_a[1] = T_in-5
dTdx_a[1] = 0
d2Tdx2_a[1] = (4*ID1*h_in_h[1]*(T_a[1]-T_h[1]))/(k_a[1]*(OD1[1]^2-ID1^2))

k_a[1] = conductivity(A$, T=T_a[1])

"Crank-Nicolson - Wall"
Duplicate i=2, N-1
T_a[i] = T_a[i-1] + (dTdx_a[i-1] + dTdx_a[i]) * (delta_x1/2)
dTdx_a[i] = dTdx_a[i-1] + (d2Tdx2_a[i-1] + d2Tdx2_a[i]) * (delta_x1/2)
d2Tdx2_a[i] =  (4*ID1*h_in_h[i]*(T_a[i]-T_h[i]))/(k_a[i]*(OD1[i]^2-ID1^2))

k_a[i] = conductivity(A$, T=T_a[i-1])
End

"Last Node - Wall (Al)"
```

```
Flux_lower * contact_area  = (T_a[N-1] - T_a[N]) / ((delta_x1/(k_a[N]*A_c1[N])) +
1/indium_resistance)
k_a[N] = conductivity(A$, T=T_a[N])


"Entropy in H2 stream"
DUPLICATE i=1,N
s_h[i] = entropy (O$, T=T_h[i], P=P_h[i])*eq_ortho1[i] + entropy (P$, T=T_h[i], P=P_h[i])*(1-
eq_ortho1[i])
END

DUPLICATE i=1, N-1
 Q_h_out[i] = m_dot[1] * (enthalpy(H$, T=T_h[i+1], P=P_h[i+1])  - enthalpy(H$, T=T_h[i],
P=P_h[i]))

m_dot[1] * s_h[i] + S_gen_h[i] = m_dot[1] * s_h[i+1] + Q_h_out[i] / ((T_a[i] + T_a[i+1])/2)
END

S_gen_h = abs( SUM(S_gen_h[i], i=1, N-1))

"Entropy in wall"
"Node 1"
Q_a_out[1] = k_a[1] * A_c1[1] * ((T_a[1] + T_a[2])/2 - T_a[2]) / delta_x1
Q_h_out[1] / ((T_a[1] + T_a[2]) / 2) + S_gen_a[1] = Q_a_out[1] / T_a[2]

"Middle Nodes"
DUPLICATE i = 2, N-2
Q_a_in[i] = k_a[i] * A_c1[i] * (T_a[i] - (T_a[i+1]+T_a[i])/2) / delta_x1
Q_a_out[i] = k_a[i] * A_c1[i] * ((T_a[i+1]+T_a[i])/2 - T_a[i+1]) / delta_x1

Q_a_in[i] / T_a[i] + Q_h_out[i] / ((T_a[i] + T_a[i+1])/2) + S_gen_a[i] = Q_a_out[i] / T_a[i+1]
END

"Node N"
Q_a_in[N-1] = k_a[N-1] * A_c1[N-1] * (T_a[N-1] - (T_a[N]+T_a[N-1])/2) / delta_x1
Q_a_in[N-1] / T_a[N-1] + Q_h_out[N-1] / ((T_a[N-1] + T_a[N])/2) + S_gen_a[N-1] =
(Flux_lower*A_c1[N])/T_a[N]

S_gen_a = abs (SUM(S_gen_a[i], i=1,N-1))

S_gen_tot1 = (S_gen_a + S_gen_h)*branches[1]
```

7.6 Code for Upper Portion of Heat Exchanger with Normal Hydrogen

```
"Assumptions"
//hydrogen is adiabatic at inlet
//all heat is removed through the Gifford-McMahon cryocooler (no environmental losses)

"Constants"
H$ = 'Hydrogen'
    //fluid
O$ = 'OrthoHydrogen'
P$ = 'ParaHydrogen'
A$ = 'Aluminum_6061'
    //wall material
T_in = 293 [K]
    //inlet temp
T_out = 30 [K]
    //outlet temp
P_in = 652933 [Pa]
    //inlet pressure
L_tot = 0.0795 [m]

RelRough = 0.01 [-]
    //relative roughness of wall, guess
P_dewar = 80 [psi]*convert(psi,Pa)
    //pressure within the dewar

T_first = 110 [K]
    //temperature of upper/first stage
T_second = 25 [K]
    //temperature of lower/second stage

m_dot_total = 0.000008 [kg/s]
Q_upper = 90 [W]
    //heat removed in upper stage

Q_lower = 30 [W]
    //heat removed in lower stage

L_tot = L1 + L2 + L3 + L4
S_gen_tot = S_gen_tot1 + S_gen_tot2 + S_gen_tot3 + S_gen_tot4
B = 4 [-]
    //number of sections in the system

N = 50 [-]
    //total number of nodes
```

```
"Number of branches in each section"
branches[1] = 1 [-]
DUPLICATE i=2, B
branches[i] = branches[i-1]*2
END

"Mass flow rate in each branch/section"
m_dot[1] = m_dot_total/branches[1]
DUPLICATE i=2, B
m_dot[i] = m_dot_total/branches[i]
END


"Heat Flux - Upper"
OD_upper1 = 12.5 [cm]*convert(cm,m)
OD_upper2 = 9 [cm]*convert(cm,m)
th_upper = 0.65 [cm]*convert(cm,m)
h_upper = 7.1 [cm]*convert(cm,m)
A_upper = PI * OD_upper2 * (h_upper - th_upper) + PI * OD_upper1 * th_upper + 2* ((PI/4) *
(OD_upper1^2 - OD_upper2^2))
Flux_upper = Q_upper/A_upper

contact_area = (PI/4) * (OD_upper1^2 - OD_upper2^2)
indium_resistance = 20 [W/K]

"Establish Nodal Network"
delta_x1 = L1/(N-1)
x[1] = 0 [m]
Duplicate i = 2, N
x[i] = x[i-1] + delta_x1
End

ID1 = 0.003175 [m]
    //tube inner diameter
A_s1 = PI* ID1 * delta_x1
    //internal surface area of tube

"Varying wall thickness"
x1 =2.15
    //exponential coeff
y1 = 0.00043
    //vertical shift, constant
f=1
                                                    //scaling factor
```

```
DUPLICATE i=1, N
OD1[i] = ID1 + th1[i]
    //varying external diameter
A_c1[i] = (PI/4) * (OD1[i]^2 - ID1^2)
    //varying cross-sectional area
th1[i] = f*x[i]^x1 + y1
    //varying wall thickness
END

"Upper Flange to first stage"
"First Node - Hydrogen"
T_h[1] = T_in
P_h[1] = P_in
Call pipeflow(H$,T_h[1],P_h[1],m_dot[1],ID1,delta_x1,RelRough:h_in_h[1], h_H_h[1],
DELTAP_h[1], Nusselt_T_h[1], f_h[1], Re_h[1])
//eq_ortho1[1] = ((-26.339285 + 40.177003 * ln(T_h[1]) -24.070739 * ln(T_h[1])^2 + 7.0854451
* ln(T_h[1])^3 - 1.0266083 * ln(T_h[1])^4 + 0.058838859 * ln(T_h[1])^5) / (1 - 0.71557425 *
ln(T_h[1]) + 0.14395723 * ln(T_h[1])^2 + 0.008041614 * ln(T_h[1])^3 - 0.0056608578 *
ln(T_h[1])^4 + 0.0004869077 * ln(T_h[1])^5)) /100
cp_h[1] = cp(H$, T=T_h[1], P=P_h[1])                    //cp(O$, T=T_h[1], P=P_h[1])*eq_ortho1[1]
+ cp(P$, T=T_h[1], P=P_h[1]) * (1-eq_ortho1[1])

"Crank-Nicolson - Hydrogen"
Duplicate i=2, N
"Hydrogen"
T_h[i] = T_h[i-1] + (dTdxi_h[i] + dtdxplus_h[i]) * (delta_x1/2)
dTdxi_h[i] = (-h_in_h[i-1]*A_s1*(T_h[i-1]-T_a[i-1]))/(m_dot[1]*cp_h[i-1]*delta_x1)
dTdxplus_h[i] = (-h_in_h[i]*A_s1*(T_h[i]-T_a[i]))/(m_dot[1]*cp_h[i]*delta_x1)

P_h[i] = P_h[i-1] - DELTAP_h[i-1]

Call pipeflow(H$,T_h[i],P_h[i],m_dot[1],ID1,delta_x1,RelRough:h_in_h[i], h_H_h[i],
DELTAP_h[i], Nusselt_T_h[i], f_h[i], Re_h[i])

//eq_ortho1[i] = ((-26.339285 + 40.177003 * ln(T_h[i]) -24.070739 * ln(T_h[i])^2 + 7.0854451
* ln(T_h[i])^3 - 1.0266083 * ln(T_h[i])^4 + 0.058838859 * ln(T_h[i])^5) / (1 - 0.71557425 *
ln(T_h[i]) + 0.14395723 * ln(T_h[i])^2 + 0.008041614 * ln(T_h[i])^3 - 0.0056608578 *
ln(T_h[i])^4 + 0.0004869077 * ln(T_h[i])^5)) /100
cp_h[i] = cp(H$, T=T_h[i], P=P_h[i])                    //cp(O$, T=T_h[i], P=P_h[i])*eq_ortho1[i] +
cp(P$, T=T_h[i], P=P_h[i]) * (1-eq_ortho1[i])
End

"First Node - Wall (Al)"
T_a[1] = T_in-1 [K]
dTdx_a[1] = 0
```

```
d2Tdx2_a[1] = (4*ID1*h_in_h[1]*(T_a[1]-T_h[1]))/(k_a[1]*(OD1[1]^2-ID1^2))

k_a[1] = conductivity(A$, T=T_a[1])

"Crank-Nicolson - Wall"
Duplicate i=2, N
T_a[i] = T_a[i-1] + (dTdx_a[i-1] + dTdx_a[i]) * (delta_x1/2)
dTdx_a[i] = dTdx_a[i-1] + (d2Tdx2_a[i-1] + d2Tdx2_a[i]) * (delta_x1/2)
d2Tdx2_a[i] =  (4*ID1*h_in_h[i]*(T_a[i]-T_h[i]))/(k_a[i]*(OD1[i]^2-ID1^2))

k_a[i] = conductivity(A$, T=T_a[i-1])
End

"Last Node - Wall (Al)"
//Flux_upper * contact_area  = (T_a[N-1] - T_a[N]) / ((delta_x1/(k_a[N]*A_c1[N])) +
1/indium_resistance)
//k_a[N] = conductivity(A$, T=T_a[N])


"Entropy in H2 stream"
DUPLICATE i=1,N
s_h[i] = entropy(H$, T=T_h[i], P=P_h[i])                //entropy (O$, T=T_h[i],
P=P_h[i])*eq_ortho1[i] + entropy (P$, T=T_h[i], P=P_h[i])*(1-eq_ortho1[i])
END

DUPLICATE i=1, N-1
 Q_h_out[i] = m_dot[1] * (enthalpy(H$, T=T_h[i+1], P=P_h[i+1])  - enthalpy(H$, T=T_h[i],
P=P_h[i]))

//Q_h_out[i] = m_dot[1] * (enthalpy(O$, T=T_h[i+1], P=P_h[i+1]) *eq_ortho[i] + enthalpy(P$,
T=T_h[i+1], P=P_h[i+1]) *(1-eq_ortho[i]) - enthalpy(O$, T=T_h[i], P=P_h[i])*eq_ortho[i]
+enthalpy(P$, T=T_h[i], P=P_h[i])*(1-eq_ortho[i]))

m_dot[1] * s_h[i] + S_gen_h[i] = m_dot[1] * s_h[i+1] + Q_h_out[i] / ((T_a[i] + T_a[i+1])/2)
END

S_gen_h = abs( SUM(S_gen_h[i], i=1, N-1))

"Entropy in wall"
"Node 1"
Q_a_out[1] = k_a[1] * A_c1[1] * ((T_a[1] + T_a[2])/2 - T_a[2]) / delta_x1
Q_h_out[1] / ((T_a[1] + T_a[2]) / 2) + S_gen_a[1] = Q_a_out[1] / T_a[2]
"Middle Nodes"
DUPLICATE i = 2, N-1
Q_a_in[i] = k_a[i] * A_c1[i] * (T_a[i] - (T_a[i+1]+T_a[i])/2) / delta_x1
```

```
Q_a_out[i] = k_a[i] * A_c1[i] * ((T_a[i+1]+T_a[i])/2 - T_a[i+1]) / delta_x1

Q_a_in[i] / T_a[i] + Q_h_out[i] / ((T_a[i] + T_a[i+1])/2) + S_gen_a[i] = Q_a_out[i] / T_a[i+1]
END

"Node N"
//Q_a_in[N-1] = k_a[N-1] * A_c1[N-1] * (T_a[N-1] - (T_a[N]+T_a[N-1])/2) / delta_x1
//Q_a_in[N-1] / T_a[N-1] + Q_h_out[N-1] / ((T_a[N-1] + T_a[N])/2) + S_gen_a[N-1] =
(Flux_upper*A_c1[N])/T_a[N]

S_gen_a = abs (SUM(S_gen_a[i], i=1,N-1))

S_gen_tot1 = (S_gen_a + S_gen_h)*branches[1]

"Node 2"
"Establish Nodal Network"
delta_x2 = L2/(N-1)
x2[1] = x[N]
Duplicate i = 2, N
x2[i] = x2[i-1] + delta_x2
End

L2 = 0.01 [m]
ID2 = 0.003175 [m]
    //tube inner diameter
A_s2 = PI* ID2 * delta_x2
    //internal surface area of tube

"Varying wall thickness"
x2 = x1
    //exponential coeff
y2 =y1
    //vertical shift, constant
DUPLICATE i=1, N
OD2[i] = ID2 + th2[i]
    //varying external diameter
A_c2[i] = (PI/4) * (OD2[i]^2 - ID2^2)
    //varying cross-sectional area
th2[i] = f*x2[i]^x2 + y2
    //varying wall thickness
END

"Upper Flange to first stage"
"First Node - Hydrogen"
T_h2[1] = T_h[N]
```

```
P_h2[1] = P_h[N]
Call pipeflow(H$,T_h2[1],P_h2[1],m_dot[2],ID2,delta_x2,RelRough:h_in_h2[1], h_H_h2[1],
DELTAP_h2[1], Nusselt_T_h2[1], f_h2[1], Re_h2[1])
//eq_ortho2[1] = ((-26.339285 + 40.177003 * ln(T_h2[1]) -24.070739 * ln(T_h2[1])^2 +
7.0854451 * ln(T_h2[1])^3 - 1.0266083 * ln(T_h2[1])^4 + 0.058838859 * ln(T_h2[1])^5) / (1 -
0.71557425 * ln(T_h2[1]) + 0.14395723 * ln(T_h2[1])^2 + 0.008041614 * ln(T_h2[1])^3 -
0.0056608578 * ln(T_h2[1])^4 + 0.0004869077 * ln(T_h2[1])^5)) /100
cp_h2[1] = cp(H$, T=T_h2[1], P=P_h2[1])              //cp(O$, T=T_h2[1],
P=P_h2[1])*eq_ortho2[1] + cp(P$, T=T_h2[1], P=P_h2[1]) * (1-eq_ortho2[1])

"Crank-Nicolson - Hydrogen"
Duplicate i=2, N
"Hydrogen"
T_h2[i] = T_h2[i-1] + (dTdxi_h2[i] + dtdxplus_h2[i]) * (delta_x2/2)
dTdxi_h2[i] = (-h_in_h2[i-1]*A_s2*(T_h2[i-1]-T_a2[i-1]))/(m_dot[2]*cp_h2[i-1]*delta_x2)

dTdxplus_h2[i] = (-h_in_h2[i]*A_s2*(T_h2[i]-T_a2[i]))/(m_dot[2]*cp_h2[i]*delta_x2)


P_h2[i] = P_h2[i-1] - DELTAP_h2[i-1]

Call pipeflow(H$,T_h2[i],P_h2[i],m_dot[2],ID2,delta_x2,RelRough:h_in_h2[i], h_H_h2[i],
DELTAP_h2[i], Nusselt_T_h2[i], f_h2[i], Re_h2[i])

//eq_ortho2[i] = ((-26.339285 + 40.177003 * ln(T_h2[i]) -24.070739 * ln(T_h2[i])^2 +
7.0854451 * ln(T_h2[i])^3 - 1.0266083 * ln(T_h2[i])^4 + 0.058838859 * ln(T_h2[i])^5) / (1 -
0.71557425 * ln(T_h2[i]) + 0.14395723 * ln(T_h2[i])^2 + 0.008041614 * ln(T_h2[i])^3 -
0.0056608578 * ln(T_h2[i])^4 + 0.0004869077 * ln(T_h2[i])^5)) /100
cp_h2[i] = cp(H$, T=T_h2[i], P=P_h2[i])              //cp(O$, T=T_h2[i],
P=P_h2[i])*eq_ortho2[i] + cp(P$, T=T_h2[i], P=P_h2[i]) * (1-eq_ortho2[i])
End

"First Node - Wall (Al)"
T_a2[1] = T_a[N]
dTdx_a2[1] = dTdx_a[N] + (d2Tdx2_a[N] + d2Tdx2_a2[1])*(delta_x2/2)
d2Tdx2_a2[1] = (4*ID2*h_in_h2[1]*(T_a2[1]-T_h2[1]))/(k_a2[1]*(OD2[1]^2-ID2^2))


k_a2[1] = conductivity(A$, T=T_a2[1])

"Crank-Nicolson - Wall"
Duplicate i=2, N
T_a2[i] = T_a2[i-1] + (dTdx_a2[i-1] + dTdx_a2[i]) * (delta_x2/2)
dTdx_a2[i] = dTdx_a2[i-1] + (d2Tdx2_a2[i-1] + d2Tdx2_a2[i]) * (delta_x2/2)
```

```
d2Tdx2_a2[i] =  (4*ID2*h_in_h2[i]*(T_a2[i]-T_h2[i]))/(k_a2[i]*(OD2[i]^2-ID2^2))


k_a2[i] = conductivity(A$, T=T_a2[i-1])
End

"Last Node - Wall (Al)"
//Flux_upper * contact_area  = (T_a2[N-1] - T_a2[N]) / ((delta_x2/(k_a2[N]*A_c2[N])) +
1/indium_resistance)
//k_a2[N] = conductivity(A$, T=T_a2[N])


"Entropy in H2 stream"
DUPLICATE i=1,N
s_h2[i] = entropy(H$, T=T_h2[i], P=P_h2[i])          //entropy (O$, T=T_h2[i],
P=P_h2[i])*eq_ortho2[i] + entropy (P$, T=T_h2[i], P=P_h2[i])*(1-eq_ortho2[i])
END

DUPLICATE i=1, N-1
Q_h_out2[i] = m_dot[2] * (enthalpy(H$, T=T_h2[i+1], P=P_h2[i+1])  - enthalpy(H$, T=T_h2[i],
P=P_h2[i]))
m_dot[2] * s_h2[i] + S_gen_h2[i] = m_dot[2] * s_h2[i+1] + Q_h_out2[i] / ((T_a2[i] +
T_a2[i+1])/2)
END

S_gen_h2 = abs( SUM(S_gen_h2[i], i=1, N-1))

"Entropy in wall"
"Node 1"
Q_a_out2[1] = k_a2[1] * A_c2[1] * ((T_a2[1] + T_a2[2])/2 - T_a2[2]) / delta_x2
Q_h_out2[1] / ((T_a2[1] + T_a2[2]) / 2) + S_gen_a2[1] = Q_a_out2[1] / T_a2[2]

"Middle Nodes"
DUPLICATE i = 2, N-1
Q_a_in2[i] = k_a2[i] * A_c2[i] * (T_a2[i] - (T_a2[i+1]+T_a2[i])/2) / delta_x2
Q_a_out2[i] = k_a2[i] * A_c2[i] * ((T_a2[i+1]+T_a2[i])/2 - T_a2[i+1]) / delta_x2

Q_a_in2[i] / T_a2[i] + Q_h_out2[i] / ((T_a2[i] + T_a2[i+1])/2) + S_gen_a2[i] = Q_a_out2[i] /
T_a2[i+1]
END

"Node N"
//Q_a_in2[N-1] = k_a2[N-1] * A_c2[N-1] * (T_a2[N-1] - (T_a2[N]+T_a2[N-1])/2) / delta_x2
//Q_a_in2[N-1] / T_a2[N-1] + Q_h_out2[N-1] / ((T_a2[N-1] + T_a2[N])/2) + S_gen_a2[N-1] =
(Flux_upper*A_c2[N])/T_a2[N]
```

```
S_gen_a2 = abs (SUM(S_gen_a2[i], i=1,N-1))

S_gen_tot2 = (S_gen_a2 + S_gen_h2)*branches[2]

"Node 3"
"Establish Nodal Network"
delta_x3 = L3/(N-1)
x3[1] = x2[N]
Duplicate i = 2, N
x3[i] = x3[i-1] + delta_x3
End

L3 = 0.01 [m]
ID3 = 0.003175 [m]
    //tube inner diameter
A_s3 = PI* ID3 * delta_x3
    //internal surface area of tube

"Varying wall thickness"
x3 = x1
    //exponential coeff
y3 = y1
    //vertical shift, constant
DUPLICATE i=1, N
OD3[i] = ID3 + th3[i]
    //varying external diameter
A_c3[i] = (PI/4) * (OD3[i]^2 - ID3^2)
    //varying cross-sectional area
th3[i] = f*x3[i]^x3 + y3
    //varying wall thickness
END

"Upper Flange to first stage"
"First Node - Hydrogen"
T_h3[1] = T_h2[N]
P_h3[1] = P_h2[N]
Call pipeflow(H$,T_h3[1],P_h3[1],m_dot[3],ID3,delta_x3,RelRough:h_in_h3[1], h_H_h3[1],
DELTAP_h3[1], Nusselt_T_h3[1], f_h3[1], Re_h3[1])
//eq_ortho3[1] = ((-26.339285 + 40.177003 * ln(T_h3[1]) -24.070739 * ln(T_h3[1])^2 +
7.0854451 * ln(T_h3[1])^3 - 1.0266083 * ln(T_h3[1])^4 + 0.058838859 * ln(T_h3[1])^5) / (1 -
0.71557425 * ln(T_h3[1]) + 0.14395723 * ln(T_h3[1])^2 + 0.008041614 * ln(T_h3[1])^3 -
0.0056608578 * ln(T_h3[1])^4 + 0.0004869077 * ln(T_h3[1])^5)) /100
cp_h3[1] = cp(H$, T=T_h3[1], P=P_h3[1])             //cp(O$, T=T_h3[1],
P=P_h3[1])*eq_ortho3[1] + cp(P$, T=T_h3[1], P=P_h3[1]) * (1-eq_ortho3[1])
```

"Crank-Nicolson - Hydrogen"
Duplicate i=2, N
"Hydrogen"
T_h3[i] = T_h3[i-1] + (dTdxi_h3[i] + dtdxplus_h3[i]) * (delta_x3/2)
dTdxi_h3[i] = (-h_in_h3[i-1]*A_s3*(T_h3[i-1]-T_a3[i-1]))/(m_dot[3]*cp_h3[i-1]*delta_x3)

dTdxplus_h3[i] = (-h_in_h3[i]*A_s3*(T_h3[i]-T_a3[i]))/(m_dot[3]*cp_h3[i]*delta_x3)

P_h3[i] = P_h3[i-1] - DELTAP_h3[i-1]

Call pipeflow(H$,T_h3[i],P_h3[i],m_dot[3],ID3,delta_x3,RelRough:h_in_h3[i], h_H_h3[i], DELTAP_h3[i], Nusselt_T_h3[i], f_h3[i], Re_h3[i])

//eq_ortho3[i] = ((-26.339285 + 40.177003 * ln(T_h3[i]) -24.070739 * ln(T_h3[i])^2 + 7.0854451 * ln(T_h3[i])^3 - 1.0266083 * ln(T_h3[i])^4 + 0.058838859 * ln(T_h3[i])^5) / (1 - 0.71557425 * ln(T_h3[i]) + 0.14395723 * ln(T_h3[i])^2 + 0.008041614 * ln(T_h3[i])^3 - 0.0056608578 * ln(T_h3[i])^4 + 0.0004869077 * ln(T_h3[i])^5)) /100
cp_h3[i] = cp(H$, T=T_h3[i], P=P_h3[i]) //cp(O$, T=T_h3[i], P=P_h3[i])*eq_ortho3[i] + cp(P$, T=T_h3[i], P=P_h3[i]) * (1-eq_ortho3[i])
End

"First Node - Wall (Al)"
T_a3[1] = T_a2[N]
dTdx_a3[1] = dTdx_a2[N] + (d2Tdx2_a2[N] + d2Tdx2_a3[1])*(delta_x3/2)
d2Tdx2_a3[1] = (4*ID3*h_in_h3[1]*(T_a3[1]-T_h3[1]))/(k_a3[1]*(OD3[1]^2-ID3^2))

k_a3[1] = conductivity(A$, T=T_a3[1])

"Crank-Nicolson - Wall"
Duplicate i=2, N
T_a3[i] = T_a3[i-1] + (dTdx_a3[i-1] + dTdx_a3[i]) * (delta_x3/2)
dTdx_a3[i] = dTdx_a3[i-1] + (d2Tdx2_a3[i-1] + d2Tdx2_a3[i]) * (delta_x3/2)
d2Tdx2_a3[i] = (4*ID3*h_in_h3[i]*(T_a3[i]-T_h3[i]))/(k_a3[i]*(OD3[i]^2-ID3^2))

k_a3[i] = conductivity(A$, T=T_a3[i-1])
End

"Last Node - Wall (Al)"
//Flux_upper * contact_area = (T_a3[N-1] - T_a3[N]) / ((delta_x3/(k_a3[N]*A_c3[N])) + 1/indium_resistance)
//k_a3[N] = conductivity(A$, T=T_a3[N])

"Entropy in H2 stream"
DUPLICATE i=1,N
s_h3[i] = entropy(H$, T=T_h3[i], P=P_h3[i]) //entropy (O$, T=T_h3[i], P=P_h3[i])*eq_ortho3[i] + entropy (P$, T=T_h3[i], P=P_h3[i])*(1-eq_ortho3[i])
END

DUPLICATE i=1, N-1
Q_h_out3[i] = m_dot[3] * (enthalpy(H$, T=T_h3[i+1], P=P_h3[i+1]) - enthalpy(H$, T=T_h3[i], P=P_h3[i]))
m_dot[3] * s_h3[i] + S_gen_h3[i] = m_dot[3] * s_h3[i+1] + Q_h_out3[i] / ((T_a3[i] + T_a3[i+1])/2)
END

S_gen_h3 = abs(SUM(S_gen_h3[i], i=1, N-1))

"Entropy in wall"
"Node 1"
Q_a_out3[1] = k_a3[1] * A_c3[1] * ((T_a3[1] + T_a3[2])/2 - T_a3[2]) / delta_x3
Q_h_out3[1] / ((T_a3[1] + T_a3[2]) / 2) + S_gen_a3[1] = Q_a_out3[1] / T_a3[2]

"Middle Nodes"
DUPLICATE i = 2, N-1
Q_a_in3[i] = k_a3[i] * A_c3[i] * (T_a3[i] - (T_a3[i+1]+T_a3[i])/2) / delta_x3
Q_a_out3[i] = k_a3[i] * A_c3[i] * ((T_a3[i+1]+T_a3[i])/2 - T_a3[i+1]) / delta_x3

Q_a_in3[i] / T_a3[i] + Q_h_out3[i] / ((T_a3[i] + T_a3[i+1])/2) + S_gen_a3[i] = Q_a_out3[i] / T_a3[i+1]
END

"Node N"
//Q_a_in3[N-1] = k_a3[N-1] * A_c3[N-1] * (T_a3[N-1] - (T_a3[N]+T_a3[N-1])/2) / delta_x3
//Q_a_in3[N-1] / T_a3[N-1] + Q_h_out3[N-1] / ((T_a3[N-1] + T_a3[N])/2) + S_gen_a3[N-1] = (Flux_upper*A_c3[N])/T_a3[N]

S_gen_a3 = abs (SUM(S_gen_a3[i], i=1,N-1))

S_gen_tot3 = (S_gen_a3 + S_gen_h3)*branches[3]

"Node 4"
"Establish Nodal Network"
delta_x4 = L4/(N-1)
x4[1] = x3[N]
Duplicate i = 2, N

```
x4[i] = x4[i-1] + delta_x4
End

L4 = 0.0495 [m]
ID4 = 0.003175 [m]
    //tube inner diameter
A_s4 = PI* ID4 * delta_x4
    //internal surface area of tube

"Varying wall thickness"
x4 = x1
    //exponential coeff
y4 = y1
    //vertical shift, constant
DUPLICATE i=1, N
OD4[i] = ID4 + th4[i]
    //varying external diameter
A_c4[i] = (PI/4) * (OD4[i]^2 - ID4^2)
    //varying cross-sectional area
th4[i] = f*x4[i]^x4 + y4
    //varying wall thickness
END

"Upper Flange to first stage"
"First Node - Hydrogen"
T_h4[1] = T_h3[N]
P_h4[1] = P_h3[N]
Call pipeflow(H$,T_h4[1],P_h4[1],m_dot[4],ID4,delta_x4,RelRough:h_in_h4[1], h_H_h4[1],
DELTAP_h4[1], Nusselt_T_h4[1], f_h4[1], Re_h4[1])
//eq_ortho4[1] = ((-26.339285 + 40.177003 * ln(T_h4[1]) -24.070739 * ln(T_h4[1])^2 +
7.0854451 * ln(T_h4[1])^3 - 1.0266083 * ln(T_h4[1])^4 + 0.058838859 * ln(T_h4[1])^5) / (1 -
0.71557425 * ln(T_h4[1]) + 0.14395723 * ln(T_h4[1])^2 + 0.008041614 * ln(T_h4[1])^3 -
0.0056608578 * ln(T_h4[1])^4 + 0.0004869077 * ln(T_h4[1])^5)) /100
cp_h4[1] = cp(H$, T=T_h4[1], P=P_h4[1])             //cp(O$, T=T_h4[1],
P=P_h4[1])*eq_ortho4[1] + cp(P$, T=T_h4[1], P=P_h4[1]) * (1-eq_ortho4[1])

"Crank-Nicolson - Hydrogen"
Duplicate i=2, N
"Hydrogen"
T_h4[i] = T_h4[i-1] + (dTdxi_h4[i] + dtdxplus_h4[i]) * (delta_x4/2)
dTdxi_h4[i] = (-h_in_h4[i-1]*A_s4*(T_h4[i-1]-T_a4[i-1]))/(m_dot[4]*cp_h4[i-1]*delta_x4)

dTdxplus_h4[i] = (-h_in_h4[i]*A_s4*(T_h4[i]-T_a4[i]))/(m_dot[4]*cp_h4[i]*delta_x4)
```

```
P_h4[i] = P_h4[i-1] - DELTAP_h4[i-1]

Call pipeflow(H$,T_h4[i],P_h4[i],m_dot[4],ID4,delta_x4,RelRough:h_in_h4[i], h_H_h4[i],
DELTAP_h4[i], Nusselt_T_h4[i], f_h4[i], Re_h4[i])

//eq_ortho4[i] = ((-26.339285 + 40.177003 * ln(T_h4[i]) -24.070739 * ln(T_h4[i])^2 +
7.0854451 * ln(T_h4[i])^3 - 1.0266083 * ln(T_h4[i])^4 + 0.058838859 * ln(T_h4[i])^5) / (1 -
0.71557425 * ln(T_h4[i]) + 0.14395723 * ln(T_h4[i])^2 + 0.008041614 * ln(T_h4[i])^3 -
0.0056608578 * ln(T_h4[i])^4 + 0.0004869077 * ln(T_h4[i])^5)) /100
cp_h4[i] = cp(H$, T=T_h4[i], P=P_h4[i])              //cp(O$, T=T_h4[i],
P=P_h4[i])*eq_ortho4[i] + cp(P$, T=T_h4[i], P=P_h4[i]) * (1-eq_ortho4[i])
End

"First Node - Wall (Al)"
T_a4[1] = T_a3[N]
dTdx_a4[1] = dTdx_a3[N] + (d2Tdx2_a3[N] + d2Tdx2_a4[1])*(delta_x4/2)
d2Tdx2_a4[1] = (4*ID4*h_in_h4[1]*(T_a4[1]-T_h4[1]))/(k_a4[1]*(OD4[1]^2-ID4^2))


k_a4[1] = conductivity(A$, T=T_a4[1])

"Crank-Nicolson - Wall"
Duplicate i=2, N-1
T_a4[i] = T_a4[i-1] + (dTdx_a4[i-1] + dTdx_a4[i]) * (delta_x4/2)
dTdx_a4[i] = dTdx_a4[i-1] + (d2Tdx2_a4[i-1] + d2Tdx2_a4[i]) * (delta_x4/2)
d2Tdx2_a4[i] =  (4*ID4*h_in_h4[i]*(T_a4[i]-T_h4[i]))/(k_a4[i]*(OD4[i]^2-ID4^2))


k_a4[i] = conductivity(A$, T=T_a4[i-1])
End

"Last Node - Wall (Al)"
Flux_upper * contact_area  = (T_a4[N-1] - T_a4[N]) / ((delta_x4/(k_a4[N]*A_c4[N])) +
1/indium_resistance)
k_a4[N] = conductivity(A$, T=T_a4[N])


"Entropy in H2 stream"
DUPLICATE i=1,N
s_h4[i] = entropy(H$, T=T_h4[i], P=P_h4[i])          //entropy (O$, T=T_h4[i],
P=P_h4[i])*eq_ortho4[i] + entropy (P$, T=T_h4[i], P=P_h4[i])*(1-eq_ortho4[i])
END

DUPLICATE i=1, N-1
```

```
Q_h_out4[i] = m_dot[4] * (enthalpy(H$, T=T_h4[i+1], P=P_h4[i+1])  - enthalpy(H$, T=T_h4[i], P=P_h4[i]))
m_dot[4] * s_h4[i] + S_gen_h4[i] = m_dot[4] * s_h4[i+1] + Q_h_out4[i] / ((T_a4[i] + T_a4[i+1])/2)
END

S_gen_h4 = abs( SUM(S_gen_h4[i], i=1, N-1))

"Entropy in wall"
"Node 1"
Q_a_out4[1] = k_a4[1] * A_c4[1] * ((T_a4[1] + T_a4[2])/2 - T_a4[2]) / delta_x4
Q_h_out4[1] / ((T_a4[1] + T_a4[2]) / 2) + S_gen_a4[1] = Q_a_out4[1] / T_a4[2]

"Middle Nodes"
DUPLICATE i = 2, N-2
Q_a_in4[i] = k_a4[i] * A_c4[i] * (T_a4[i] - (T_a4[i+1]+T_a4[i])/2) / delta_x4
Q_a_out4[i] = k_a4[i] * A_c4[i] * ((T_a4[i+1]+T_a4[i])/2 - T_a4[i+1]) / delta_x4

Q_a_in4[i] / T_a4[i] + Q_h_out4[i] / ((T_a4[i] + T_a4[i+1])/2) + S_gen_a4[i] = Q_a_out4[i] / T_a4[i+1]
END

"Node N"
Q_a_in4[N-1] = k_a4[N-1] * A_c4[N-1] * (T_a4[N-1] - (T_a4[N]+T_a4[N-1])/2) / delta_x4
Q_a_in4[N-1] / T_a4[N-1] + Q_h_out4[N-1] / ((T_a4[N-1] + T_a4[N])/2) + S_gen_a4[N-1] = (Flux_upper*A_c4[N])/T_a4[N]

S_gen_a4 = abs (SUM(S_gen_a4[i], i=1,N-1))

S_gen_tot4 = (S_gen_a4 + S_gen_h4)*branches[4]
```

7.7 Code for Lower Portion of Heat Exchanger with Normal Hydrogen

```
"Assumptions"
//hydrogen is adiabatic at inlet
//all heat is removed through the Gifford-McMahon cryocooler (no environmental losses)

"Constants"
H$ = 'Hydrogen'
    //fluid
O$ = 'OrthoHydrogen'
P$ = 'ParaHydrogen'
A$ = 'Aluminum_6061'
    //wall material
```

```
T_in = 100 [K]
    //inlet temp
T_out = 20 [K]
    //outlet temp
P_in = 652933 [Pa]
    //inlet pressure
L_tot = 0.239 [m]

RelRough = 0.01 [-]
    //relative roughness of wall, guess
P_dewar = 80 [psi]*convert(psi,Pa)
    //pressure within the dewar

T_first = 110 [K]
    //temperature of upper/first stage
T_second = 25 [K]
    //temperature of lower/second stage

m_dot_total = 0.000008 [kg/s]
Q_upper = 110 [W]
    //heat removed in upper stage

Q_lower = 30 [W]
    //heat removed in lower stage

L_tot = L1
S_gen_tot = S_gen_tot1
B = 1 [-]
    //number of sections in the system

N = 50 [-]
    //total number of nodes

"Number of branches in each section"
branches[1] = 8 [-]
DUPLICATE i=2, B
branches[i] = branches[i-1]*2
END

"Mass flow rate in each branch/section"
m_dot[1] = m_dot_total/branches[1]
DUPLICATE i=2, B
m_dot[i] = m_dot_total/branches[i]
END
```

```
"Heat Flux - Lower"
OD_lower1 = 6.8 [cm]*convert(cm,m)
OD_lower2 = 5 [cm]*convert(cm,m)
th_lower = 0.6 [cm]*convert(cm,m)
h_lower = 6.2 [cm]*convert(cm,m)
A_lower = PI*h_lower*OD_lower2 + (PI/4)*(OD_lower1^2-OD_lower2^2) +
PI*OD_lower1*th_lower + (PI/4) * OD_lower1^2
Flux_lower = Q_lower/A_lower

contact_area = (PI/4) * (OD_lower1^2 - OD_lower2^2)
indium_resistance = 20 [W/K]

"Establish Nodal Network"
delta_x1 = L1/(N-1)
x[1] = 0 [m]
Duplicate i = 2, N
x[i] = x[i-1] + delta_x1
End

ID1 = 0.003175 [m]
    //tube inner diameter
A_s1 = PI* ID1 * delta_x1
    //internal surface area of tube

"Varying wall thickness"
x1 =2.1
    //exponential coeff
y1 = 0.0009
f = 0.3
    //vertical shift, constant
DUPLICATE i=1, N
OD1[i] = ID1 + th1[i]
    //varying external diameter
A_c1[i] = (PI/4) * (OD1[i]^2 - ID1^2)
    //varying cross-sectional area
th1[i] =  f*x[i]^x1 + y1
    //varying wall thickness
END

"Upper Flange to first stage"
"First Node - Hydrogen"
T_h[1] = T_in
P_h[1] = P_in
```

```
Call pipeflow(H$,T_h[1],P_h[1],m_dot[1],ID1,delta_x1,RelRough:h_in_h[1], h_H_h[1],
DELTAP_h[1], Nusselt_T_h[1], f_h[1], Re_h[1])
//eq_ortho1[1] = ((-26.339285 + 40.177003 * ln(T_h[1]) -24.070739 * ln(T_h[1])^2 + 7.0854451
* ln(T_h[1])^3 - 1.0266083 * ln(T_h[1])^4 + 0.058838859 * ln(T_h[1])^5) / (1 - 0.71557425 *
ln(T_h[1]) + 0.14395723 * ln(T_h[1])^2 + 0.008041614 * ln(T_h[1])^3 - 0.0056608578 *
ln(T_h[1])^4 + 0.0004869077 * ln(T_h[1])^5)) /100
cp_h[1] = cp(H$, T=T_h[1], P=P_h[1])                    //cp(O$, T=T_h[1], P=P_h[1])*eq_ortho1[1]
+ cp(P$, T=T_h[1], P=P_h[1]) * (1-eq_ortho1[1])
"Crank-Nicolson - Hydrogen"
Duplicate i=2, N
"Hydrogen"
T_h[i] = T_h[i-1] + (dTdxi_h[i] + dtdxplus_h[i]) * (delta_x1/2)
dTdxi_h[i] = (-h_in_h[i-1]*A_s1*(T_h[i-1]-T_a[i-1]))/(m_dot[1]*cp_h[i-1]*delta_x1)
dTdxplus_h[i] = (-h_in_h[i]*A_s1*(T_h[i]-T_a[i]))/(m_dot[1]*cp_h[i]*delta_x1)

P_h[i] = P_h[i-1] - DELTAP_h[i-1]

Call pipeflow(H$,T_h[i],P_h[i],m_dot[1],ID1,delta_x1,RelRough:h_in_h[i], h_H_h[i],
DELTAP_h[i], Nusselt_T_h[i], f_h[i], Re_h[i])

//eq_ortho1[i] = ((-26.339285 + 40.177003 * ln(T_h[i]) -24.070739 * ln(T_h[i])^2 + 7.0854451
* ln(T_h[i])^3 - 1.0266083 * ln(T_h[i])^4 + 0.058838859 * ln(T_h[i])^5) / (1 - 0.71557425 *
ln(T_h[i]) + 0.14395723 * ln(T_h[i])^2 + 0.008041614 * ln(T_h[i])^3 - 0.0056608578 *
ln(T_h[i])^4 + 0.0004869077 * ln(T_h[i])^5)) /100
cp_h[i] = cp(H$, T=T_h[i], P=P_h[i])                    //cp(O$, T=T_h[i], P=P_h[i])*eq_ortho1[i] +
cp(P$, T=T_h[i], P=P_h[i]) * (1-eq_ortho1[i])
End

"First Node - Wall (Al)"
T_a[1] = T_in-5
dTdx_a[1] = 0
d2Tdx2_a[1] = (4*ID1*h_in_h[1]*(T_a[1]-T_h[1]))/(k_a[1]*(OD1[1]^2-ID1^2))

k_a[1] = conductivity(A$, T=T_a[1])

"Crank-Nicolson - Wall"
Duplicate i=2, N-1
T_a[i] = T_a[i-1] + (dTdx_a[i-1] + dTdx_a[i]) * (delta_x1/2)
dTdx_a[i] = dTdx_a[i-1] + (d2Tdx2_a[i-1] + d2Tdx2_a[i]) * (delta_x1/2)
d2Tdx2_a[i] =  (4*ID1*h_in_h[i]*(T_a[i]-T_h[i]))/(k_a[i]*(OD1[i]^2-ID1^2))

k_a[i] = conductivity(A$, T=T_a[i-1])
End

"Last Node - Wall (Al)"
```

```
Flux_lower * contact_area  = (T_a[N-1] - T_a[N]) / ((delta_x1/(k_a[N]*A_c1[N])) +
1/indium_resistance)
k_a[N] = conductivity(A$, T=T_a[N])


"Entropy in H2 stream"
DUPLICATE i=1,N
s_h[i] = entropy(H$, T=T_h[i], P=P_h[i])                //entropy (O$, T=T_h[i],
P=P_h[i])*eq_ortho1[i] + entropy (P$, T=T_h[i], P=P_h[i])*(1-eq_ortho1[i])
END

DUPLICATE i=1, N-1
 Q_h_out[i] = m_dot[1] * (enthalpy(H$, T=T_h[i+1], P=P_h[i+1])  - enthalpy(H$, T=T_h[i],
P=P_h[i]))

m_dot[1] * s_h[i] + S_gen_h[i] = m_dot[1] * s_h[i+1] + Q_h_out[i] / ((T_a[i] + T_a[i+1])/2)
END

S_gen_h = abs( SUM(S_gen_h[i], i=1, N-1))

"Entropy in wall"
"Node 1"
Q_a_out[1] = k_a[1] * A_c1[1] * ((T_a[1] + T_a[2])/2 - T_a[2]) / delta_x1
Q_h_out[1] / ((T_a[1] + T_a[2]) / 2) + S_gen_a[1] = Q_a_out[1] / T_a[2]

"Middle Nodes"
DUPLICATE i = 2, N-2
Q_a_in[i] = k_a[i] * A_c1[i] * (T_a[i] - (T_a[i+1]+T_a[i])/2) / delta_x1
Q_a_out[i] = k_a[i] * A_c1[i] * ((T_a[i+1]+T_a[i])/2 - T_a[i+1]) / delta_x1

Q_a_in[i] / T_a[i] + Q_h_out[i] / ((T_a[i] + T_a[i+1])/2) + S_gen_a[i] = Q_a_out[i] / T_a[i+1]
END

"Node N"
Q_a_in[N-1] = k_a[N-1] * A_c1[N-1] * (T_a[N-1] - (T_a[N]+T_a[N-1])/2) / delta_x1
Q_a_in[N-1] / T_a[N-1] + Q_h_out[N-1] / ((T_a[N-1] + T_a[N])/2) + S_gen_a[N-1] =
(Flux_lower*A_c1[N])/T_a[N]

S_gen_a = abs (SUM(S_gen_a[i], i=1,N-1))

S_gen_tot1 = (S_gen_a + S_gen_h)*branches[1]
```